Titin regulation and maintenance in the cardiac sarcomere

By

Adrian Gabriel Cadar

Dissertation

Submitted to the Faculty of the

Graduate School of Vanderbilt University

in partial fulfillment of the requirements

for the degree of

DOCTOR OF PHILOSOPHY

in

Molecular Physiology & Biophysics

August 11, 2017

Nashville, Tennessee

Approved:

Charles E. Cobb, Ph.D.

Wenbiao Chen, Ph.D.

Charles C. Hong, M.D./Ph.D.

Anne K. Kenworthy, Ph.D.

Chee Chew Lim, Ph.D.

Owen P. McGuinness, Ph.D

This work is dedicated to my supportive family and friends

ACKNOWLEDGEMENTS

This would not have been possible without the help and support of individuals listed below. First, I would like to thank my mentors, Drs. Charles Hong and Chee Lim; your mentorship has truly impacted my scientific career. Dr. Hong, thank you for being a wonderful mentor. You are great role model for anyone that wants to become a physician scientist. I always appreciated the critical input and valued the translational component you placed in my work. Dr. Lim, thank you for teaching me how to be independent, critical, thoughtful, and confident with regards to my scientific reasoning. I should also take this time to thank my dissertation committee chair Dr. Charles Cobb and committee members Drs. Anne Kenworthy, Owen McGuiness, and Wenbiao Chen. You all have provided tremendous support and council throughout this process. Dr. Don Brunson, without you, I would have never considered Vanderbilt. Thank for your support and friendship. Drs. Roger Chalkey, Linda Sealy, Christina Keeton, and the IMSD, thank you for your unyielding support. The IMSD program without a doubt helped shaped me to become not only a successful scientist but a leader as well. Dr. T.K. Feaster, Juan Gneeco, and Mohamed Elmonoufy, thank you for your help and support. Drs. Lili Wang, Kevin Bersell, and Bjorn Knollmann, thank you for your scientific contributions to my studies.

SOURCE OF FUNDING

This study was funded in part by National Institutes of Health (NIH) grant RO1HL095813 and Vanderbilt University Stahlman to C.C.L., 5R01HL104040, 5R01HL095813, and P50GM115305 to C.C.H., Graduate Research Assistant Supplement RO1HL095813-S1 and Center for Advancing Translational Sciences Award No. UL1TR000445 to A.G.C. Live cell imaging were performed in part through the use of the VUMC Cell Imaging Shared Resource (supported by NIH grants CA68485, DK20593, DK58404, DK59637 and EY08126).

TABLE OF CONTENTS

LIST OF TABLES

Table Page

LIST OF FIGURES

Chapter 1

Introduction

1.1 The sarcomere

The heart's primary role is to pump blood throughout the body. This feat is accomplished by the precise coordination of excitation-contraction coupling of approximately 2-3 billion terminally differentiated cells known as cardiomyocytes. Cardiomyocytes (mononucleated and or binucleated) constitute a third of the heart and are connected to each other in a branched pattern via gap junctions where their signal propagation is transmitted through[1]. Within cardiomyoctes are myofibrils, which are made up of a series of contractile units known as sarcomeres. The first historical observation of sarcomeres was in 1682 by Anton Van Leeuwenhoek when he noted the banded patterns of beef muscle with his early miscorscope[2]. Corresponding with Robert Hooke, he described muscle as chords made up of strings that were composed of filaments that were most likely composed of lower filaments[2]. These were the early descriptions of muscle and since then significant progress has been made in the structure and function of sarcomeres.

The sarcomere is the basic contractile unit of striated muscle and is composed of an ordered arrangement of myofilaments and accessory proteins that are important for force generation (Fig 1). One sarcomere is defined by two neighboring Z-lines which is derived from the German word *zwischenscheibe,* meaning in between[3,4]. Under polarized light, sarcomeres give rise to alternating light and dark bands. The light band is denoted as the I-band (isotropic) and the dark band is denoted as the A-band (anisotropic). The M-band (mittel, German for middle) bifurcates the A-band. The I-band gives rise to the thin filaments (actin, troponins and tropomyosin) and the A-band gives rise to the thick filaments (myosin). At 2.97-3.7mDa, titin is

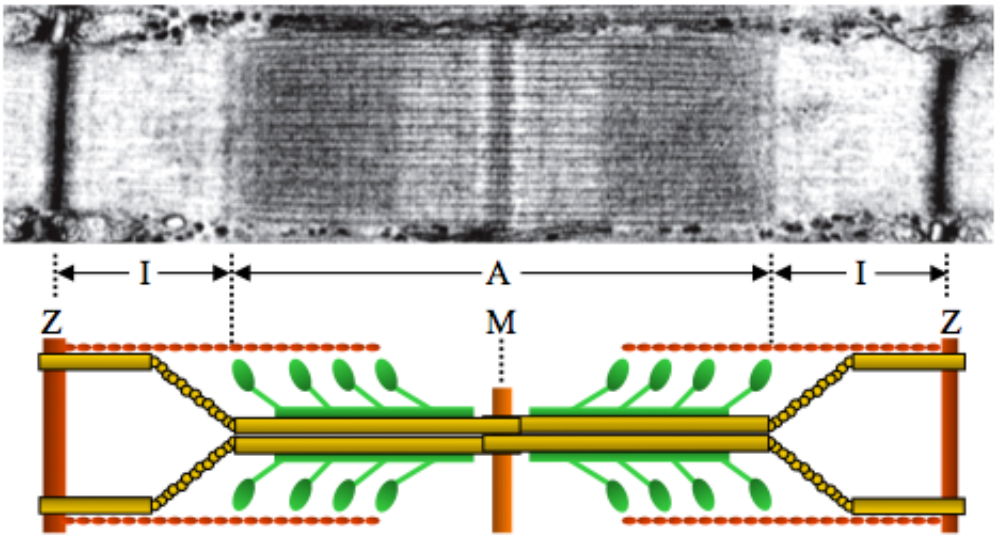

Figure 1 Schematic of the sarcomere. Top: Electron micrograph of the cardiac sarcomere. Bottom: Cartoon representation of the sarcomere. Dark orange - Z-disk; light orange - M-band; yellow – titin; red - actin filament; green - myosin heavy chain.

the largest and third most abundant myofilament protein after actin and myosin[5]. Titin spans the half-sarcomere with its N-terminal domain anchored at the Z-line and its C-terminal domain at the M-band serving as a molecular scaffold for the organization of contractile and many other sarcomeric proteins (Fig. 1)[5,6].

1.2 Discovery of the third myofilament

A.F. Huxley and R. Nidergerke (1954) and H.E. Huxley and J. Hanson (1954) independently proposed the sliding filament theory, which describes how muscle contracts[7,8]. The authors demonstrated how the A-band remained constant throughout contraction and observed how only the I-band changed in length. This allowed them to propose a model in which the actin filaments slide past the myosin filaments in order to generate contraction. Their model accounted for contraction of two filaments as it was unknown whether a third filament existed.

In 1953, Hanson et al provided direct evidence that myosin was located at the A-band by extracting myosin from myofibrils by irrigating the myofibril preparations with a Hasselbach-Schneider pyrophosphate and Guba-Strab-ATP solution[9]. After treatment, Hanson et al observed the disappearance of the A-band as the sarcomere was left intact which they noted as "sarcomere ghosts"[9]. If they used trypsin after removing myosin heavy chain, Hanson et al observed collapsing of the sarcomeres[9]. This was indirect evidence of the potential existence of a third myofilament that provided structural integrity to the sarcomere. The question became, what was holding the sarcomere intact? This third myofilaments concept was further expanded in Huxley and Hanson's landmark sliding filament model of muscle contraction manuscript. Again, after removing myosin heavy chain, the actin filaments were still present and connected to the Z-bands, Huxley this time postulated the existence of an elastic S substance (S-filament) that

connected the Z-bands and actin filaments which could explain why the sarcomere was intact[8,10,11]. Later, Hanson and Huxley further demonstrated that extracted myosin component contained an unknown substance (X-protein) which was presumably pieces of titin[11,12].

Although the two-filament model explained many features of muscle contraction, it did not account for the passive tension observed in myofibrils therefore it was hypothesized that something else could account for that force[13]. Further interest into the third myofilament hypothesis resulted from electron microscopy images of stretched sarcomeres. Thin filaments called "gap filaments" were in the I-band as well as in between the half A-bands were postulated to hold the sarcomeres intact after they had been stretched beyond their physiological length[14,15]. This finding allowed for the proposal of a third myofilament hypothesis by Locker and Leet[13].

In 1976, Maruyama et al extracted all soluble proteins from isolated rabbit myofibrils and observed that the myofibrils were still intact and remained elastic even though there were no observable filaments between the Z-lines[16]. From this prep, Maruyama et al isolated an elastic protein that was distinct from elastin and collagen[16]. Maruyama further characterized the amino acid composition of this insoluble elastic protein and determined that it was not was not reticulin therefore, naming this new elastic protein connectin[17]. Concurrently in 1976, Etlinger et al set out to elucidate the molecular composition of the sarcomere by extracting and purifying large molecular weight protiens (>200,000 daltons) from myofibrils in order to develop a tool to understand myofibrillogenesis[18]. Etlinger's observations of large unknown sarcomeric proteins laid the foundation for the discovery of titin as Wang et al set out to identify and characterize these large molecular weight proteins in 1979[19]. Wang et al observed two large molecular weight bands in an SDS-PAGE gel of thiol-reduced, denatured rabbit myofibril lysates and collectively named these two larges bands, titin after the deity Titan, given its size[13,19]. Wang et

al purified titin via agarose gel filtration and developed a polyclonal antibody which localized titin to the Z-line and M-line via immunofluorescence which generated confusion about titin's localization in the sarcomere[19]. Unfortunately, there was even more confusion in the field as Maruyama and Wang had identified the same protein but named it differently. Maruyuma's characterization of connectin stemmed via a chemical analysis of mixture of insoluble proteins that contained titin whereas Wang's was a pure protein isolation[13]. Marayuma later confirmed that connectin and titin were one and the same[20].

1.3 Titin: the third myofilament

In humans and mice, titin is encoded by a single gene composed of 363 exons on the long arm of chromosome 2 with a coding capacity of a ~4.2 mDa protein thus making it the largest single encoded protein known (Fig. 2)[21]. To date, only a 3.8 mDa protein has been identified, due to the extensive alternative splicing that occurs at the spring domain of titin which gives rise to 2.97-3.7mDa proteins[22]. In striated muscle, titin is the largest and third most abundant myofilament protein, after actin and myosin, accounting for 10% of the total protein in the cardiomyocyte[5]. At ~1 μm in length, titin spans the entire half-sarcomere with its N-terminal domain anchored at the Z-line and its C-terminal domain at the M-band serving as a molecular scaffold for the organization of contractile and many other sarcomeric proteins[5,6]. Approximately 90% of titin consists of two types of protein domains, an immunoglobulin-like (Ig) and fibronectin type-III (FNIII) domain along with several unique sequences and a kinase domain (Fig. 2)[5,23]. Differential splicing of approximately 230 exons within the titin spring domain results in three main titin isoforms in adults; cardiac N2B (~3 mDa), cardiac N2BA (~3.2-3.8 mDA), and skeletal N2A (~3-3.8 mDa) with the exception of a fetal isoform and rare

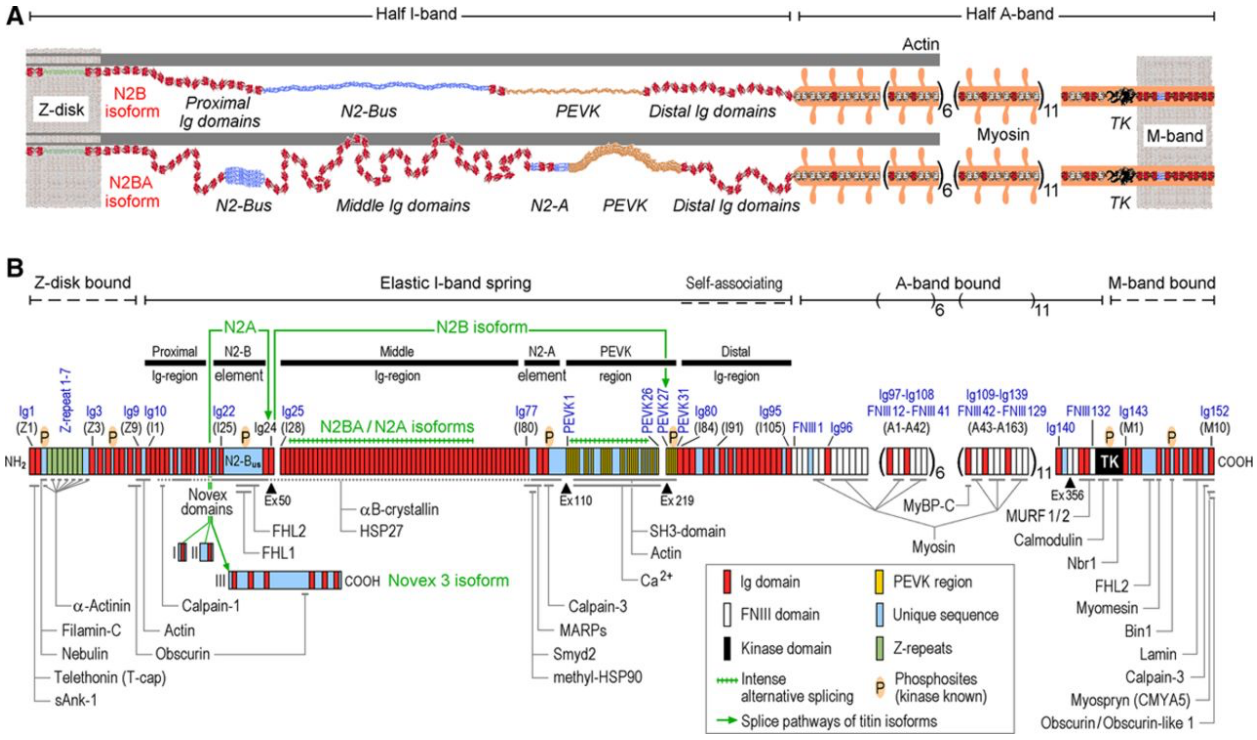

Figure 2 Domain structure of titin-isoforms and binding sites of titin ligands. A) Layout of titin-isoforms in the cardiac half-sarcomere, showing stiff N2B coexpressed with compliant N2BA. B) Domain structure of the canonical titin sequence (UniProtKB identifier Q8WZ42-1), main splicing pathways (green lines), and binding sites of known titin ligands. Domain numbers in blue refer to UniProtKB entry Q8WZ42-1, black numbers in parentheses to Ref. 11. Bin1 indicates bridging integrator-1; CMYA5, cardiomyopathy-associated protein-5; Ex, exon in genomic human titin sequence; FHL1 and 2, four-and-a-half-LIM-domain protein-1 and -2; FNIII, fibronectin type III–like domain; HSP27, heat shock protein-27; HSP90, heat shock protein-90; Ig, immunoglobulin-like domain; MARPs, muscle ankyrin repeat proteins; MURF1/2, muscle-specific RING-finger protein-1/-2; MyBP-C, myosin-binding protein-C; Nbr1, neighbor of BRCA1 gene-1; P, titin phosphosite (kinase known); PEVK, titin region rich in proline, glutamate, valine, and lysine; sANK-1, small-ankyrin-1 isoform; Smyd2, SET and MYND domain–containing protein-2; and TK, titin kinase domain.

isoforms such as Novex-1, Novex-2, and Novex-3 (625-700 kDA)[21,22,24].

The N2B, N2BA, and N2A isoforms have differential spring compositions that define titin's passive tension[24,25]. Titin's elastic spring domain also functions as a bidirectional spring that accounts for the majority of restoring force after systole[22,25,26]. Within the left ventricle, the N2BA/N2B titin isoform expression ratio in humans is 30%/60% verses 20%/80% in rodents[22,27]. The N2BA/N2B ratio varies across the area of the heart. The N2BA/N2B ratios are higher in the right side of the heart and the atria when compared to the left side of the heart and the ventricles[28]. The following section will break down the 4 main sarcomere domains of titin.

1.3a Z-line titin

Titin is the only continuous myofilament in the sarcomere with overlapping N-terminal and C-terminal domains at the Z-line and M-band. The Z-line portion of human titin is integrated into the sarcomere Z-line and is composed of 9 (Ig1-9) domains coalesced with unique sequences and 45 amino acid residue repeats (Z-repeats)[22]. Two titin molecules from the same half-sarcomere are crosslinked to telethonin in an antiparallel manner via their Ig2 domains forming a stable titin/telethonin complex that functions to orient the N-terminal domain of titin into the Z-line[29,30]. The titin/telethonin complex also functions as a hub for proteasomal signaling as telethonin interacts with E3 ubiquitin ligase, mouse-double-minute-2-homolog[30]. Promoting Z-line structural integrity, alpha-actinin dimers crosslink titin from opposite half-sarcomeres in an antiparallel fashion via their C-terminal domain to the titin Z-repeats[31]. Alpha-actin dimers also crosslink to actin filaments through their actin binding domains[29]. Although the individual titin/alpha-actinin interaction are relatively weak, it is summation of multiple titin/alpha-actin interactions in the z-repeats that promote Z-line stability[31]. The final Z-line titin Ig9 domain and

peripheral Z-line edge Ig10 domain bind to the actin filament system[32]. Together, the Z-line is an integrated and complex protein network that requires the movement of many molecules in order to orientate and stabilize titin.

1.3b I-band titin

Titin accounts for 90% of passive tension under physiological sarcomere lengths (1.9-2.2 microns) whereas collagen accounts for the majority of passive tension beyond physiological sarcomere lengths[33]. This elastic I-band titin region stems from the spring domain which is composed of 3 extensible tandem Ig elements, the proximal-Ig (Ig10-20), middle-Ig (Ig24-76, nomenclature off due to alternative splicing), and distal-Ig (Ig80-95)[22]. The I-band portion of titin also contains 2 unique extensible sequences, the N2-B element and a unique series of 26-28 repeating domains rich in proline, glutamate, valine and lysine known as PEVK domains[34]. The N2B titin isoform is generated from the splicing of exon 49/50 (Ig27) to exon 219 (Ig84). The cardiac N2BA and skeletal N2A titin isoforms also contain an N-2A element as well additional PEVK domains due to the inclusion of alternative exons between exons 49 through 119 however N2A titin almost always excludes the N2B exon 50[22,34,35]. The fetal cardiac titin isoform is larger than the N2B and N2BA titin isoforms due to the retention of alternately spliced exons within the spring domain and progressively become shorter throughout developement[25,35]. Titin splicing is important for cardiac function as heterozygous mutations in a 5 amino acid hotspot in exon 9 of RNA Binding Motif Protein 20 (RBM20), a cardiac splicing protein, is known to cause dilated cardiomyopathy (DCM)[36,37]. Mutations in the RBM20 RS-domain, critical for protein-protein interactions, lead to largest isoform of titin ever discovered (N2BA-Giant, ~4.0 mDa) which is primarily due the retention and expression of alternative exons in the spring domain of titin[36].

The I-band of titin is thought of as a 3 part entropic spring. During stretch, the tandem Ig domains first unfold followed by the PEVK domain and the N2B domain leading to an increase in passive tension[38]. The expression of titin isoforms play an important role in the tuning cardiomyocyte stiffness as the majority of titin passive tension derives from the extensibility of the PEVK domains such that longer N2BA molecules are more compliant than the stiffer N2B isoforms[34]. The spring domains of titin are important for cardiomyocyte function as mouse knockout of studies of the tandem Ig, N2B, and PEVK domains all result in diastolic dysfunction with increased titin stiffness[39-41]. Together the titin isoforms work together to set myocardial passive tension. In some end stage heart failure cases, the N2BA/N2B ratio increases and is thought to be compensatory response to volume overload[22]. Apart from general isoform switching to augment tension, post-translational modifications either through direct phosphorylation, disulfide bonding or S-glutathionylation have been shown to fine-tune the titin tension[22]. Phosphorylation via PKA, PKG, and CaMKII have been shown to decrease titin tension whereas PKCα increases titin tension[22]. So far, only ~20 phosphosites have been identified with many more to be elucidated nevertheless, phosphorylation of titin in a pathological setting remains an active area of research. Aside from post-translational modification, free calcium binding to the PEVK domain has been demonstrated to increase titin stiffness[42]. Overall, cardiomyocyte stiffness is a combination of titin isoform expression and spring domain modulation.

Aside from elasticity, the spring domain of titin also functions as signaling hub for proteins involved in contraction, energy homeostasis, protein quality control and mechanosensing, The thin filament system binds to titin at two major sites, one at the Z-line/I-

band junction and the other at the PEVK domain therefore bridging together the two myofilament systems[32,43].

The N2B domain of titin is a major signaling network as it directly binds to the four and a half LIM domain proteins (FHL1 and FHL2), muscle-ankyrin repeat proteins (MARPS) heat shock protein 27 (HSP27), and αβ-crystalin[22]. The N2A domain of titin also binds to MARPs as well as HSP90[22]. The FHL2/FHL1 protein complexes signal via the mitogen-activated protein kinase pathway (MAPK) to promote cardiac hypertrophy upon biochemical stress[44,45]. Knockout of the N2B domain confirms the role of FHL2 in regulating cardiac growth as the mice exhibit cardiac atrophy[39]. Within the MARP family, ANKD1/ERK/GATA4 signaling complex can translocate from the N2A domain of titin to the nucleus in order to activate cardiac gene expression to promote pathological growth[46]. Together these studies support the role of titin as a biomechanical sensor. Aside from signaling, the titin spring domain is a dynamic region that is continually undergoing mechanical stress; the chaperones αβ-crystalin HSP27 and HSP90 have been demonstrated to protect regions of I-band titin during stretch[22].

1.3c A-band titin

The A-band portion of titin mainly functions as a molecular ruler for the assembly and organization of the thick filaments[5]. The entire A-band region of titin is a rigid structure composed of Ig and FNIII domains that are arranged into two types of super-repeats, a 6x, 7 domain (Ig97-Ig108/FNIII12-FNIII41) and an 11x, 11 domain (Ig109-Ig139/FNIII42-FNIII129)[22]. The super-repeats together with additional Ig and FNIII domains account for the largest portion of titin's size (~2.1 mDa)[5]. The titin A-band FNIII domains interact with myosin heavy chain; specifically six titin molecules interact with the myosin filaments (~294 filaments)

per half-sarcomere[24,47]. The first Ig domains of the 11 domain super-repeat interact with myosin binding protein c which in turn connects titin to myosin heavy chain[48].

1.3d M-band titin

The M-band functions as a structural component of the sarcomere where overlapping thick filaments are centered[49]. The terminal titin exons 258-363 (Ig domains Ig143-152; also known as M1-10) define the M-band region of titin are dispensable for sarcomere formation but absolutely required for sarcomere integrity and maintenance[50,51]. Although the exact structure of the M-band remains to be elucidated, the current accepted model is a stable ternary network of the titin, obscurin, obscurin-like-1 (obscurin homolog) and myomesin filaments[52,53]. The C-terminal domains of myomesin form antiparallel homodimers where their N-terminal domains crosslink opposing myosin filaments together. Within the myomesin molecule, the linker fibronectin domains (My4-6) interact with titin's Ig M4 domain therefore connecting opposing titin molecules from each half-sarcomere promoting stability[54]. Obscurin or obscurin-like-1 attaches to both titin and myomesin creating a stable ternary structure[29].

Although the M-band appears static, the M-band portion of titin is major signalosome regarding protein quality control. Titin exon 358 and 359 encode a serine-threonine kinase domain and its kinase activity is regulated in a two-step mechanism via mechanical strain[55,56]. Mechanical strain opens the ATP binding site on the titin kinase domain by moving a C-terminal regulatory tail, allowing for ATP to bind[55]. Once ATP is bound, autophosphorylation of the an inhibitory tyrosine-170 residue allows for full activation of the kinase[55]. Although direct titin kinase targets have yet the be identified, it is an important domain as deletion results in heart failure and mutations in the titin kinase domain result in autosomal dominant heredity myopathy

with early respiratory failure[50,57]. The kinase domain of titin is involved in controlling muscle gene expression as it serves as hub for the strain sensing Nbr1/p62/MuRF2 complex. Upon mechanical strain, the E3 ubiquitin ligase, MuRF2, in turn translocates to the nucleus to target serum response factor (transcription factor) for degradation in order to reduce muscle gene expression[50]. Adjacent to the kinase domain is a binding site for MuRF1[58,59]. MurR1 is the primary E3 ligase in the heart and has been demonstrated to directly ubiquitylate cardiac troponin I and myosin heavy chain thus promoting their degradation[58]. Whether titin is a substrate of MuRF1 remains to be determined[60]. Calcium dependent protease Calpain-3 binds to titin and serves to regulate sarcomere proteolysis[61]. Titin also binds FHL2 at the M-band, which in turn recruits metabolic enzymes to the M-band[45]. In summary, 152 Ig and 132 FNIII along with unique domains constitute titin[22]. Each region of titin plays an important role scaffolding, signaling, and function; therefore it is not surprising that perturbations in the titin gene would result in cardiovascular and skeletal muscle disease.

1.4 Clinical significance: Titin and cardiovascular disease

In the United States, heart failure is projected to increase by 46% from 2012-2030 thus affecting over 8 million Americans adults[62]. Cardiomyopathies are the leading cause of congestive heart failure after coronary artery disease[63]. Non-ischemic dilated cardiomyopathy (DCM, a subset of cardiomyopathy) affects 1 in 250 individuals and is characterized by dilation in one or both ventricles and is accompanied with progressive systolic dysfunction[63,64]. With respect to myopathies, titin is considered to be major disease gene as ~133 mutations in titin have been described giving rise to DCM but also hypertrophic cardiomyopathy, arrhythmogenic right ventricular cardiomyopathy, and skeletal myopathy (Fig. 3)[22]. In a landmark study, Herman

et al reported that ~25% of idiopathic dilated cardiomyopathies are caused by titin truncating variants (TTNtvs) in the titin gene, making it the most commonly known genetic contributor to DCM (Fig. 3)[65]. Using whole exome sequencing, Herman et al identified 25 nonsense, 23 frameshift, and 23 splicing mutations in the titin transcripts which are predicted to result in a truncated titin protein[65]. Although they found no differences in gross muscle morphology, the group did not investigate whether the truncated mutations affected sarcomere ultrastructure, function, and stability. Their reporting of the widespread prevalence of TTNtvs moved the field into an active area of research as independent groups began to investigate the pathophysiology of DCM via TTNtvs. Clinically, TTNtv-positive DCM patients present with lower ejection fractions and thinner left ventricular walls than DCM positive TTNtv-negative patients[64]. Interestingly, there is a difference in the composite endpoint LV assist device implant, cardiac transplant and all cause mortality as TTNtv-positive patients reach these endpoints sooner thus highlighting its clinical significance[64]. The TTNtvs are predominantly located in the titin A-band in DCM patients with mutations distributed throughout the entire length of titin (Fig. 3)[65]. The observation that distal A-band truncations were more pathogenic than proximal I-band truncations suggests a dominant-negative mechanism, whereby titins with distal A-band truncations are more likely to incorporate into the sarcomere and interfere with wild-type titin protein function. I-band truncations are believed to be more tolerated due to the extensive alternative splicing in the titin I-band[64]. Regardless, it has been difficult to detect even low amounts of truncated TTN proteins in DCM tissue samples[64,66,67]. Currently, the prevailing hypothesis is that titin truncating variants cause disease through haploinsufficiency; however, convincing evidence is needed to support this claim as there have been no observable reduction in total titin protein levels in TTNtv-positive DCM tissue[64,67].

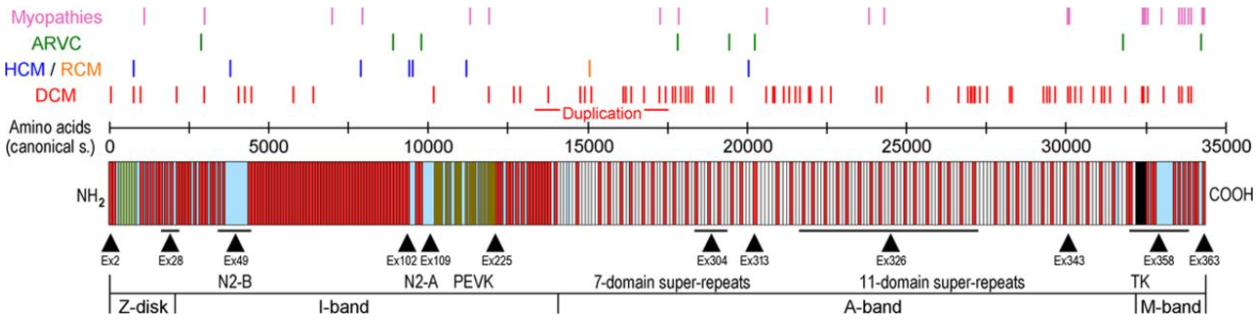

Figure 3 Titin mutations identified in human heart and skeletal muscle disease. Titin-domain arrangement and positions of mutations according to the canonical titin sequence (UniProtKB entry Q8WZ42-1). An annotated list of these mutations (current as of December 2013) is provided in Online Table I. ARVC indicates arrhythmogenic right ventricular cardiomyopathy; DCM, dilated cardiomyopathy; HCM, hypertrophic cardiomyopathy; PEVK, titin region rich in proline, glutamate, valine, and lysine; RCM, restrictive cardiomyopathy; and TK, titin kinase domain. Reprinted from Wolfgang A. Linke, Nazha Hamdani, Gigantic Business Titin Properties and Function Through Thick and Thin, Circulation Research, Volume 114, Issue 6, pg 1052-1068, http://circres.ahajournals.org/content/114/6/1052 , Copyright 2014, License number 4067130110862, with permission from Wolters Kluwer Health, Inc.

The general consensus of whether TTNtv cause DCM via haploinsufficiency or a dominant negative mechanism has been a controversial area of research.

Recent attempts at demonstrating if TTNtv-DCM occur via a dominant negative mechanism have remained inconclusive. In one clinical case, a 2-bp insertion (c.43628insAT) in exon 226 was found to be a cause of DCM in humans[68]. Given the invasiveness of a cardiac biopsy, a skeletal muscle biopsy was taken instead and the truncated titin was identfied[68]. Gramlich et al tried to recapitulate the DCM phenotype by generating an A-band truncation mouse model via 2-bp knock-in mutation at exon 326[66]. The homozygous mutant mice exhibited defects in sarcomerogenesis during development and consequently died before embryonic day 9.5[66]. Heterozygous mice were viable with normal cardiac morphology and function; however, when chronically stressed with angiotensin or isoproterenol these mice developed a severe DCM phenotype when compared to control[66]. Gramlich et al could only detect low levels of truncated titin, less than 1% of total titin levels, with no observable reduction of total titin protein between wild-type and heterozygous AT knock-in mice. Even in our I-band (exon 190) patient TTNtv DCM tissue, we were unable to detect a truncated titin protein (Fig. 4).

In support of the haploinsufficiency hypothesis, Hinson et al used human induced pluripotent stem cell derived cardiomyocytes (hiPSC-CMs) from patients with a TTNtv to recapitulate the DCM phenotype and demonstrated reduced contractile performance and general sarcomere disorganization[67]. Although they found the presence of the truncated titin protein in some A-band TTNtv hiPSC-CM lines, there was discrepancy due to the little to no protein expression in human clinical biopsies. Regardless, they concluded that TTNtv DCM was caused by titin haploinsufficiency even though wild-type titin levels were not different between control and TTNtv samples. Hinson et al postulated that the truncated titin was rapidly turned over and

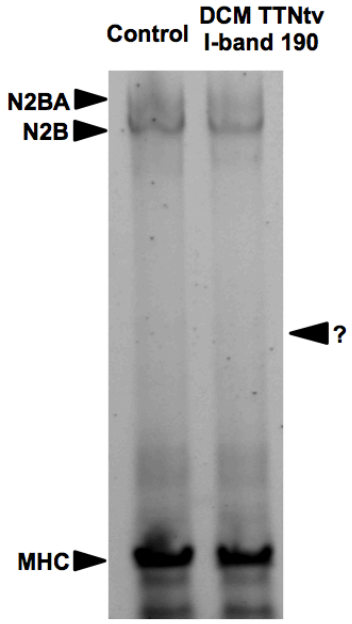

Figure 4. Truncated titin is not detected in TTNtv exon 190 DCM patient sample. Control and DCM TTNtv lysates were ran on a 1% vertical agarose gel. Total protein was detected via SYPRO Ruby. N2BA, N2B denote titin isoforms, MHC denotes myosin heavy chain.

stated that titin haploinsufficiency resulted in sarcomere insufficiency which progressed to DCM[67].

Adding to the complexity of TTNtv biology, 1% of the general population have a TTNtv without the presentation of DCM[65,69]. How the heart can tolerate these truncations remain to be elucidated; nevertheless, the general population with TTNvs are at a greater risk of adverse cardiac events[69]. Therefore, it is important that the field understands the pathophysiological developments of TTNtvs in DCM. However, before the field can make strides in understanding these molecular events mediating TTNtv in DCM, research is needed in the overall understanding of sarcomere maintenance regarding the synthesis, incorporation and removal of titin molecules as well as other myofilament proteins in the macromolecular structure of the sarcomere.

1.5 Sarcomere maintenance

On average, the heart will beat over 2.5 billion times in one's lifetime[70]. This mechanical feat is accomplished by the actin-myosin power stroke in the sarcomeres of cardiomyocytes. Nevertheless, in order to maintain functional sarcomeres, there must be an active balance of *de novo* synthesis and incorporation proteins into the sarcomere coupled to the removal and degradation of old/damaged proteins. The clear mechanism as to how these molecules are incorporated and removed from the sarcomere in active terminally differentiated cardiomyocytes remains poorly understood.

In the 1940s, electron microscopy provided one of the first clear images that illustrated the complex crystalline architecture of the sarcomere[71]. Given such higher order of structure, the field generally believed the sarcomere was a static structure whereby its only function was to

produce force[72]. In the 1980's, radioisotope labeling provided early insight in sarcomere protein turnover as the protein half-lives of myosin heavy chain (5.4 days), actin (10 days), troponin T (3.5 days), troponin I (3.2 days), troponin C (5.3 days) have been estimated in the adult rat heart[73,74]. These long proteins half-lives and the crystalline sarcomere structure supported the hypothesis that the sarcomere was a static structure with proteins turning over at their respective rates.

Investigators interested in myofibrillogenesis clearly showed that the assembly of sarcomeres was a dynamic process thus challenging the view of the sarcomere. Sanger et al microinjected rhodamine-tagged alpha-actinins into cultured embryonic chick cardiomyotes and observed rapid reincorporation at both the peripheral side of the cell (*de novo* sarcomerogenesis) and pre-existing sarcomeres[75,76]. Although the embryonic cardiomyocyte model provided insight into sarcomere protein incorporation, there are fundamental differences between neonatal/embryonic cardiomyocytes versus adult cardiomyocytes such as their sarcomere organization and ultrastructure[77]. Opting for a more representative model, Sanger's group confirmed rapid (within minutes) incorporation of rhodamine-tagged alpha-actinins in pre-existing sarcomeres in adult rat cardiomyocytes[78]. These experiments laid the foundation for more quantitative assessments of sarcomere protein incorporation and exchange as investigators began performing fluorescence recovery after photobleaching (FRAP) in live cardiomyocytes.

1.6 Modeling incorporation of sarcomeric proteins

The discovery of green fluorescent protein (GFP) from *Aequorea victoria* revolutionized microscopy as this protein could be used as a live cell reporter to distinctly map protein localization in real-time[79,80]. An innovative technology, FRAP, emerged in the 1970's as a

valuable assay to directly quantify protein dynamics in living cells. FRAP didn't gain full traction in the field until the 1990's as it required specialized instrumentation[80,81]. Moreover, it was the combination of tagging proteins with GFP and performing FRAP that allowed for the ability to assay direct protein dynamics.

In FRAP, a region of interest (ROI) within a live cell expressing a protein of interest fused to a fluorescent reporter is photoablated. The dark photobleached ROI represents the area where the fluorescently tagged molecules were once fluorescent are now in an irreversible dark state[80,82]. Due to the diffusion of the fluorescent molecules from the non-bleached area, the photobleached area begins to recover over time.[80] If the recovering pixel intensity of the ROI is plotted as a function over time, a FRAP curve can be extrapolated which allows investigators to empirically quantify two important parameters about the fluorescent protein of interest 1) the total mobile fraction of fluorescent proteins, 2) the rate of fluorescent protein mobility[80]. Figure 5 illustrates a hypothetical FRAP curve where fluorescence intensities of region of interest (ROI) are acquired over time prior to photobleaching (pre-bleach, F_i), immediately after bleaching (F_0), and recovery ($F\infty$). The recovery phase is dictated by fluorescence recovery until a steady state is reached ($F\infty$). F_i, F_0, and $F\infty$ can be used to extrapolate a mobile fraction (mf) via the equation below:

$$mf = \frac{F\infty - F_0}{F_i - F_0}$$

The immobile fraction can be calculated by subtracting 1- mf. FRAP also provides information on the rate of recovery of said fluorescent protein of interest where the fluorescent intensities of the ROI is normalized and often fitted into a one phase associated equation in which an exchange half-life be extrapolated.

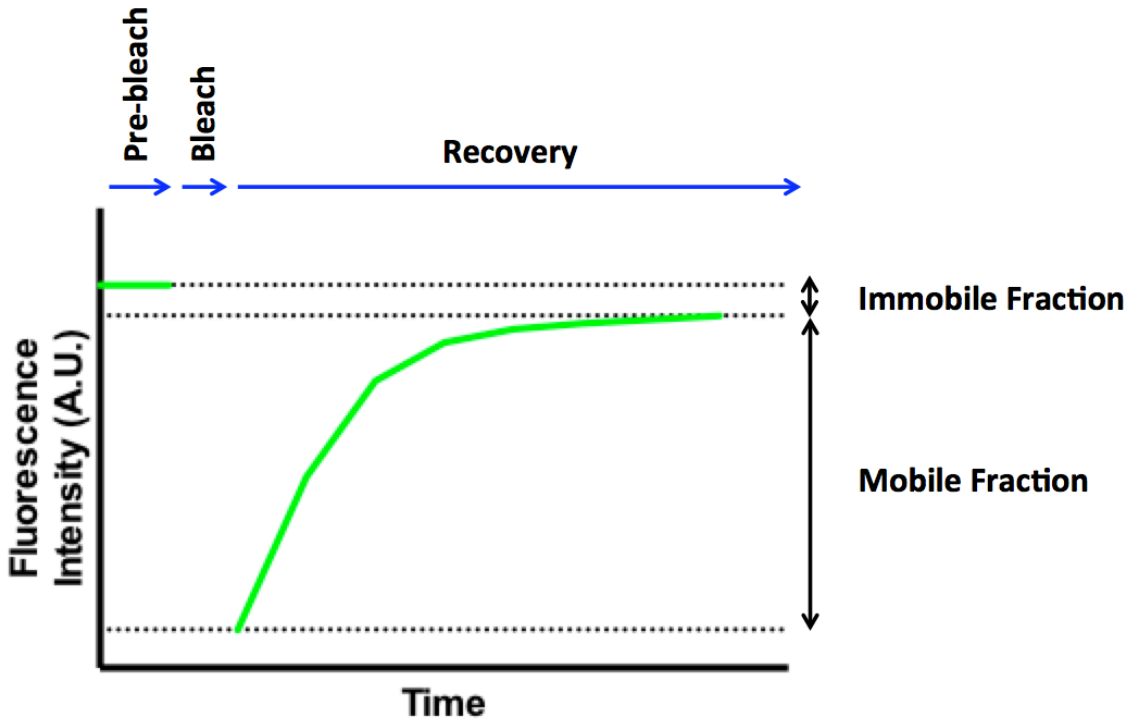

Figure 5. Hypothetical FRAP curve. The green line shows the plotted fluorescent intensity of a protein of interest during a FRAP assay. There is a baseline fluorescence established during the pre-bleach phase followed by significant drop fluorescent intensity to ~zero during the transition from the pre-bleach to bleach phase. Over time, the fluorescence intensity begins to recover during the recovery phase until the curve reaches a steady state.

Specifically in the heart, FRAP has allowed investigators to examine the dynamic state of the sarcomere in real-time. In neonatal ventricular myocytes, α-actin and β-actin have exchange half-lives 1 minute and 30 minutes[83] whereas β-myosin heavy chain has an exchange half-life of 32 minutes in adult rat cardiomyocytes[84]. Cardiac troponin T and C have similar exchange half-lives of approximately 20 minutes in mouse embryonic cardiomyocytes[85]. Collectively, these observations suggest that sarcomere protein components may in fact recycle among myofibrils either through a pool of sarcomeric (bound) and nonsarcomeric (unbound) molecules. This is particularly germane to titin given its role in the sarcomere.

1.7 Titin turnover

Titin is essential for sarcomere assembly and for maintaining the contractile integrity of mature sarcomeres as both knockdown and knockout of titin in cell models fail to develop and or maintain sarcomeres[86,87]. Furthermore, impaired thick filament assembly and organization is observed in the titin knockout cell (BHK-21-Bi) line thus demonstrating titin's crucial role as a molecular scaffold for sarcomere assembly[86]. With respect to sarcomereogenesis, titin plays a key role in assembly via its N-terminal domain anchoring alpha-actinin to the Z-bodies which together with actin filaments form IZI bodies[88]. These IZI bodies are ~1μM apart; mature Z-lines are ~2μM suggesting an important role for the C-terminal end of titin at the A-band and M-line in the assembly, spacing and incorporation of the thick filaments at the A-band[88]. Titin is the only continuous myofilament system in the sarcomere suggesting its importance as a molecular ruler. The majority of studies on titin have focused on developmental, structural and mechanical roles in the sarcomere; however, the mechanisms regulating titin turnover in the mature cardiac sarcomere are currently unknown. Given the observable *in situ* sarcomere protein exchange rates,

are all the myofilament proteins (i.e., actin, alpha-actin, myosin heavy chain) that readily detachable? Could the same be true with regards to titin?

Early insight into titin turnover stemmed from da Silva Lopes et al's titin-eGFP knockin mouse model where eGFP was inserted at titin's terminal exon creating a titin-eGFP fusion protein. Da Silva Lopes et al used FRAP to study titin eGFP mobility *in situ* via using isolated neonatal titin-eGFP cardiomyocytes[89]. They reported a fluorescence exchange half-life of ~2.5 hours which was unexpected given that the molecular half-life of titin is 72 hours by pulse-chase experiments[90]. To determine if *de novo* synthesis accounted for titin-eGFP recovery, da Silva Lopes et al treated titin-eGFP cells with a protein translational inhibitor, cylcoheximide, prior to and during FRAP and reported no change in titin-eGFP mobility suggesting that pre-existing titin accounted for the majority of recovery. Da Silva Lopes et al also demonstrated that titin-eGFP recovered in similar mobile fractions in regions where sarcomeres were bleached longitudinally (down the myofibril) and laterally (across multiple myofibrils) thus saying that titin recovery occurs uniformly throughout the myofibrils. Although mechanical arrest did not affect titin recovery, high calcium conditions significantly limited titin exchange.

These findings laid the paradigm that the sarcomere was a dynamic structure undergoing rapid exchange (recycling) between a pool of sarcomeric (bound) and nonsarcomeric (unbound) titin molecules (Fig. 6). Given the direct live cell imaging evidence, it became easy for investigators to adopt this new hypothesis. This seminal paper laid the groundwork for this dissertation, as the original goal was to develop human version of the titin-eGFP mouse model in order to elucidate the molecular mechanisms governing sarcomere turnover with respect to titin as well as identify novel regulators involved in titin trafficking.

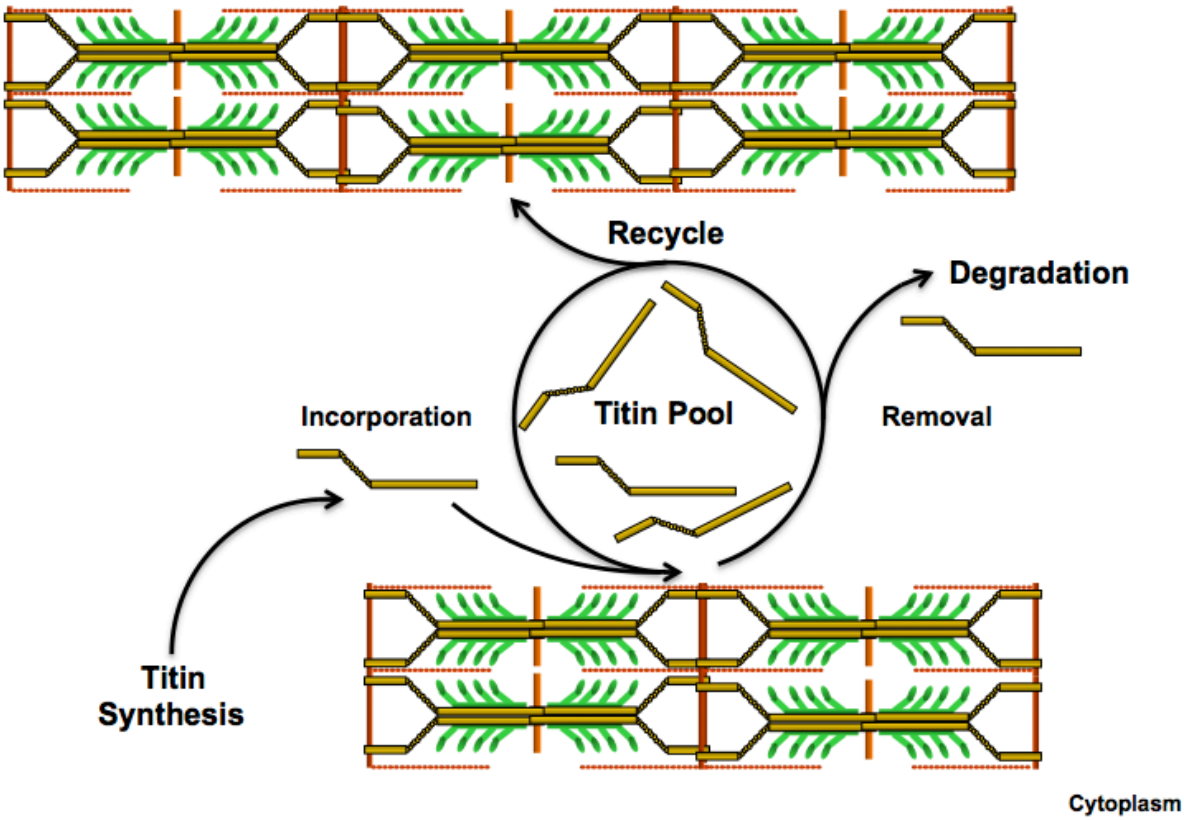

Figure 6. Titin life cycle prior to dissertation. Newly translated titin protein is incorporated into sarcomere. Over time, titin is removed from the sarcomere and either reincorporated into another sarcomere or sent for degradation. The mechanism as to how titin is transported is unknown. Titin turnover occurs once titin is removed from sarcomere and sent for degradation.

1.8 Human induced pluripotent stems to model cardiovascular biology

Cardiovascular disease is the leading cause of mortality worldwide[91]. Ergo, there is an urgent need for appropriate model systems to investigate the disease pathophysiology as well as understand the basic cardiovascular biology.

In 1981, the first embryonic stem cells (ES) were isolated and cultured from the inner cell mass of mouse blastocyte cavity[92,93]. These ES cells had ability to self renew without spontaneous differentiation, nevertheless, the ES had the remarkable ability to differentiate into all three germ layers: endoderm, mesoderm and ectoderm, which raised promise in the field of regenerative medicine research[92]. In 1998, this feat was later replicated as the first human ES cell lines were generated from early human embryos[94]. However, this accomplishment and subsequent research raised significant ethical concerns and controversy ultimately resulting in restricted federal support which impacted the field[95].

In 2006, the reprograming of adult somatic cells into induced pluripotent stem cells (iPSCs) revolutionized biomedical research[96]. Yamanaka first generated iPSCs from mouse embryonic cells and adult mouse fibroblasts as well as adult human dermal fibroblasts via the transfection of 4 essential transcription factors: Oct3/4, Sox2, Klf4, and c-Myc[96,97]. These reprogramed cells had recapitulated many key features of ES thus circumventing ES controversy and revolutionizing their adaptation for biological research.

Recent advances in human induced pluripotent stem cell (hiPSC) biology have led to reliable and efficient methods of differentiating hiPSCs into hiPSC-cardiomyoctytes (hiPSC-CM) for research and disease modeling[67,98,99]. Therefore, they are increasingly being valued as a useful model and surrogate for human cardiomyocyte studies[98,100,101]. Initially, the majority of physiological readouts using hiPSC-CMs have focused on electrophysiology and calcium

handling measurements since they were the easiest to assess since methods of functional evaluation were difficult to perform. Assessment of single cell contractility, cell shortening, has been limited due to the lack of cell shortening due to the aberrant spherical morphology of hiPSC-CMs cultured on standard substrates. To circumvent this issue, biophysical approaches such as atomic force microscopy, traction force microscopy, and micropost deflection have been employed to assess the contractile forces of single cell hiPSC-CMs [102-104]. Although quantitative, these methods are technically challenging and require specialized lab equipment, which limits their adoptability. Recently, a novel method termed the Matrigel Mattress has emerged which promotes elongation and robust cell shortening of individual cardiomyocytes allowing for quantitative assessment of cell contractility and calcium handling[100]. Collectively, these methods validate the use of hiPSC-CMs to model cardiomyocyte biology.

1.9 CRISPR/CAS9 gene editing

CRISPR/Cas9 gene editing has revolutionized our ability to model human diseases. Briefly, CRISPR/Cas9 takes advantage of the cell's endogenous repair mechanisms to generate site specific insertions/deletions (indels) that can be used for targeted genome editing[105]. Introduction of a guide RNA (gRNA), a fusion of the CRISPR RNA (crRNA) and transactivating CRISPR RNA (tracrRNA), along with Cas9 protein allows for specific target site cutting. The gRNA functions by binding and recruiting the Cas9 nuclease to the target site. The first twenty nucleotides of the crRNA portion of the gRNA is the protospacer portion, which binds to complementary target DNA sequence. In order for site-specific cleavage to occur, the protospacer must be adjacent to the 5' end of the 5'-NGG protospacer adjacent motifs (PAM) sequence. The Cas9 nuclease generates a double stranded break (DSB) 3 nucleotides down the

PAM sequence which can be repaired by nonhomologous end-joining (NHEJ) and or homology directed repair (HDR)[106]. HDR can be utilized to insert exogenous specific DNA sequences though recombination. This technique coupled with hiPSC has the potential to elucidate novel insights in cellular biology.

1.10 Objective

During the average human lifespan, the heart will beat on average over 2.5 billion times[70]. This raises the intriguing question as to how mechanically contracting sarcomeres are able to maintain their precise organizational structure while requiring constant replenishing of worn out and/or damaged proteins. At ~3-3.8 mDa, titin is the largest known protein and given its massive size, several questions related to its synthesis emerge. What are the mechanisms regulating titin gene expression? Where is titin synthesized, and how is it transported and incorporated into a mechanically contracting cardiomyocyte? Is titin replacement uniform throughout the cardiomyocyte? Does the replacement of titin require partial or complete break down of the myofilaments? Given its ~3 day half-life, why is titin exchange that fast? These questions merge into the overall aim of this dissertation:

To develop a novel human induced pluripotent stem cell-derived cardiomyocyte model in order to further investigate the mechanisms mediating titin exchange and turnover in real-time.

This dissertation will delineate 3 important mechanisms of the regulation of titin in the cardiac sarcomere. The first two studies will address the important contributions of the

untranslated regions (UTRs) in titin post-transcriptional regulation. The first study specifically demonstrates how the 5'-UTR serves as a translational brake in titin synthesis. The second study will elucidate the importance of microRNA 26a and 26b (miR-26a/b) in post-transcriptionally regulating titin gene expression at the 3'-UTR. Finally, the last study will describe the generation of a novel titin hiPSC model via CRISPR/Cas9 editing to directly observe titin incorporation and turnover in sarcomeres of live beating cells in order test and expand on the model put forth by da Silva Lopes et al[89].

Chapter 2

Upstream open reading frame in 5'-untranslated region reduces titin mRNA translational efficiency

2.1 Chapter abstract

Titin is the largest known protein and a critical determinant of myofibril elasticity and sarcomere structure in striated muscle. Accumulating evidence that mRNA transcripts are post-transcriptionally regulated by specific motifs located in the flanking untranslated regions (UTRs) led us to consider the role of titin 5'-UTR in regulating its translational efficiency. Titin 5'-UTR is highly homologues between human, mouse, and rat, and sequence analysis revealed the presence of a stem-loop and two upstream AUG codons (uAUGs) converging on a shared in frame stop codon. We generated a mouse titin 5'-UTR luciferase reporter construct and targeted the stem-loop and each uAUG for mutation. The wild-type and mutated constructs were transfected into the cardiac HL-1 cell line and primary neonatal rat ventricular myocytes (NRVM). SV40 driven 5'-UTR luciferase activity was significantly suppressed by wild-type titin 5'-UTR (~70% in HL-1 cells and ~60% in NRVM). Mutating both uAUGs was found to alleviate titin 5'-UTR suppression, while eliminating the stem-loop had no effect. Treatment with various growth stimuli: pacing, PMA or neuregulin had no effect on titin 5'-UTR luciferase activity. Doxorubicin stress stimuli reduced titin 5'-UTR suppression, while H_2O_2 had no effect. A reported single nucleotide polymorphism (SNP) rs13422986 at position -4 of the uAUG2 was introduced and found to further repress titin 5'-UTR luciferase activity. We conclude that the uAUG motifs in titin 5'-UTR serve as translational repressors in the control of titin gene

expression, and that mutations/SNPs of the uAUGs or doxorubicin stress could alter titin translational efficiency. [1]

2.2 Introduction

The cardiac sarcomere is the basic contractile unit of the heart and is comprised of a large assembly of myofilament proteins that are responsible for force generation. At ~3-3.7mDa, titin (TTN) is the largest and third most abundant myofilament protein in striated muscle[6]. Titin serves as a molecular scaffold for contractile and many other sarcomeric proteins to organize around. Physiologically, titin accounts for the majority of passive tension during diastole and restoring force after systole[6]. The majority of studies on titin have focused on genomic mutations, structural and mechanical roles in the sarcomere; however, the mechanisms regulating titin gene expression are virtually unknown.

Regulation of gene expression is a complex orchestration of events and is controlled at multiple levels including transcription, mRNA processing/decay, and protein translation[107,108]. Even though changes in mRNA transcript levels are commonly extrapolated to reveal functional differences at the protein level, the correlation between mRNA and protein expression is highly variable and this discrepancy may be due to post-transcriptional regulation[109,110]. Indeed, Schwanhäusser et.al. demonstrated in NIH3T3 fibroblasts that only 40% of cell protein levels were determined by mRNA levels and stressed the importance of translational control as the main regulator of protein abundance[111]. Cap-dependent translational initiation occurs when 43S ribosomal complex binds near the 5'-7-methylguanylate cap of the untranslated region (UTR) and scans in a 5' to 3' direction until it recognizes the AUG start codon of the main open reading

[1] Reprinted from Publication title, Volume 453, Issue I /, Adrian G. Cadar, Lin Zhong, Angel Lin, Mauricio O. Valenzuela, Chee C. Lim, Upstream open reading frame in 5′-untranslated region reduces titin mRNA translational efficiency, pages 185-191, Copyright (2014), with permission from Elsevier.

frame (mORF)[112]. Upon recognition, the 60S ribosomal subunit joins and translational elongation occurs until a stop codon is read resulting in termination of translation[112]. It is increasingly being recognized that the 5'-UTR can contain *cis*-regulatory elements such as upstream AUGs (uAUGs), secondary structure, and upstream ORF (uORF) which are thought to repress translational efficiency[107,113]. uORFs are thought to reduce translational efficiency by a process called leaky scanning in which the 43S ribosomal complex either recognizes the uORF and initiates translation or scans past the uORF to the mORF. In the case of translating the uORF, the translating ribosome can either scan through and reinitiate at the mORF or stall which leads to mRNA degradation[107,113,114]. Overall, uORFs reduce translational initiation at the mORF. Calvo et al. reported 50% of human and mouse protein coding genes contain an uORF and further demonstrated that these uORF repress translational activity by 30-80%[114]. Secondary structures such as stem loops have been demonstrated to repress translational efficiency by reducing the 43S ribosomal complex's ability to scan[112]. To examine whether titin is post-transcriptionally regulated by its 5'-UTR, we performed *in silico* analysis of titin 5'-UTR and identified a stem loop and two uORF that were highly conserved between human and mouse. We hypothesized that titin gene expression is post-transcriptionally regulated by *cis*-regulatory elements within its 5'-UTR.

2.3 Materials and methods

All experiments involving animals were approved by the Animal Care and Use Committee at Vanderbilt University Medical Center, and carried out in accordance with the Guide for the Care and Use of Laboratory Animals of the National Institutes of Health.

2.3a Cardiomyocyte isolation and cell culture

Neonatal rat ventricular myocytes (NRVMs) were isolated from hearts of 1-2-day old Sprague-Dawley rat pups (Charles River Laboratory) as previously described[115] and cells were cultured in DMEM low glucose supplemented with 7% FBS. Adult rat ventricular myocytes (ARVMs) were isolated from the hearts of adult male Sprague-Dawley rats (Charles River Laboratory) as previously described.[115] The HL-1 cardiac cell line was kindly provided by Dr. Claycomb and maintained according to instructions (Claycomb, PNAS, 1998). The human embryonic kidney 293 (HEK-293) cell line was purchased from ATTC and cultured in DMEM supplemented with 7% FBS.

2.3b Titin half-life

NRVM were treated with transcriptional inhibitor actinomyocin D (Sigma) or Dimethyl sulfoxide (DMSO, Sigma) vehicle for 1hr, 6hr, 12hr, 24hr and 48hr. Total RNA was isolated using TRIzol® Reagent. RNA was treated using DNA-*free*™ DNA Removal Kit (Life Technologies™). Total RNA was converted into cDNA using High-Capacity cDNA Reverse Transcription Kit (Applied Biosystems). RT-PCR was performed using SsoAdvanced™ Universal SYBR® Green Supermix (Bio-Rad) in a CFX96™ Real-Time PCR Detection System. Primers were designed using Primer3: WWW Software Tool. Primers used for this study rat Ttn, sense 5'-AAGCCAAGAAACAGGAACCA-3' and antisense 5'-TGCAATAGCCTTTCCATCCT-3'; rat 18s RNA, sense 5'-GTGGAGCGATTTGTCTGGTT-3' and antisense 5'-CGCTGAGCCAGTCAGTGTAG-3'. Titin mRNA expression was normalized to 18s RNA. A standard curve was generated to normalized titin mRNA expression to

log[cDNA] of titin. Data was fitted into a nonlinear one phase exponential decay model (PRISM Software) to calculate the mRNA half-life.

2.3c Titin 5'-UTR fluorescence in situ hybridization

Cardiomyocyte mRNA *in situ* hybridization was performed according to the method of Cripe et al.[116] Briefly, adult cardiomyocytes were fixed in a 1:9 formaldehyde/methanol (vol/vol) and hybridized with a digoxigenin labeled 222 nucleotide probe directed against the 5'-UTR of titin or a 265 nucleotide labeled probe against myosin heavy chain mRNA (5565-5830 nucleotides of X15938). The probes were detected using a rhodamine labeled antidigoxigenin conjugate.

2.3d 5' RACE and plasmids

RNA was extracted from c57BL/6 mice cardiac and skeletal muscle tissue using Trizol. The titin 5'-UTR sequence was identified using 5' Rapid Amplification of cDNA Ends kit (Ambion). Gene specific antisense primers used for the 5' RACE study: outer 5'-GCTGACTGAAGTTGGGTGGT-3'; inner 5'- TGGCTCTCAGGGAGTATCGT-3'. The titin 5'-UTR PCR product was cloned into TOPO TA vector and subjected for Sanger sequencing. The 5'-UTR of titin was subcloned downstream of an SV40 promoter and upstream the firefly luciferase gene in a pGL3 reporter (Promega) using HindIII and NcoI restriction sites (New England Biolabs). All mutagenesis were performed using the QuikChange lightening mutagenesis kit (Agilent Technologies). Stem-loop reporter construct was generated by mutating three nucleotides , and loss of the stem loop structure was confirmed by Mfold[117] (Data not

shown). Mutagenesis of uAUG1 and/or uAUG2 was performed by mutating the ATG to AAG**,** rs13422986 SNP reporter construct was generated by mutating the G to A in the 5'-UTR.

2.3e Cell transfection and stimulation

NRVMs were serum starved overnight (1% FBS/DMEM) followed by transient transfection with 200ng of pGL3 control or 5'-UTR pGL3 reporter constructs, along with 100ng of pRL-TK *Renilla* luciferase construct or pRL-null *Renilla* luciferase construct (Promega) via Lipofectamine 2000 delivery (Life Technologies). Following 24 h transfection, NRVM were either electrically paced at 2 Hz, 30V, 10ms using a Ion Optix myopacer, or treated with, neuregulin 20ng/mL, phorbol 12-myristate 13-acetateor (PMA, 200μM), doxorubicin (Doxo,0.5 μM), H_2O_2 50 μM, blebbistatin 3 μM for 24hrs.

2.3f Luciferase reporter assay

Following treatment, cells were harvested and assayed for luciferase activities using a GloMax-Multi Detection system (Promega). The ratio of firefly:*Renilla* luciferase activities was calculated to normalize for differences in cell number and transfection efficiency. Each experiment was run in triplicate and the ratio values were normalized to control to allow for between-experiment comparison.

2.3g Statistical analysis

Data are reported as mean±SD. Where appropriate, results were either analyzed by Student's t-test or ANOVA with a Bonferroni's multiple comparison post hoc test. $P<0.05$ was considered statistically significant.

2.4 Results

2.4a Titin mRNA half-life and localization in cardiomyocytes

To assess the half-life of titin mRNA, NRVM were treated with transcriptional inhibitor actinomyocin D and measured steady state titin mRNA levels at various time points. Fitting the data to a one phase exponential decay model, titin mRNA half-life was estimated at 66hr (Fig. 7A). Subcelluar mRNA targeting provides a mechanism to control gene expression[118]. We used fluorescent *in situ* hybridization (FISH) and observed that titin mRNA was localized to the sarcomere (based on the periodic staining pattern) and in the cytoplasm (Fig 7B, top panels). This striation pattern appeared to be specific for titin mRNA as the mRNA for another myofilament protein, myosin heavy chain, was non-sarcomeric and diffusely distributed (Fig. 7B, bottom left panel). The relatively long half-life of titin mRNA and its sarcomeric localization is presumed to place greater importance on post-transcriptional control as a means of regulating protein expression.

2.4b Identification of mouse titin 5'-UTR

The UTRs of mRNA transcripts are known to regulate protein translation; in this study we specifically investigated the role of titin 5'-UTR on regulating translational efficiency. To identify titin 5'-UTR we performed a 5' RACE and amplified two RACE PCR products from mouse cardiac and skeletal muscle total RNA (Fig. 8A). The expected 508 bp product contained the 223 nt canonical titin 5'-UTR as determined by sanger sequencing. The faint 400 bp product was a PCR artifact in both cardiac and skeletal muscle. The 5'-UTR sequence was

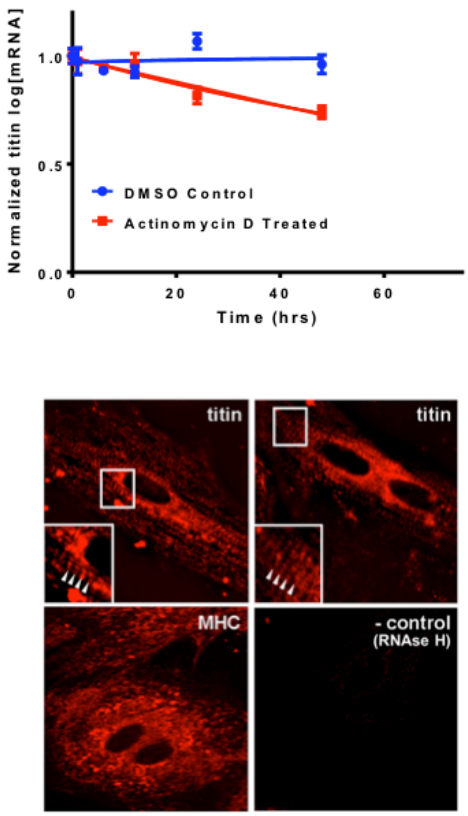

Figure 7. Titin mRNA half-life and subcellular localization in cardiomyocytes. A) NRVM were treated with Actinomyosin D or DMSO control for 0, 1, 6, 12, 24, and 48hrs. Titin gene expression was analyzed by qRT-PCR and normalized to 18S ribosomal RNA. Normalized ct values were normalized to a standard curve of titin gene expression. Data was fitted to a one-phase exponential decay model to calculate titin mRNA half-life. Data is presented as mean ± SEM, (n=3). B) Titin mRNA is localized to the sarcomere and cytoplasm. Top panels: Striated appearance of titin mRNA staining (see arrowheads in inset) characteristic of muscle sarcomeres. Bottom panels: MHC mRNA staining was diffuse with no detectable periodicity. A sample subjected to Rnase treatment served as a negative control.

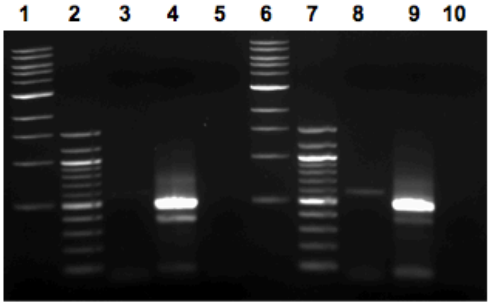

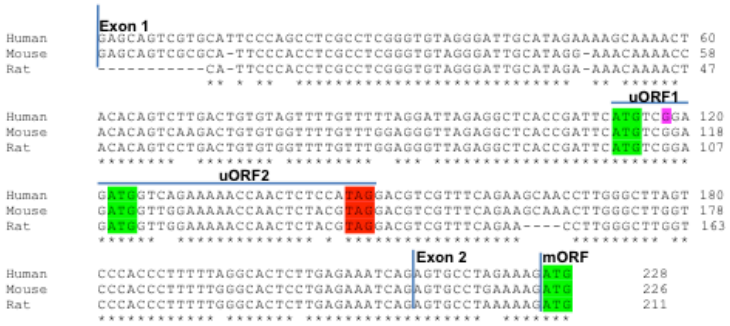

Figure 8. 5' RACE identifies single titin 5' UTR in mouse cardiac and skeletal tissue. A) 5' RACE assay was performed using mouse cardiac and skeletal tissue. 5' RACE assay identifies single expected 514 bp RACE product. Lanes 1 and 6 are 1 kb ladder. Lanes 2 and 7 are 100bp ladder. Lanes 3, 4 and 5 are cardiac outer PCR reaction, cardiac inner PCR reaction and cardiac TAP treated negative control respectfully. Lanes 8, 9 and 10 are skeletal outer PCR reaction, skeletal inner PCR reaction and skeletal TAP treated negative control respectfully. B) Clustal Omega multiple sequence alignment of titin 5'-UTR between human, mouse and rat. Titin 5'-UTR sequence spans from exon 1 to part of exon 2. Human, mouse and rat 5'-UTR sequences are >87% homologous. uAUG1, uAUG2 and the mORF between human, mouse and rat (shown in green) are conserved. The in frame TAG stop codon for uAUG1 and uAUG2 is shown in red. Overline blue depicts the uORF reading frames. SNP rs13422986 is shown in purple.

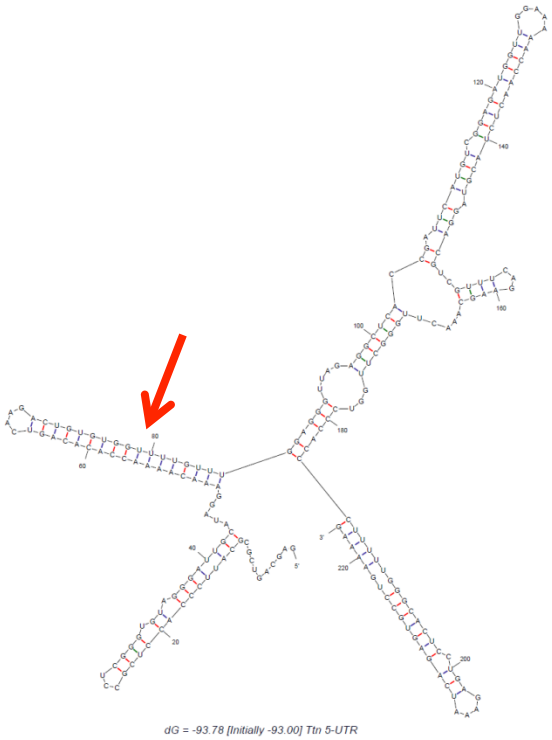

Figure 9. Mfold was used to generate the mRNA structure of titin's 5'-UTR. The red arrow depicts the portion of the stem-loop that was targeted for mutagenesis**.**

entirely consistent with Genebank's mouse annotation, and sequence alignment shows high homology (>87%) between mouse, human and rat (Fig 8B). We performed *in silico* analysis of titin 5-'UTR and were able to identify two uAUGs (uAUG1 and uAUG2) that were both in frame with the same stop codon which we will denote as uORF1 and uORF2. We used the Mfold computer program to predict the secondary structure of the 5'-UTR sequence and were able to identify a highly stable stem loop structure (Fig. 9). Importantly, these motifs were conserved in human, mouse, and rat suggesting regions of greater regulatory importance.

2.3c Characterization of functional cis regulatory elements within mouse titin 5'-UTR

To determine if titin 5'-UTR regulates titin translation, we subcloned the 223 nucleotide 5'-UTR into the pGL3 firefly luciferase reporter vector. The wild-type titin 5'-UTR reporter activity showed significant repression in transiently transfected HL-1 cells (Fig. 10). To determine the functional relevance of the 5'-UTR stem-loop, we mutated 3 sites in the stem-loop that according to Mfold resulted in complete disruption of the stem-loop[117]. Dual luciferase reporter assays in HL-1 cells showed that the mutated stem-loop had no effect on titin 5'-UTR suppression of luciferase activity (Fig.10). To investigate the role of the two uAUGs we mutated each individually (uAUG1 and uAUG2) and in combination (uAUG+uAUG2). The results demonstrated that mutated uAUG1 had no effect, while mutated uAUG2 increased luciferase activity when compared to 5'-UTR reporter activity. Mutated uAUG1+uAUG2 reporter generally restored firefly luciferase activity to pGL3 control reporter levels (Fig. 10). These results were confirmed in NRVM showing that titin 5'-UTR resulted in 57% repression compared to pGL3 control luciferase activity while mutated uAUG1+uAUG2 resulted in near complete de-repression of titin 5'-UTR activity (Fig. 10). Addition of the mouse titin 3'-UTR

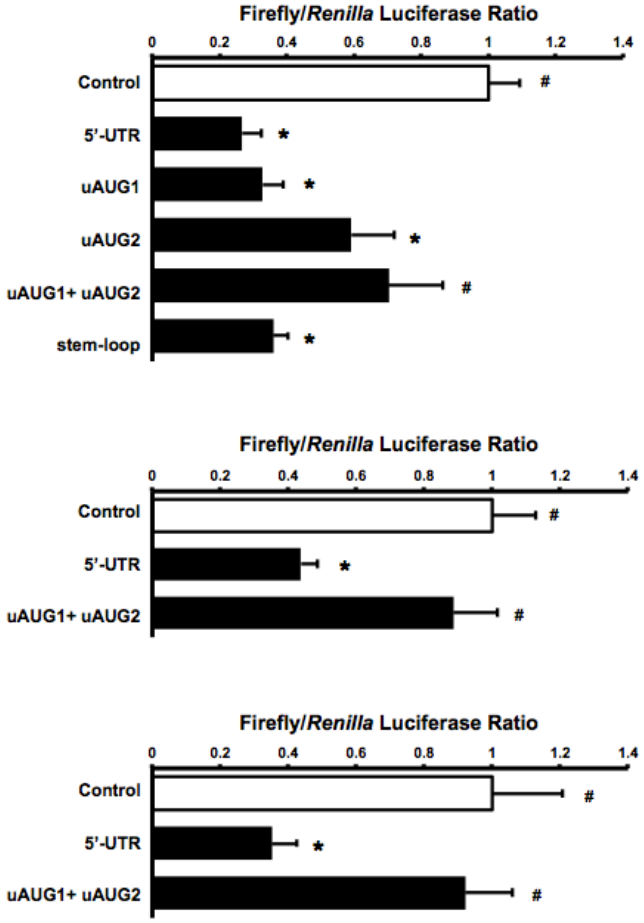

Figure. 10 Titin 5'-UTR suppresses pGL3 reporter activity. A) HL-1 cells were transiently transfected with 100ng RTK and 200ng of either pGL3 control, wild-type Ttn 5'-UTR, or mutant Ttn 5'UTR reporter constructs (uAUG1, uAUG2, uAUG1+ uAUG2, stem-loop). Cells were lysed and assayed for firefly and *Renilla* luciferase activities (n=5-6 for each group). B) NRVM were transfected with pGL3 control, wild-type, or mutant uAUG1+uAUG2 Ttn 5'-UTR reporter construct and assayed for firefly and *Renilla* luciferase activity (n=3-4 for each group). C) HEK 293 cells were transfected with pGL3 control, wild-type 5'-UTR, or mutant uAUG1+uAUG2 Ttn 5'-UTR reporter construct and assayed for firefly and *Renilla* luciferase actvity (n=4-6 for each group). All data displayed as Mean ± SEM, * $p<0.05$ vs. pGL3 control; # $p<0.05$ vs. 5' UTR; groups compared by ANOVA.

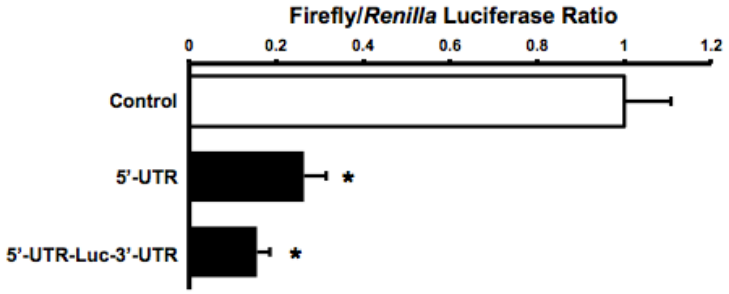

Figure 11. Addition of Titin 3' UTR reduces titin translational efficiency. NRVM were transiently transfected with pGL3 control, 5'-UTR, or combined 5'-UTR-Luc-3'-UTR reporter for 24hrs and cells were lysed and assayed for luciferase activity. Data presented as Mean ± SEM (n=3); *$p<0.05$ vs Control. Groups were compared by ANOVA.

did not significantly reduce luciferase activity in NRVM (Fig. 11), thus we conclude that under basal conditions titin 5'-UTR is the main regulatory component controlling titin translation

To determine if the repressive effect of titin 5'-UTR is cardiac specific, we transfected the titin 5'-UTR reporter plasmids into non-muscle HEK293 cells. Similar to the results observed in cardiac cells, 5'-UTR luciferase activity was significantly suppressed in HEK 293 cells (Fig. 10), and by and large the suppression stems from the uAUGs.

Taken together, these data suggests that the presence of uAUG motifs in titin 5'-UTR results in innate suppression of translational efficiency.

2.4d Titin 5'-UTR stimulation

To test whether cardiac hypertrophic stimuli could enhance titin translational efficiency via 5'-UTR de-repression, we transiently transfected NRVM with the titin 5'-UTR reporter and electrically paced cells at 2 Hz or treated cells with neuregulin 20ng/ml and phorbol 12-myristate 13-acetateor (PMA 200μM). PMA and neuregulin stimulation did not alter titin promoter activity (data not shown), suggesting that these growth stimuli did not alter titin mRNA transcripts. Neither electrical stimulation nor any of the growth factors tested altered titin 5'-UTR luciferase activity (Fig. 12A-C). Since NRVM spontaneously contract in culture we also mechanically arrested NRVM with blebbistatin treatment, but again found no change in titin 5'-UTR luciferase activity. Stress stimuli, such as doxorubicin and oxidative stress enhance overall protein degradation which has been shown to stimulate *de novo* protein synthesis. NRVMs treated with doxorubicin significantly enhanced titin 5'-UTR luciferase activity compared to the untreated controls (Fig. 13A). H_2O_2, on the other hand, had no effect titin 5'-UTR luciferase

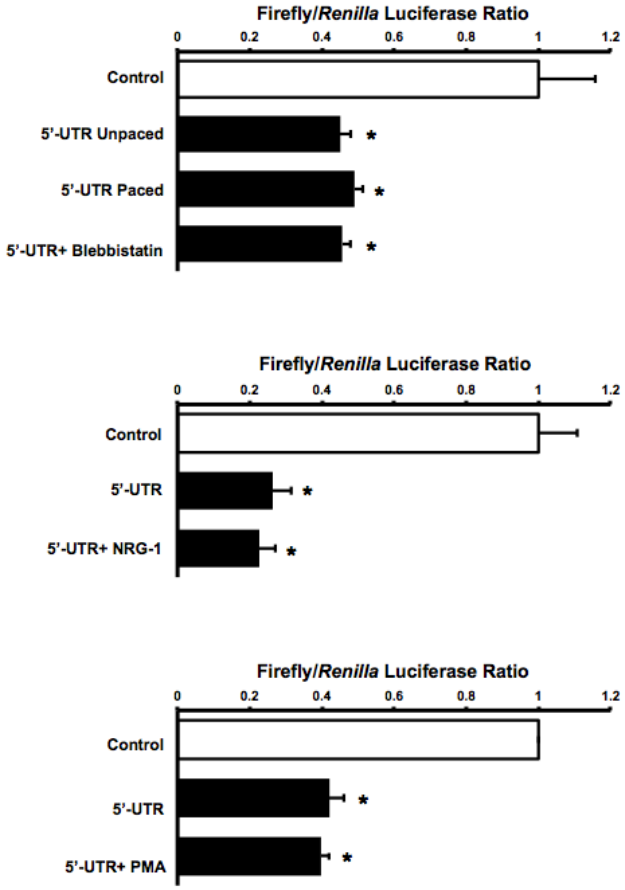

Figure 12. Pacing, blebbistatin, NRG-1 and PMA do not modulate titin translation efficiency. A) NRVM were transiently transfected with pGL3 control or Ttn 5'-UTR for 24 hours. NRVM were either unpaced, paced at 30 V, 2 Hz, 10ms for 24hrs, or treated with 3μM blebbistatin. Cells were lysed and assayed for luciferase activities. Data presented as Mean ± SEM (n=3-4). B) NRVM were transiently transfected with reporter constructs as above and were either treated with vehicle or 20ng/mL NRG-1 for 24 hours, and cells lysed and assayed for luciferase activity. Data presented as Mean ± SEM, (n=3). C) NRVM were transiently transfected with reporter constructs as above and were treated with vehicle or 200μM PMA, and cells lysed and assayed for luciferase activity. Data presented as Mean ± SEM, (n=3). * $p<0.05$ vs control, groups were analyzed by ANOVA.

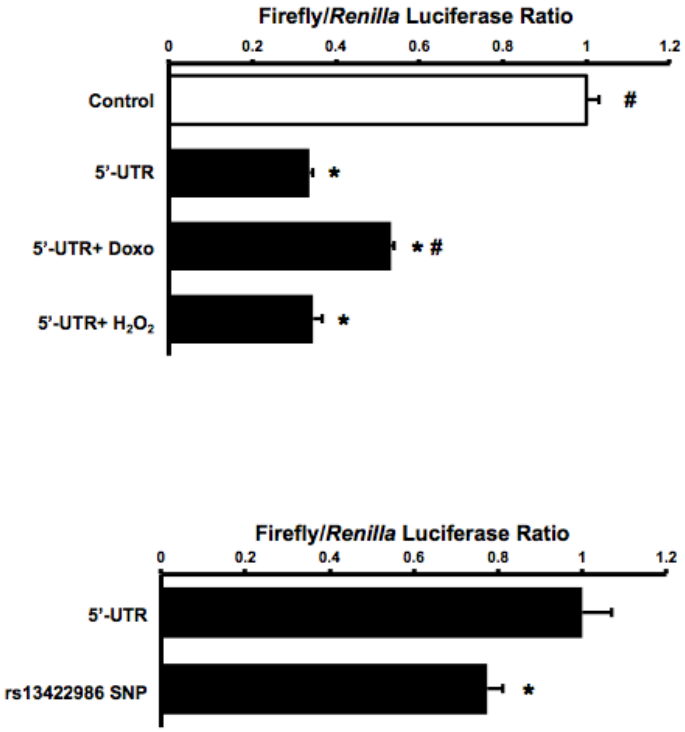

Figure 13. Regulation of titin translational efficiency. A) NRVM were transiently transfected with 100ng RTK and 200ng pGL3 Control or Ttn 5' UTR via lipofectamine delivery for 24 hours. NRVM were either treated with vehicle, 0.5µM of doxorubicin or 50µM H_2O_2 for 24hrs. Cells were lysed and assayed for luciferase activities (n=3). B) NRVM were transiently transfected with 100ng RTK and 200ng Ttn 5'-UTR or mutated rs13422986 5'-UTR for 24hrs. Cells were lysed and assayed for luciferase activities (n=4). All data presented as Mean ± SEM, *p<0.05 vs 5'-UTR. Groups were analyzed by ANOVA or student's t-test.

activity. These data suggest that growth stimuli do not, but stress stimuli such as doxorubicin could modulate titin translational efficiency via its 5'-UTR.

2.3e SNPs in titin 5'-UTR

We scanned the NIH SNP database and found several SNPs throughout the 5'-UTR titin; however, none modulated the generation or loss of uORF. We did find a SNP in the -4 position of uAUG2 Kozak sequence that may alter translation initiation efficiency of the uAUG2. Strong Kozak sequences contain conserved -3 and +4 sites (underlined) of the GCCA/GCC**AUG**G which promotes efficient 43S ribomosomal complex recognition [119,120]. Given that uAUG2 most likely accounts for the suppression of titin 5'-UTR translational efficiency, we hypothesized that SNP at the -4 position of uAUG2 could alter titin reporter function. We generated the SNP 5'-UTR reporter and were able to show that the rs13422986 SNP significantly decreased titin 5'-UTR luciferase activity by 17% in NRVM (Fig. 13B).

2.5 Discussion

Titin is the largest known protein (~3-3.7 mDa) and presumably the costliest to synthesize. In this report, we found that titin mRNA is localized at the sarcomere and has a relatively long half-life of ~3 days which would favor control of titin protein expression at the post-transcriptional level. We provide evidence that titin 5'-UTR represses its translation efficiency through a conserved uAUG. Mutations/SNP in the titin 5'-UTR or stress stimuli could alter titin translational efficiency and ultimately affect cardiac growth.

Schwanhäusser et.al. analyzed the global mRNA half-lives in mammalian NIH3T3 cells via pulse labelling mRNA followed by deep sequencing and found that median mRNA half-life

is 9 hours [111]. We found that titin mRNA is remarkably stable with a half-life of ~3 days, which is similar to the reported protein half-life of titin in skeletal muscle cells in culture[90]. Housekeeping genes are abundantly expressed and energetic constraints placed on the cell may explain why these genes tend to have stable mRNAs and proteins[111]. We speculate that stable titin mRNAs and proteins may have evolved in part to minimize the energetic cost of transcription, synthesis and transport of large proteins in a cell. Our *in situ* hybridization study together with previous reports showing that titin mRNA is striated and co-localized with titin protein as well as sarcomeric 60S ribosomal subunit, suggests that titin mRNA is targeted to the sarcomere directly at the site of protein localization and translation [121,122]. This close spatial proximity between titin translation and sarcomere incorporation may facilitate local feedback regulation of mRNA post-transcriptional control.

The control of gene expression via the 5'-UTR represents one important mechanism of control within the complex network of gene regulation. Identification of cis-regulatory elements such as secondary structure, uAUGs, uORFs have been shown to negatively regulate translational efficiency [113,114,123]. Mutations in the 5'-UTR of protein coding genes have been associated with diseases, further highlighting the importance of the 5'-UTR in control on protein expression [113]. Moreover, alternative transcriptional start sites for a gene when expressed in different tissues or in disease have been reported that have altered 5'-UTR control of translational efficiency [124,125]. We identified a single 223 nt titin 5'-UTR transcript via 5'RACE assay in wild-type mouse cardiac and skeletal muscle. The absence of any additional bands signifies that titin 5'-UTR does not stem from alternative promoters, transcriptional initiation sites, and RNA processing events under normal conditions. Whether alternative transcriptional start sites exist for titin with muscle development or disease remains to be determined.

The -3 and +4 nucleotides of the consensus Kozak sequence are key nucleotides involved in binding eIF2α of the mammalian 43S subunit and are present in uAUG2 but absent in uAUG1 of titin 5'UTR [120]. Thus, uAUG1 does not have a strong Kozak sequence and may be skipped over by the ribosome in a process called leaky scanning [113]. Our results are consistent with this notion as uAUG2 accounted for most of titin 5'-UTR translational repression, while uAUG1 had a negligible effect. Short hairpin motifs in the 5'-UTR have been shown to repress translational efficiency by impeding ribosomal scanning [112]. We found a conserved short hairpin motif in titin 5'-UTR, however, mutation of the short hairpin motif within the 5'-UTR did not relieve repression, suggesting that this motif does not play a role in titin translational regulation. It is possible that our mutagenesis may not have sufficed to fully disrupt the hairpin, regardless our data suggest that the titin 5'-UTR translational repression comes primarily from uAUG2.

A further question relates to the degree of titin 5'-UTR translational control following treatment with growth factors. We compared growth stimuli neuregulin (PI-3-kinase and $p70^{S6K}$ activation) and PMA (ERK activation) on titin 5'-UTR translational efficiency. We also investigated the effect of electrical pacing which was previously shown in feline cardiomyocytes to increase 5'-UTR translational efficiency of c-jun 5'-UTR reporter[126]. On the other hand, mechanical inactivation of spontaneously beating NRVM has been shown to depress alpha myosin heavy chain mRNA translation and result in cellular atrophy [127]. Neither growth stimuli, electrical pacing, nor mechanical arrest in cardiomyocytes altered titin 5'-UTR reporter activity, thus it appears that stimuli modulating cardiac growth do not affect titin protein synthesis at the 5'-UTR level.

Our data shows that doxorubicin stress was able to increase 5'-UTR activity. This observation is interesting because doxorubicin has been shown to induce calpain mediated titin

degradation [115]. Increasing titin protein synthesis via enhanced 5'-UTR translational efficiency could act as a compensatory feedback mechanism under conditions of stress-induced titin degradation. Support for stress induced translational upregulation stems from a study in which endoplasmic reticulum stress in kidney cells bypassed the inhibitory uORF in the 5'-UTR of PKD2 mRNA thereby increasing it translation [128].

Calvo *et al*. reported that SNPs generated or deleted uORFs in the 5'-UTRs of at least 507 human genes and showed that all SNPs resulted in a 30-60% decrease in reporter levels when compared to control reporters [114]. Currently there are 24 disease conditions associated with SNPs altering uORF function [113]. A SNP at the -6 position of the Kozak sequence of cardiac transcription factor GATA4 was shown to co-segregate with atrial septal defect [129]; in vitro experiments showed that this SNP resulted in decreased translational initiation and protein expression of GATA4. We demonstrated that the titin rs13422986 T/C SNP at the uAUG2 Kozak sequence decreases titin translational efficiency. This SNP has a minor allele count of T=0.015/32 in 1000 genomes project. We therefore speculate that the population harboring the rs13422986 SNP is synthesizing less titin which may potentially affect cardiac growth.

It should be noted that the 3'-UTR of titin mRNA may be another important control mechanism at the post-transcriptional level[130]; we are currently investigating this notion. Nevertheless, our result showing that addition of the titin 3'-UTR to the 5'-UTR reporter did not alter luciferase activity suggests that the 5'-UTR is the main regulatory component of basal titin mRNA translational efficiency.

In summary, our study found that titin mRNA translational has a long half-life and is localized at the sarcomere. We provide evidence that titin translational efficiency is controlled in part by its 5'-UTR mainly through a *cis*-regulatory uORF. Given that titin synthesis is

energetically costly, we believe that the uORF could play a role in fine tuning titin mRNA translation by serving as a passive brake to prevent overproduction of titin and hence wasting of cellular resources.

Chapter 3

miR26a/b regulate titin gene expression at the 3'-UTR

3.1 Chapter abstract

At ~3-3.7 mDa, titin is the largest known protein and critical component of sarcomere structure and function. Recent evidence highlighting the significance of the titin 5'-UTR led us to consider the role of the titin 3'-UTR in regulating its translational efficiency. We performed a 3' RACE and identified two titin 3'-UTRS in both mouse and human heart tissue. Using the canonical titin 3-UTR sequence, we generated a mouse titin 3'-UTR reporter and found that it significantly repressed translation efficiency by 56% in NRVM and 30% HEK293 cells. *In silco* analysis of titin 3'UTR identified a conserved miRNA binding site, miR-26a/b. To determine if titin 3' UTR is regulated by mIR-26a/b, we transfected WT titin 3'-UTR or mutant titin miR-26a/b 3' UTR along with miR-26a, miR-26b or scramble mimics into Cos7 cells. Results for titin 3'-UTR showed that miR-26a and miR-26b both significantly repressed titin luciferase activity by 33% and 28% respectively. Transient transfections of miR-26a, miR-26b mimics into NRVM significantly repress titin gene expression by 53% and 56% respectively when compared to scramble control treated cells. Our results imply that titin is post-transcriptionally regulated by miR-26a/b.

3.2 Introduction

The cardiac sarcomere is the basic contractile unit of the heart and composed of several myofilament and accessory proteins that function to produce force. At ~3.0-3.7 mDa, titin is the

largest and third most abundant myofilament after actin and myosin[5]. One molecule of titin spans the entire half-sarcomere from its N-terminal domain at the Z-disk to and its C-terminal domain at the M-line thus serving as a molecular ruler for sarcomere spacing[22]. Additionally, titin functions as a bidirectional spring by providing passive tension during diastole and the restoring force after systole[22].

Although much is known about the structure and function of titin, the mechanisms regulating its gene expression are virtually unknown. Gene expression is harmonization of complex events that are regulated at multiple levels including epigenetic, transcriptional, post-transcriptional, and translational control[131-133]. Recently, Cadar et. al., provided evidence highlighting the importance of titin's 5-UTR by identifying uORFs that negatively regulate titin translational efficiency as uORFs reduce translation from the mORF[134]. The control of translational initiation is mediated by synergy between the 5'-UTR and 3'-UTR as the poly(A)-binding protein (PABP) binds to the eukaryotic initiation factor 4G (eIF4G) thus promoting recruitment of the eIF4F complex to the 5' cap and circularization of mRNA[135,136]. At the 3'-UTR, *cis*-regulatory elements have been shown to modulate mRNA stability, localization, and translational control[137].

MircoRNAs (miRNAs) are evolutionally conserved, eukaryotic small, 21-22 nt, noncoding RNAs that bind to (microRNA response element) MREs in the 3' UTR of genes[138]. They function to recruit miRNA-induced silencing complex in order to promote mRNA repression via decapping, deadenylation, and or decay[138]. To examine whether titin is post-transcriptionally regulated by miRNAs, we performed *in silico* analysis of titin 3'-UTR and identified miR-26a/b as a putative target. The miR-26a/b (miR-26a-1, miR-26a and miR-26b) family is transcribed from the introns encoding carboxy-terminal domain RNA polymerase II

polypeptide A small phosphatase (CTD) family (CTDSPL, CTDSP2, and CTDSP1 respectfully). These phosphatases have been shown to dephosphorylate the CTD of RNA polymerase II and phosphorylated prb protein[139,140]. Specifically in the heart, miRNA 26b (miR-26b) was shown to post-transcriptionally regulate GATA4, an important transcription factor in cardiogenesis and sarcomere maintaince[141,142]. We hypothesized that titin gene expression is post-transcriptionally regulated by miR-26a/b.

3.3 Materials and methods

All experiments involving animals were approved by the Animal Care and Use Committee at Vanderbilt University Medical Center, and carried out in accordance with the Guide for the Care and Use of Laboratory Animals of the National Institutes of Health.

3.3a Cardiomyocyte isolation and cell culture

Neonatal rat ventricular myocytes (NRVMs) were isolated from hearts of 1-2-day old Sprague-Dawley rat pups (Charles River Laboratory) as previously described[115] and cells were cultured in DMEM low glucose supplemented with 7% FBS. The human embryonic kidney 293 (HEK-293) cell line was purchased from ATTC and cultured in DMEM supplemented with 7% FBS.

3.3b 3' RACE and plasmids

RNA was extracted from c57BL/6 mouse and human cardiac tissue using Trizol. The titin 3'-UTR sequence was identified using 5' Rapid Amplification of cDNA Ends kit (Ambion). Gene specific antisense primers used for the 3' RACE study: mouse outer 5'-GTACAGAAACAAGATGGCGGACTTT-3', mouse inner 5'-

ATGGCGGACTTTATACCCTAAGCTT-3', human outer 5'-GTACAGAAACAAGATGGTGGACTTT-3', and human inner 5'-GATGGTGGACTTTATACCCTGAGTT-3'. The mouse titin 3'-UTR PCR product was cloned into TOPO TA vector and subjected for Sanger sequencing. The 3'-UTR of titin was subcloned downstream of the firefly luciferase gene in a pGL3 reporter (Promega) using XbaI restriction sites (New England Biolabs). All mutagenesis were performed using the QuikChange lightening mutagenesis kit (Agilent Technologies). Muatant titin 3'-UTR construct was generated by mutating 7 nucleotides (TACTTGA to GCGGCTG) at the seed sequence. Mutagenesis was confirmed by Sanger sequencing.

3.3c Cell transfection and luciferase reporter assay

NRVM were serum starved overnight (1% FBS/DMEM low glucose) followed by transient transfection with 100ng RTK, 200ng pGL3 control or Ttn 3'-UTR for 24 hours via lipofectamine delivery. HEK 293 cells were serum starved overnight (1% FBS/DMEM high glucose) followed by treated with 100ng RTK, 200ng pGL3 Control or Ttn 3' -TR for 24 hours via lipofectamine delivery. COS-7 cells were serum starved overnight (1% FBS/DMEM high glucose) followed by transient transfection 100ng RTK, 200ng Ttn 3'-UTR or Mutant Ttn 3'-UTR pGL3 reporter constructs along with 25nM miRNA scramble, or 25nM miR-26a or 25nM miR-26b for 24 hours via lipofectamine delivery. Following treatments, cells were harvested and assayed for luciferase activities using a GloMax-Multi Detection system (Promega). The ratio of firefly:*Renilla* luciferase activities was calculated to normalize for differences in cell number and transfection efficiency. Each experiment was run in triplicate and the ratio values were normalized to control to allow for between-experiment comparison.

3.3d Titin gene expression

NRVM were treated with 100nM of scramble, miR-26a, or miR26b mimic for via Lipofectamine 2000 delivery (Life Technologies) for 72 hours. Total RNA was isolated using TRIzol® Reagent. RNA was treated using DNA-*free*™ DNA Removal Kit (Life Technologies™). Total RNA was converted into cDNA using High-Capacity cDNA Reverse Transcription Kit (Applied Biosystems). RT-PCR was performed using SsoAdvanced™ Universal SYBR® Green Supermix (Bio-Rad) in a CFX96™ Real-Time PCR Detection System (Bio-Rad). Primers were designed using Primer3: WWW Software Tool. Primers used for this study rat Ttn, sense 5'-AAGCCAAGAAACAGGAACCA-3' and antisense 5'-TGCAATAGCCTTTCCATCCT-3'; rat 18s RNA, sense 5'-GTGGAGCGATTTGTCTGGTT-3' and antisense 5'-CGCTGAGCCAGTCAGTGTAG-3'. Titin mRNA expression was normalized to 18s RNA.

3.3e Titin gel electrophoresis

NRVM were treated with 100nM of scramble, miR-26a mimic for 72 hours via Lipofectamine 2000 delivery (Life Technologies). Titin was analyzed as in Warren et. al.[143]. Briefly, NRVM were washed with cold PBS twice before addiotion of sample buffer : 8 M urea, 2 M thiourea, 0.075 DTT, 0.050 M Tris HCL and 3% w/v SDS at pH 6.8. NRVM were scraped and transferred to a cold glass homogenizer. Cells were homogenized for 30 seconds and transferred into an eppendorf tube and incubated in a 60° C water bath for 5 min. Samples were centrifuged at 12,000 RPM for 3 minutes at 4° C. Supernatant was loaded on to a 1% agarose gel. After gel electrophoresis, total protein was visualed via SYPRO Ruby stain.

3.3f Statistical analysis

Data are reported as mean ± SD. Where appropriate, results were either analyzed by Student's t-test or ANOVA with a Bonferroni's multiple comparison post hoc test. $P<0.05$ was considered statistically significant.

3.4 Results

3.4a Identification of mouse titin 3'-UTR

The UTRs of mRNA transcripts are known to regulate protein translation; in this study we specifically investigated the role of titin 3'-UTR on regulating translational efficiency. To identify titin 3'-UTR we performed a 3' RACE and amplified two RACE PCR products, a canonical 1050 nt and a short 447 nt PCR product (Fig. 14A). Sanger sequencing confirmed the 1050 conical titin 3'-UTR sequence within the 1.2kb band. The short PCR band product contained the first 447 nt of the titin 3'-UTR. The canonical 3'-UTR sequence was entirely consistent with Genebank's mouse annotation, and sequence alignment shows high homology (>81%) between mouse, human and rat (Fig. 15).

3.4b Titin 3'-UTR controls titin gene expression

To determine if titin 3'-UTR regulates titin translation, we subcloned the 1050 nt nucleotide 3'-UTR downstream of the firefly luciferase gene in the pGL3 control vector (Fig. 14B). The titin 3'-UTR reporter activity showed significant repression in transiently transfected NRVM (56% decrease) and HEK293 cells (30% decrease) (Fig.16A,B).

3.4c miR-26a/b regulate titin gene expression at the 3' UTR

We performed an *in silico* analysis using www.microRNA.org to identify potential miRNAs targeting the titin 3'-UTR. *In silico* analysis identified miR-26a and miR-26b (miR26a/b) as potential hits. miR-26a/b target the 151-173 nt span of the mouse titin 3'-UTR and 145-167 nt span of the human 3'-UTR (Fig 17A). To verify if miR-26a/b target titin, we transiently transfected the pGL3 titin 3'-UTR reporter along with either a miR-26a, miR-26b, and scrambled control mimic into COS7. We found that miR-26a reduces titin 3'-UTR translational efficiency by 33 % and miR-26b by 28% (Fig. 17B). We choose to use COS7 cells which are derived from the African green monkey kidney as a non-cardiac screening cell line. To confirm specificity, we mutated the seed sequence (5 nt bp change) of the titin 3'-UTR pGL3 reporter found no change in luciferase activity in the presence of control, miR-26a/b mimics (Fig. 17B)

After confirming target specificity, we tested whether miR-26a/b downregulated titin mRNA expression *in vitro.* We report that both miR-26a and miR-26b significantly reduce titin mRNA expression by 53% and 56% in NRVMs (Fig. 18). We next examined titin protein levels and found that miR-26a reduces titin protein expression in NVRMs (Fig. 19).

We next aimed to generate a human titin 3'-UTR model so we performed a 3' RACE and amplified two RACE PCR products, a canonical 1050 nt and a short 447 nt PCR product (Fig. 20). Sanger sequencing confirmed the 1050 conical titin 3'-UTR sequence within the 1.2kb band. The short PCR band product contained the first 447 nt of the titin 3'-UTR. We have yet to generate such a reporter.

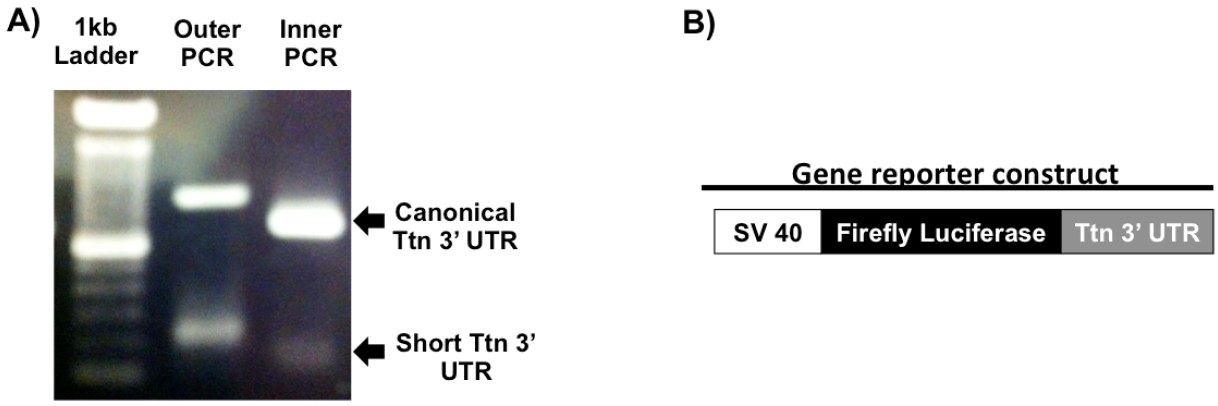

Figure 14. 3' RACE identifies two titin 3'-UTR transcripts in mouse cardiac tissue. A) 3' RACE assay was performed using mouse cardiac tissue. 3' RACE assay identifies the canonical 1047 nt and a short 447 nt 3'-UTR products. B) The titin 3' UTR produce was cloned downstream the firefly luciferase gene.

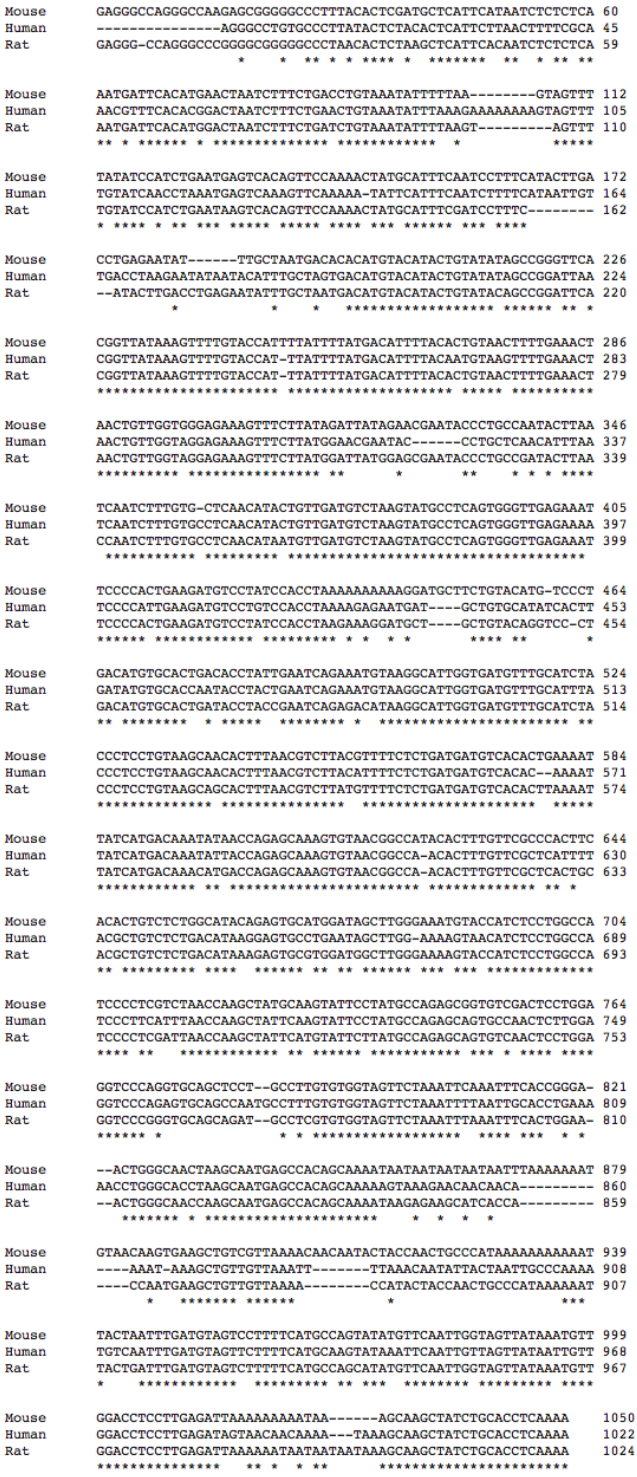

Figure 15. Clustal Omega multiple sequence alignment of titin 3'-UTR between mouse, human, rat. Titin 3'-UTR sequence is on exon 363. Mouse, human, and rat 3'-UTR sequences are >81% homologous.

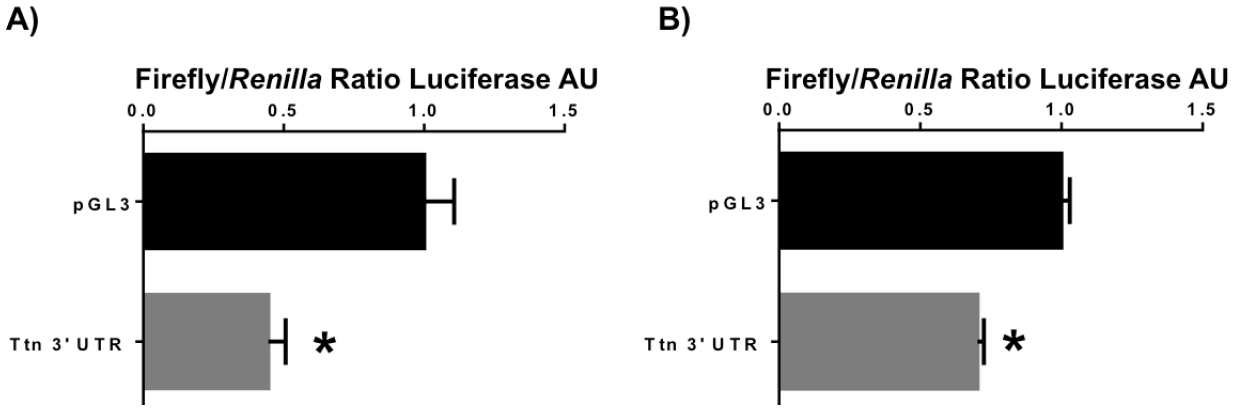

Figure 16. Titin 3'-UTR suppresses titin translational efficiency. A) NRVM were treated with 100ng RTK, 200ng pGL3 control or 3'-UTR for 24 hours via lipofectamine delivery. Cells were lysed and assayed for firefly and *Renilla* luciferase activities (n=3). Data displayed as Mean±SEM, * $P<0.05$, t-test comparison. B) HEK 293 cells were treated with 100ng RTK, 200ng pGL3 Control or Ttn 3'-UTR for 24 hours via lipofectamine delivery. Cells were lysed and assayed for firefly and *Renilla* luciferase activities (n=3). Data displayed as Mean±SEM, * $P<0.05$, t-test comparison.

(A

```
miR-26a              3′ UCGGAUAGGACCUAAUGAACUU 5′
                        | |||||    |||||||
Mmu Ttn 3′UTR 151:5′ UUUCAAUCCUUUCAUACUUGAC 3′:173
                        | |||||    |||||||
miR:26b              3′  UGGAUAGGACUUAAUGAACUU 5′

miR-26a              3′ UCGGAUAGGACCUAAUGAACUU 5′
                        | ||| |    || |||
Hsa TTN 3′UTR 145:5′ UUUCAAUCUUUUCAUAAUUGUU 3′:167
                        | ||| |    || |||
miR:26b              3′  UGGAUAGGACUUAAUGAACUU 5′
```

B)

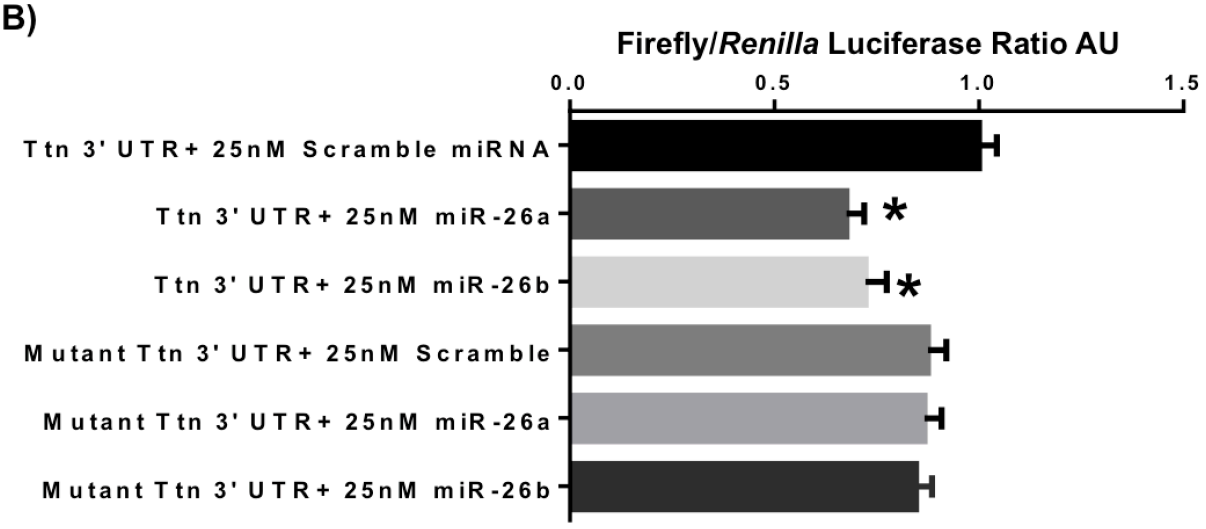

Figure 17. miR-26a/b regulates the titin 3'-UTR. A) Schematic of miR-26a/b binding site in mouse titin 3' UTR. The seed sequence is bolded. B) COS-7 cells were treated with 100ng RTK, 200ng Ttn 3' UTR or Mutant Ttn 3' UTR along with 25nM miRNA scramble or 25nM miR-26a/b for 24 hours via lipofectamine delivery. Cells were lysed and assayed for firefly and *Renilla* luciferase activities (n=4). Data displayed as Mean±SEM, * $p<0.05$ vs Ttn 3' UTR + 25nM Scramble miRNA, groups compared by ANOVA.

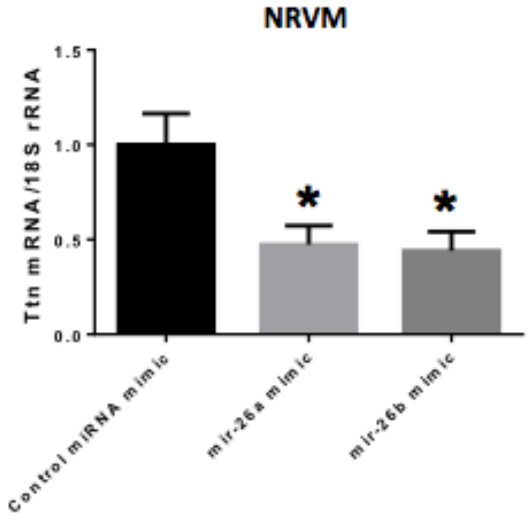

Figure 18. MiR26a/b reduces titin gene expression. NRVM were treated with 100nM of scramble, miR-26a, or miR26b mimic for 72 hours. Real-time PCR was performed to assess titin gene expression. Data displayed as Mean±SEM, * $p<0.05$ vs control miRNA mimic, groups compared by ANOVA.

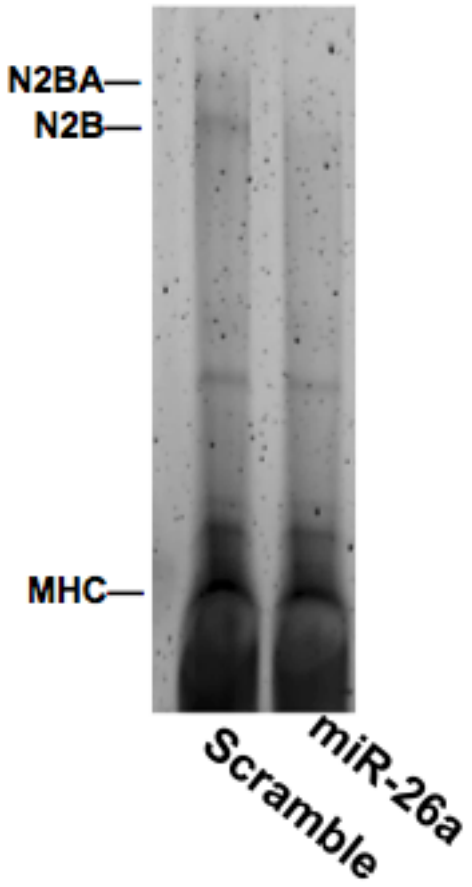

Figure 19. miR-26a reduces titin protein expression. NRVM were treated with 100nM of scramble or miR-26a mimic for 72 hours. Lysates ran on 1% agarose gel. Titin was visualized using SYPRO Ruby stain.

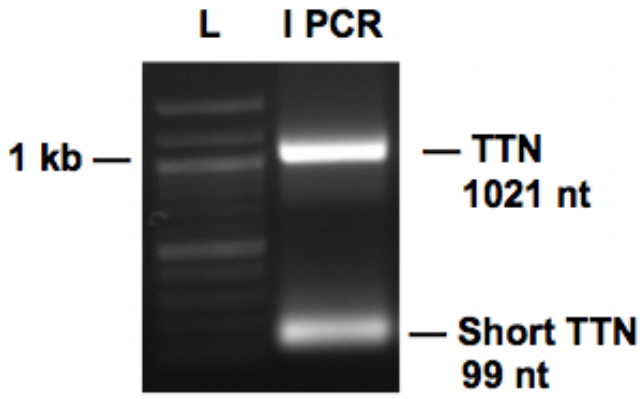

Figure 20. 3' RACE identifies two titin 3'-UTR transcripts in human cardiac tissue. 3' RACE assay was performed using human cardiac tissue. 3' RACE assay identifies the canonical 1021 nt and a short 99 nt 3'-UTR products.

3.5 Discussion

At ~3-3.7 mDa titin is the largest and presumably the metabolically taxing protein to synthesize. In this chapter, we found that titin 3'-UTR represses its translational efficiency as well as provide evidence that miR-26a/b regulate titin at the 3'-UTR. Together, these studies along with the prior chapter highlight the UTRs as an important mechanism in controlling titin gene expression.

With a stable mRNA half-life of ~66 hrs and sarcomeric localization, control of titin gene expression would favor regulation at the post-transcriptional level[134]. In mouse and human hearts, we identified the canonical titin (1050 nt mouse, 1021 nt human) 3'-UTR as well as a novel short (447 nt mouse, 99 nt human) 3'-UTR via 3'RACE. The canonical mouse, human and rat titin 3'-UTRS share greater than 87% sequence homology suggesting evolutionary conservation. Using a luciferase as a reporter, we demonstrate that the titin 3'-UTR represses translational activity by 56%, which is approximately equal in repression to its 5'-UTR counterpart[134]. This duality in repression suggests that both the titin 5'-UTR and 3'-UTR work together in sync to repress titin gene expression in order to prevent an overproduction of titin which could be metabolically wasteful.

Regarding the short titin 3'-UTRs, alternative cleavage and polyadenylation (APA) serve as an important 3' processing event in the maturation of mRNA. Approximately 70% of mammalian genes undergo APA demonstrating that it is a widespread occurrence. Furthermore, APA have functional consequences as 3' end processing may affect mRNA metabolism, localization and stability[144]. Given the identification of multiple titin 3'-UTRs, we speculate that titin mRNA may undergo alternative cleavage and polyadenylation.

MicroRNAs have been demonstrated to be important mediators in the control of gene expression in mammalian cells and tissues[145]. Specifically within the heart, miRNAs have been shown to have important roles in cardiogenesis as dicer knock out mice result in dilated cardiomyopathy, progressing to heart failure and post-natal lethality thus highlighting their importance in cardiac function. Nevertheless, overexpression of miRNAs can have negative consequences such as miR-1 overexpression resulting in decreased ventricular myocyte proliferation[146]. In the heart, miRNAs have been implicated in modulating cardiac hypertrophy, fibrosis, regeneration, angiogenesis and apoptosis[138].

We sought to determine if titin was regulated by miRNAs therefore we performed an *in silico* analysis and identified miR-26a/b as a putative target. We confirmed that miR-26a/b directly targets the titin 3'-UTR from our luciferase reporter assays. We also demonstrate that both miR-26a/b target titin at the mRNA level as titin mRNA levels decrease with miR-26a/b treatment. We also provide preliminary evidence that miR-26a treatment downregulates titin protein expression in NRVM; however, it should be noted that it was an N=1 thus warranting further investigation. While we provide evidence that miR-26a/b target the mouse titin 3'-UTR *in vitro*, it would be important to recapitulate this using a human titin 3'-UTR reporter as well as confirming a physiological interaction *in vivo* using an unbiased approach such as crosslinking immunoprecipitation coupled with high-throughput sequencing (HITS-CLIP) in mouse and human tissue[147]. Such an experiment would also allow for the identification of other novel binding miRNAs as mRNAs have been shown to be the target of multiple miRNAs[148].

Initial studies on the miR-26a/b family focused on their regulation of cell cycle activity where they blocked the G1/S transition by down regulating key cell cycle regulators, CDK6 and cyclin E1[140]. In a zebrafish ventricular resection model, miR-26a was downregulated in

proliferating cardiomyocytes[149]. Additional support for miR-26a in regulating cell growth stems from the finding that miR-26a was downregulated in a rat transaortic constriction pressure overload model[150]. MiR-26 was shown to post-transcriptionally regulate GATA4, an important transcription factor in cardiogenesis and sarcomere maintaince[141,142]. Our evidence demonstrates that miR-26a/b acts as a novel titin regulator. Nevertheless, the roles of miR-26a/b family and titin play in its relation to cell growth remains to be elucidated.

Chapter 4

Real-time visualization endogenous titin reveals extensive reversible photobleaching in human induced pluripotent stem cell-derived cardiomyocytes

4.1 Chapter abstract

The cardiac sarcomere is the elemental contractile unit of the heart and is composed of a complex array of highly ordered structural, regulatory, and contractile proteins designed to generate force. Titin, the largest known protein, is indispensable for the structural integrity and function of the cardiac sarcomere, however, little is known regarding the turnover of titin within the complex macromolecular sarcomere structure in contracting cardiac myocytes. To directly visualize sarcomeric titin incorporation and turnover, we used CRISPR/Cas9 genome editing in human induced pluripotent stem cells (hiPSC) to knock-in a photoconvertible fluorescent protein, mEos3.2, into the C-terminus of titin. Upon cardiac induction, the titin-mEos3.2 fusion protein is expressed and integrated in the sarcomeres of hiPSC-derived cardiomyocytes (hiPSC-CMs). Fluorescence recovery after photobleaching (FRAP) revealed a baseline titin-mEos3.2 sarcomere exchange half-life of ~1.2 hours with a 68% mobile fraction. Cycloheximide treated titin-mEos3.2 hiPSC-CMs displayed no significant changes in mobility whereas paraformaldehyde fixed and permeabilized titin-mEos3.2 hiPSC-CMs surprisingly revealed a 55% mobile fraction. Whole cell FRAP analysis in paraformaldehyde fixed, cycloheximide treated and untreated titin-mEos3.2 hiPSC-CMs displayed no significant differences in recovery. Our results reveal that reversible photobleaching accounts for the majority of titin recovery demonstrating that titin is not a dynamic molecule as previously thought.

4.2 Introduction

During the average human lifespan, the heart beats over 2.5 billion times[70]. This remarkable feat is accomplished by terminally differentiated mechanically contracting cardiac myocytes. In turn, cardiomyocyte contraction at the subcellular level is orchestrated by a highly complex and integrated protein system known as the sarcomere, where force is generated by bidirectional sliding of thin actin filaments past the thick myosin filaments. To maintain functional sarcomeres, it is assumed that precise turnover of proteins is required that balances protein synthesis and incorporation into the sarcomere with removal and degradation of worn out or damaged proteins. With the use of radioisotopes, the protein half-lives have been estimated for myosin heavy chain (5.4 days), actin (10 days), troponin T (3.5 days), Troponin I (3.2 days), troponin C (5.3 days) in the adult rat heart[73,74]. These long protein half-lives supported the notion that the sarcomere was a static structure with proteins turning over at their respective rates.

Fluorescence recovery after photobleaching (FRAP) is a commonly used microscopy technique to quantify fluorescently tagged protein dynamics in living cells[80]. Specifically in the heart, FRAP has allowed investigators to examine the dynamic state of the sarcomere in real-time. In neonatal ventricular myocytes, β-actin has a 30 minute exchange half-life [83] whereas β-myosin heavy chain has an exchange half-life of 32 minutes in adult rat cardiomyocytes[84]. Cardiac troponin T and C have exchange half-lives on the order of 20 minutes in mouse embryonic cardiomyocytes[85]. Collectively, these observations suggest that sarcomere protein components may in fact recycle among myofibrils either through a pool of sarcomeric (bound) and nonsarcomeric (unbound) molecules. This is particularly germane to titin, an enormous (up to 4 mDa) structural component of the thick filament spanning the half-sarcomere.

Titin serves as a molecular scaffold for sarcomere assembly, maintenance, and function[5,6]. With its N-terminal domain anchored at the sarcomeric Z-line and its C-terminal domain at the M-band, titin also functions to center the thick filament between the thick filaments and to stabilize relative positions of the two filaments to prevent overstretch. In addition, titin possesses a bidirectional spring domain responsible for most of the sarcomere's elastic recoil[22,25,26]. Given titin's vital importance in sarcomere structure and function, surprisingly little is known about the dynamics of titin turnover in a continuously contracting cardiomyocyte. With multiple isoforms ranging in molecular weights of 2.97-3.7 mDa, modeling titin dynamics has been problematic. To study sarcomere turnover *in situ*, da Silva Lopes et al created a titin-eGFP knockin mouse model to isolate neonatal mouse cardiomyocytes and study titin-eGFP mobility using FRAP[89]. They report that the half-life for fluorescent titin recovery in the sarcomere was 2.5 hours, which was unexpected given that the molecular half-life of titin is 72 hours by pulse-chase experiments[90]. They concluded that the sarcomere is a dynamic rather than a static structure with rapid exchange between a pool of sarcomeric (bound) and nonsarcomeric (unbound) titin molecules.

The reprograming of adult somatic cells into induced pluripotent stem cells has revolutionized biomedical research[96]. With standard protocols available coupled to emerging technologies i.e (Matrigel Mattress, microcontact printing), hiPSC-CMs are increasing being valued as a useful model and surrogate for human cardiomyocyte studies[98,100,101]. Complemented with the versatility of CRISPR/Cas9 gene editing, one can generate genetically modified hiPSC-CMs for research[151]. To more closely examine the dynamics of sarcomeric titin turnover, *in situ*, we used the CRISPR/Cas9 genome editing technology to generate the first-of-its-kind titin fused with a photoconvertible fluorescent protein to directly track titin incorporation and turnover in

sarcomeres of live, beating hiPSC-derived cardiomyocytes. We used our model to test the hypothesis that titin is a dynamic and mobile protein in hiPSC-CMs

4.3 Materials and methods

All protocols were approved by the Vanderbilt University Institutional Review Board.

4.3a Human induced pluripotent stem cell (hiPSC) reprograming

Dermal fibroblasts were isolated from a 2-mm dermal punch biopsy from a healthy male volunteer with no history of heart disease. Fibroblasts from the second passage were reprogrammed into hiPSCs using electroporation delivery (Neon) of non-integrating episomal vectors (Epi5™ Episomal iPSC Reprogramming Kit (ThermoFisher)). After episomal delivery, fibroblasts were plated on a standard cell culture grade 10-cm plate. iPSC-like colonies were manually moved to hES-grade Matrigel (Corning) coated 24-well plates between day 14-30 post-electroporation. Individual colonies were expanded for validation and line maintenance.

4.3b hiPSC validation: stem cell markers

HiPSC were validated by presence of stem cell associated markers via immunostain for OCT4 (Cell Signaling, #2750), SSEA4 (DSHB, MC-813-70), SSEA3 (Millipore, MAB4303) , TRA-1-60 (Millipore, MAB4360). The presence of stem cell-associated alkaline phosphatase was detected by commercially available colorimetric assay (Stemgent, 00-0055).

4.3c hiPSC validation: pluripotency

HiPSCs were grown in suspension on low adherence plates in DMEM/F12 w/ GlutamaX (Invitrogen, 10565) supplemented with 20% knockout serum replacement (Invitrogen , 10828-028), 1% non-essential amino acids (Sigma, M7145), 1% penicillin/streptomycin (MediaTech,15140122). On day 5 of differentiation, individual embryoid bodies were replated on growth factor reduced Matrigel (Corning) for 14 days in media listed above. Presence of cells in the endoderm, mesoderm, and ectoderm lineages were visualized by immunofluorescent detection of proteins associated with each of the three germ layers: GATA4 (Abcam, ab84593) for endoderm, alpha-smooth muscle actin (Abcam, ab7817) for mesoderm, and betaIII-tubulin (Millipore, MAB1637f) for ectoderm.

4.3d hiPSC validation: chromosomal assessment

Twenty hiPSCs were screened for large chromosomal abnormalities by commercial karyotype analysis (Genetics Associates, Nashville, TN).

4.3e hiPSC maintenance

hiPSCs were maintained as described in Feaster et. al[100]. Briefly, hiPSCs were on cultured on growth factor-reduced Matrigel (Corning) coated plates (1:200 dilution, DMEM/F12) in mTeSR1 medium (Stemcell Technologies). Cells were passaged every 4 days using 0.5 mM EDTA (Life Technologies) in D-PBS without $CaCl_2$ or $MgCl_2$ (Life Technologies). 10 μM Rho kinase inhibitor Y-27632 (CalBiochem) was added for the first 24 hours after passaging. Cells were maintained at 37 °C, with 5% CO_2 and 5% O_2.

4.3f Guide RNA design

The human titin exon 363 sequence was uploaded into the CRISPR Design Tool (crispr.mit.edu) for gRNA generation. Guide sequence 5'-TCTGTACGTCCATGATGATC-3' was cloned into pSpCas9(BB)-2A-Puro (PX459) (gift from Feng Zhang, Addgene plasmid # 4813). Sanger sequencing confirmed correct gRNA insertion.

4.3g T7 endonuclease assay

Hek 293 cells were transiently transfected via lipofectamine delivery with 1 μg of PX459 plasmid encoding the titin gRNA and Cas9 for 36 hours. HEK 293 cells were then subjected to antibiotic selection (1μg/mL ampicillin) for 48 hours. HEK 293 cells were then harvested for DNA extraction using QuickExtract solution (Epicentre, QE0905T). Indels were detected using GeneArt Genomic Cleavage Detection Kit (Invitrogen, A24372) per manufacturer's protocol. A 423 bp loci where the double stranded breaks occurred was PCR amplified using Left Primer sequence 5'-AGCAGGCATAAGAGGTGAGC-3' and Right Primer sequence 5'-CAGTGGCAGAGTCAGATCCA-3'. DNA was ran on 2% agarose gel and was visualized by EtBr staining. % cleavage ((sum of cleaved band intensities/ total band intensities)*100) was quantified by band densitometry.

4.3h CRISPR/Cas9 gene editing

hiPSC were dissociated with electroporated with 10 μg of gRNA and 500 ng of titin mEos3.2 homology directed repair template. Cells were plated on 1:200 Matrigel coated plates with in mTesSR1 with 10 μM Y-27632 for 24 hours. Media was changed after 24 hours to remove Y-27632. At 36 hours post-electroporation, cells were subjected to puromyocin selection

at 500ng/mL for 48 hours. Individual colonies were picked and expanded for screening. Individual colonies hiPSC were screened for mEos3.2 insertion by PCR using primers flanking the outside of the repair template, Right primer sequence 5'-CAGCGTAAAATGAGCGAACA-3', left primer sequence 5'-TGCAAGGAAGCTTCTCGTCT-3'. mEos3.2 was confirmed via Sanger sequencing.

4.3i hiPSC cardiac differentiation and culture

Cardiac induction was achieved by small molecule delivery as previously described[100]. Briefly, at day 0 hiPSC were switched from mTeSR1 medium to RPMI 1640 (Life Technologies, 11875) supplemented with B27 minus insulin (Life Technologies, A1895601), 6 μM CHIR99021 (Selleck Chemicals) for 2 days. At Day 2, media was changed to RPMI 1640 with 2% B27 minus insulin. At day 3, media was changed to RPMI 1640 with B27 minus insulin and 5 μM IWR-1 (Sigma) for two days. At day 5, medium was changed to RPMI 1640 with 2% B27 minus insulin for two days and changed every other day until day 10. At day 10, media was changed to RPMI 1640, no glucose (Life Technologies, 11879) for two days and changed every other day until day 16. At day 16, medium was changed to RPMI 1640 with 2% B27 complete (Life Technologies, 17504044) with 1% penicillin/streptomycin (Gibco, 15140122) for 2 days and changed every other day until day 30.

4.3j hiPSC-CM dissociation

Day 30, hiPSC-CMs were washed with PBS without $CaCl_2$ and $MgCl_2$ and dissociated with TrypLE Express (ThermoFisher Scientific, 12604013) for 15 min at 37° C. Single hiPSC-CMs were replated on Growth Factor Reduced Matrigel (Corning) (1:200 dilution in

DMEM/F12) coated MatTek) dishes (MatTek Corporation, P35G-1.5-14-C with phenol free RPMI 1640 with 2% B27 complete and 1% penicillin/streptomycin

4.3k Video based edge detection

Day 30 control or titin-mEos3.2 hiPSC-CMs were dissociated as described above and replated on the Matrigel Mattress for 5 days as in Feaster et. al[100]. Cellular shortening was assessed by video edge based detection as in Feaster et al[100].

4.3l Drug treatments

Day 30 titin-mEos3.2 hiPSC-CMs were treated with 0.1% DMSO (Sigma), 10 μg/mL cycloheximide (CHX) (Sigma),) 1 hour prior to and throughout image acquisition. Fixed hiPSC-CMs were treated with 4% PFA for 15 min and permeablized with 0.5% Triton X-100 in PBS for 15 min before FRAP.

4.3m Protein synthesis assay

Global protein synthesis was detected via Protein Synthesis Assay kit (Cayman Chemicals) per manufacture's protocol. Briefly, day 30 hiPSC-CMs were plated on a 1:200 Matrigel coated 96 well plate. Cells were pretreated with vehicle or CHX (10 μg/mL) for 30 min in culture. Cells were then treated with a metabolic probe O-propargyl-puromycin (OPP), OPP+ CHX or no O-Propargyl-puromycin for 1 hour in culture. Cells were then fixed and treated with 5-FAM-Azide for OPP probe detection. Fluorescence was detected (excitation/emission, 485nm/535nm) via Promega Glomax reader.

4.3n Fluorescence recovery after photobleaching

FRAP experiments were conducted by using a Zeiss laser scanning LSM 710 META Inverted confocal microscope. Titin-mEos3.2 hiPSC-CMs on MatTek dishes were kept at 37° C and 5% CO_2 using ZEISS live cell system. For FRAP, a 63x / 1.40 Plan-APOCHROMAT OIL objective was used with a pinhole set at 1.4 μm. Images were taken before an after photobleaching in the 488 nm channel at 4% laser power. An ROI of 2 sarcomeres was bleached by 100% laser power in the 488 nm channel for 20 iterations. FRAP images were acquired every 30 min for 9 hours. Pixel intensities of the ROI, background and whole cell were acquired using Zen software. Background was subtracted from ROI and whole cell measurements. The ROI was normalized to whole cell pixel intensities. Data was fitted into a one-phase association equation to calculate titin-mEos3.2 exchange half-life. Mobile fractions were calculated by (end recovered fluorescence intensity- postbleach fluorescence intensity/ (prebleach fluorescence intensity- postbleach fluorescence intensity)*100.

For whole cell FRAP, images were taken before an after photobleaching in the 488 nm channel at 4% laser power. A region encompassing the whole cell was bleached by 100% laser power in the 488 nm channel for 200 iterations. FRAP images were acquired every 30 min for 9 hours. Pixel intensities of the ROI (2 sarcomeres) and background were acquired. Background was subtracted from ROI. Images were normalized to pre-bleach intensities. Data was fitted into a one-phase association curve. Mobile fractions were calculated as described above.

4.3o Statistical analysis

All data displayed as Mean ± SEM. Differences between two groups were assesed by a two tailed Student's *t*-test. Differences between more than two groups were assessed by a one-

way ANOVA with a Dunnett's multiple comparison post hoc test. $p < 0.05$ was considered statistically significant. Statistical analysis was performed using Graphpad Prism 6.

4.4 Results

4.4a Generation and validation of titin-mEos3.2 hiPSC model

Briefly, dermal fibroblasts were isolated from a healthy male volunteer with no history of heart disease and reprogramed into hiPSC. Isolated control hiPSC colonies displayed stem cell morphology via the presence of pluripotent markers Oct4, SSEA4, SSEA3 and Tra-1-60 as well as exhibited alkaline phosphatase activity with no changes in genomic integrity (Fig. 21A-C). Pluripotency was validated via *in vitro* differentiation assay of hiPSC (Fig. 21D). We next used CRISPR/Cas9 gene editing in hIPSC to replace the stop codon in titin's terminal exon 363 with an in-frame knock-in of photoconvertible fluorescent protein, mEos3.2[152] (Fig. 22). We designed a gRNA to target titin exon 363 for cleavage. We focused on tagging the C-terminal end of titin since N-terminal tagging of titin with GFP was shown to result in sarcomere dissasembly[153]. T7 endonuclease assay demonstrated gRNA cleavage activity (65.7%) in HEK-293 cells (Fig. 22B) Next, we electroporated hiPSC with the titin targeting gRNA and the mEos3.2 homology directed repair template. Successful and correct genomic mEos3.2 integration was confirmed by screening single hiPSC colonies by PCR using primers that flanked outside the repair template (Fig. 22C). mEos3.2 sequence integration was confirmed by Sanger sequencing (Fig. 22D). The newly derived titin-mEos3.2 hiPSCs retained their stem cell markers (Fig. 23).

Cardiac differentiation of the titin-mEos3.2 hiPSC resulted in the expression of striated titin-mEos3.2 protein at the sarcomere, which was not detectable in the unedited control hiPSC-CM by confocal microscopy (Fig. 24A). Our model labels all main isoforms of titin with the

exception of the novex isoforms[21,24]. Correct sarcomeric localization was confirmed by co-immunnostaining for α-actinin (Z-disk) and myomesin (M-band) (Fig. 24B). The alternating signal peaks of α-actinin and colocalization peaks of myomesin confirm proper titin-mEos3.2integration at the sarcomere. We next determined whether the mEos3.2 tag affected cardiomyocyte function by assessing cell-shortening mechanics. We found no change in resting cell length and no differences in the contraction and relaxation kinetics in titin-mEos3.2 hiPSC-CM when compared to controls (Fig. 24C, D). Our data support the validation of the titin-mEos3.2 hiPSC line to model sarcomere biology.

4.4b Titin-mEos3.2 mobility in live hiPSC-CMs

We assessed the baseline kinetics of endogenous titin-mEos3.2 exchange using day 30 hiPSC-CM. As a metric for quality control, all cells imaged were spontaneously beating unless stated otherwise. We used FRAP to quantify titin-mEos3.2 mobility and exchange. At baseline, we found titin-mEos3.2's recovery reached a steady state within 9 hours after photoablation. We found the titin-mEos3.2 exchange half-life to be ~1.2 hours with a mobile fraction of 68.1 ± 5.7% (Fig. 25A, B, and Table 1) in untreated control titin-mEos3.2 hiPSC-CMs. These results are consistent with those of da Silva Lopes et al[89].

To determine whether the rapid sarcomeric titin-mEos3.2 recovery was dependent on *de novo* synthesis, we treated hiPSC-CMs with the cycloheximide (CHX), translational inhibitor, for one hour prior to and during FRAP. We found a significant increase in the exchange half-life from 1.2 hours (untreated control) to 2.1 hours (CHX) with no significant difference in titin-mEos3.2 mobile fractions (68.1 ± 5.7% untreated control versus 62.8% ± 5.2% CHX) (Fig. 25A, B, and Table 1). Since CHX was dissolved in DMSO, we treated titin-mEos3.2 hiPSC-CMs with

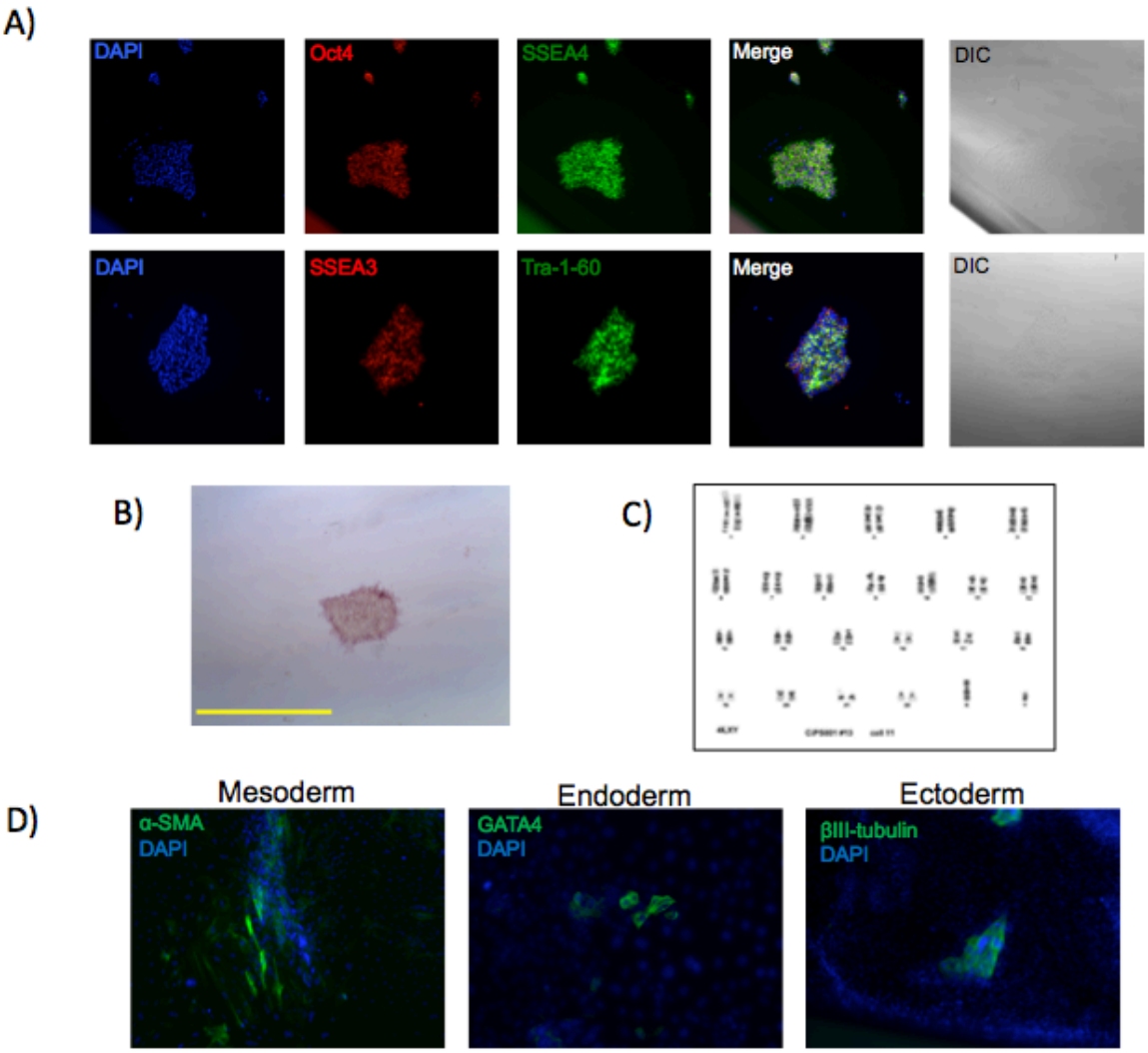

Figure 21. Control human iPSC characterization and validation. A) Control hiPSCs express stem cell markers. Control hiPSC were immunostained for OCT4, SSEA4, SSEA3, Tra-1-60 and Dapi. B) Control hiPSC colony stained positive for alkaline phosphatase. Scale bar is 50μm. C) Chromosomal assessment of control hiPSCs. D) Pluirpotency validation.HiPSCs were differentiated into embryoid bodies for 2 weeks. Embryoid bodies were immunostained for alpha smooth muscle actin (α-SMA), GATA4 and class III beta-tubulin (βIII-tubulin), markers of mesoderm, endoderm, and ectoderm, respectively.

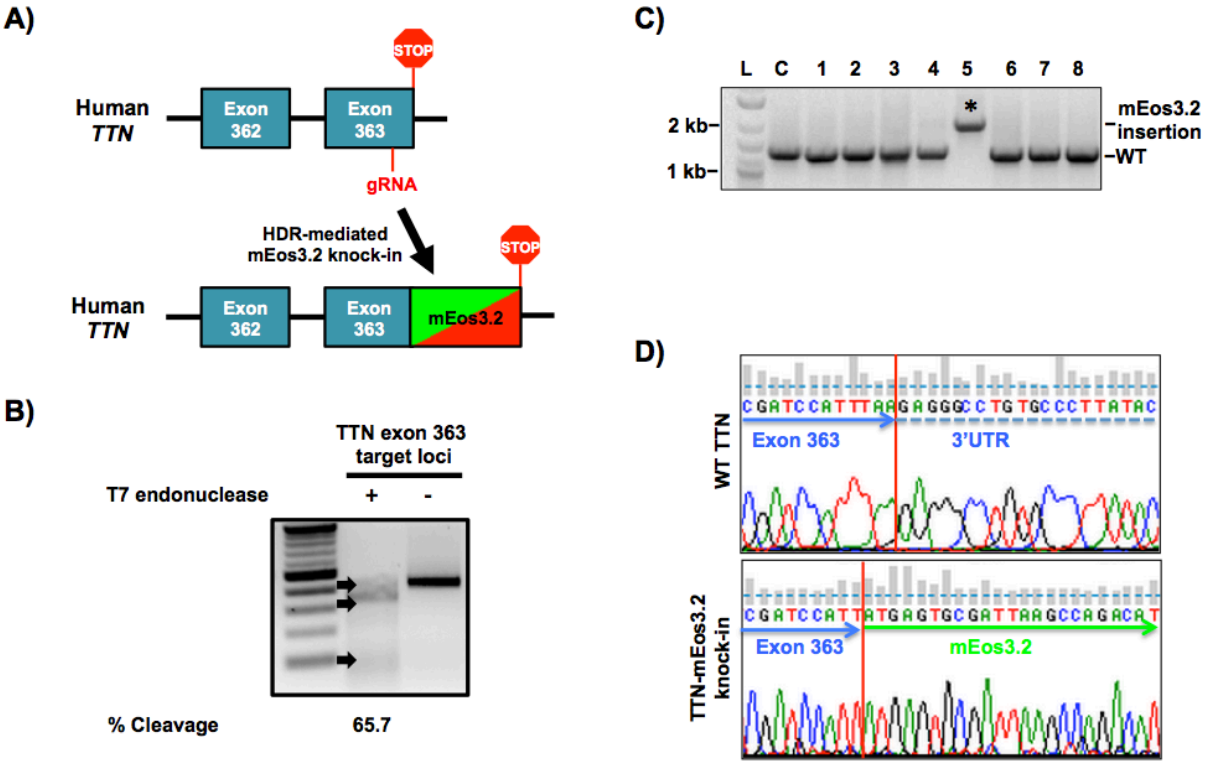

Figure 22. Generation of titin-mEos3.2 knock-in model in hiPSC. A) Titin-mEos3.2 knock-in strategy to replace the stop codon in titin's terminal exon 363 with an in frame mEos3.2 knock-in into titin's terminal exon 363. A gRNA targeting titin exon 363 for cleavage was co-electroporated with a homology directed repair template (mEos3.2, with 600 bp titin flanking homology arms) in human induced pluripotent stem cells. B) Gel image of T7 endonuclease assay demonstrates Titin specific gRNA targets exon 363 for cleavage in HEK 293 cells. Briefly, HEK 293 were transiently transfected with 1 µg of PX 459 plasmid encoding a titin specific gRNA and Cas9 for 36 hours. HEK 293 cells were then subjected to antibiotic selection (500ng/mL, puromyocin) for 48 hours. HEK 293 cells were then harvested for DNA extraction. An 421 bp loci where the double stranded breaks occurred was PCR amplified. The PCR product was denatured and reannealed before being subjected to T7 endonuclease. Lane 1 100 bp ladder. Lane 2 was treated with T7 endonuclease; lane 3 was not. DNA was visualized by EtBr staining and % cleavage ((sum of cleaved band intensities / (total band intensities))*100) was quantified by band densitometry. C) Gel image of mEos3.2 sequence integration in hiPSC. hiPSC were electroporated with 10 µg of gRNA and 500 ng of titin-mEos3.2 HDR template. Individual colonies hiPSC were screened for mEos3.2 insertion by PCR using primers flanking outside of the repair template. PCR products were ran on a 1% agarose gel and stained with EtBr. L lane is 100 bp ladder. Lane C is control. Lane 1-8 are individual hiPSC clones. * in Lane 5 denotes mEos3.2 sequence integration. D) Chromatogram of genomic sequences from hiPSC with and without mEos3.2 sequence integration.

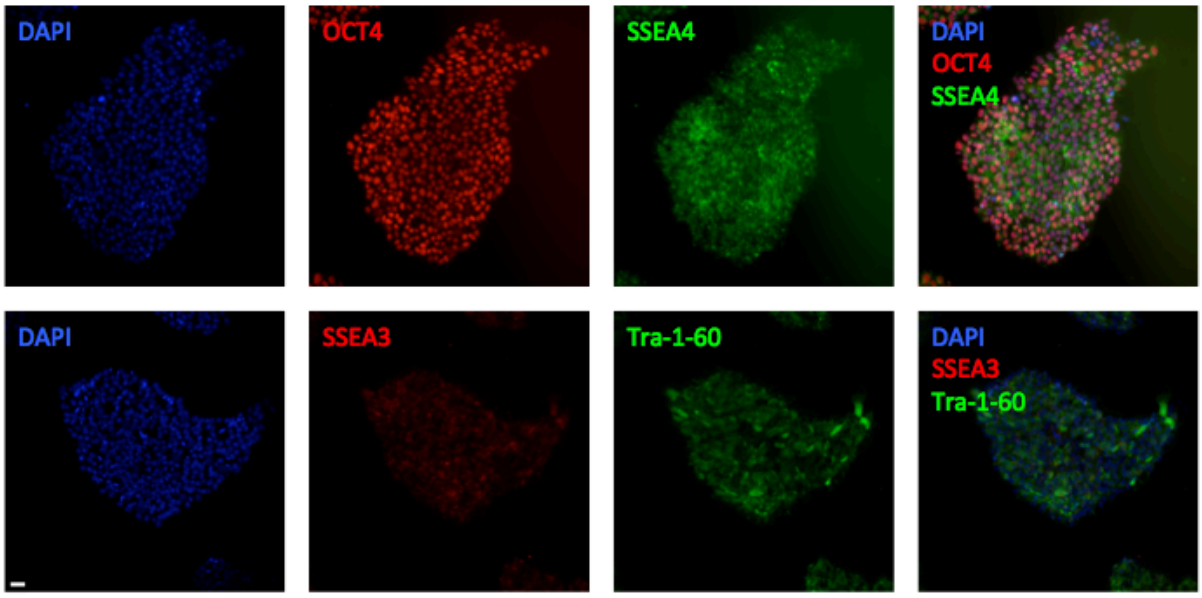

Figure 23. Titin-mEos3.2 hiPSCs express stem cell markers. Titin-mEos3.2 hiPSCs were immunostained for OCT4, SSEA4, SSEA3, Tra-1-60 and Dapi. Scale bar, 100 μm.

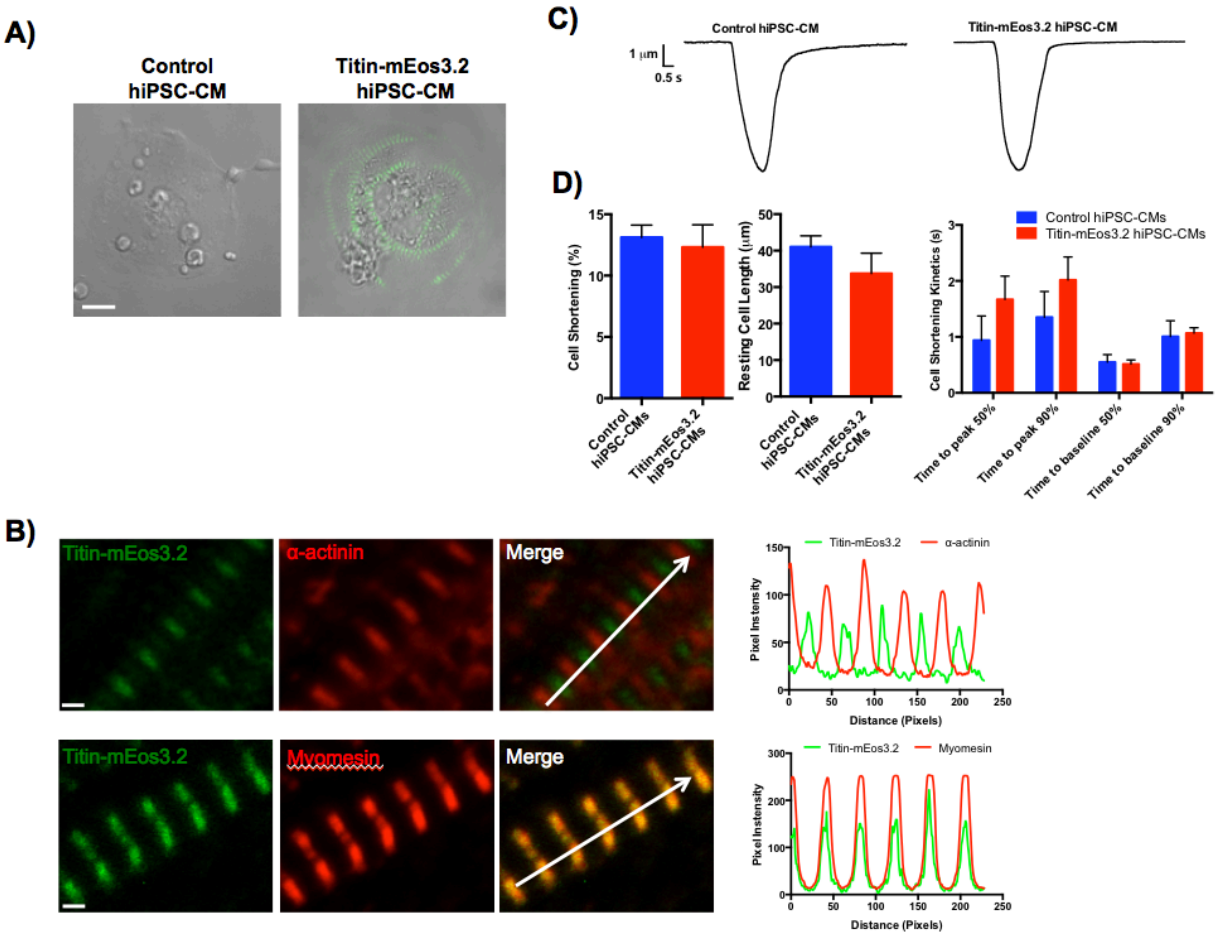

Figure 24. Titin-mEos3.2 hiPSC-CMs express endogenous striated titin-mEos3.2 and are functional. A) Live cell bright field image overlaid with green fluorescence image of day 30 unedited control and titin-mEos3.2 hiPSC-CM. Scale bar is 10μm. B) Day 30 titin-mEos3.2 hiPSC-CMs were fixed and immunostained for Z-disk protein, α-actinin (red, top panels) or M-band protein, myomesin (red, bottom panels). Scale bar is 1 μm . The top panel merged image shows alternating bands of titin-mEos3.2 (green) with α-actinin (red), while the bottom panel merged image shows co-localziation of myomesin (red) and titin-mEos3.2 (green). Shown on the right is the corresponding pixel intensity along the white arrow in the merged images. Scale bar is 1 μm. C) Representative contraction trace of control hiPSC-CM and titin-mEos3.2 (unpaced). D) Contractility evaluation of cell shortening (left) resting cell length (middle) and cell shortening kinetics in control (n=6) and titin-mEos3.2 (n=4) hiPSC-CMs. Panels C and D were performed by Lili Wang, Ph.D.

0.1% DMSO to account for potential solvent toxicity and found no difference in the titin exchange half-life and mobile fraction (Fig. 25A, B, and Table 1). As a control, we assayed for global protein synthesis and found that our CHX dose treatment reduced global protein translation indicating that the fluorescence recovery observed in CHX treated titin-mEos3.2 hiPSC-CMs may be due to pre-existing titin molecules (Fig 26). Our initial results are in agreement with those of da Silva Lopes *et al*[89] suggesting that sarcomeric titin molecules are freely 1) recycled between sarcomeres and/or 2) exchanged between a precursor pool.

4.3c Titin-mEos3.2 reversible photobleaching occurs in fixed hiPSC-CMs

In order to determine if titin-mEos3.2 recovery was due to *de facto* titin movement, we fixed titin-mEos3.2 hiPSC-CMs in 4% PFA for 15 min and permeablized their membranes before performing FRAP. Surprisingly, fixed titin-mEos3.2 hiPSC-CMs had a 55.5 ± 5.3% mobile fraction and a ~3.1 hour exchange half-life which suggested a phenomena known as reversible photobleaching[154] (Fig. 25A,B). One presumption in FRAP is the irreversible quenching of GFP from a bright state to a dark state upon photoablation; however accumulating evidence has suggested otherwise[154,155].

While our initial FRAP assays only quantified the recovery of 2 sarcomeres in the presence of pre-existing fluorescent titin-mEos3.2 molecules, our observable fixed cell fluorescent recovery may in fact be due to, but unlikely, poor sample fixation. However, we postulated that this is not the case; therefore, we employed a secondary confirmatory method where we bleached the entire titin-mEos3.2 cell in order to quench all fluorescence so that any observable recovery will not be due to pre-existing molecules. We first performed whole cell FRAP in untreated control cells and observed a 67.9 ± 8.0 mobile fraction (Fig. 27A-C). We then

Table 1. Mobile fractions and exchange half-lives of titin-mEos3.2 hiPSC-CMs

Treatment	Mobile fraction %	$t_{1/2}$ [h]
Untreated Control (n=4)	68.1 ± 5.7	1.2 ± 0.19
DMSO (n=4)	63.4 ± 5.0	1.3 ± 0.20
Cycloheximide (CHX) (n=3)	62.8 ± 5.2	2.1 ± 0.02*
Fixed (n=3)	55.5 ± 5.3	3.3 ± 0.35*

Data presented as MEAN ± SEM, *, p< 0.05 vs. control, groups compared by ANOVA

Table 1. Mobile fractions and exchange half-lives of titin-mEos3.2 hiPSC-CMs
Data presented as MEAN ± SEM, *, p< 0.05 vs. control, groups compared by ANOVA

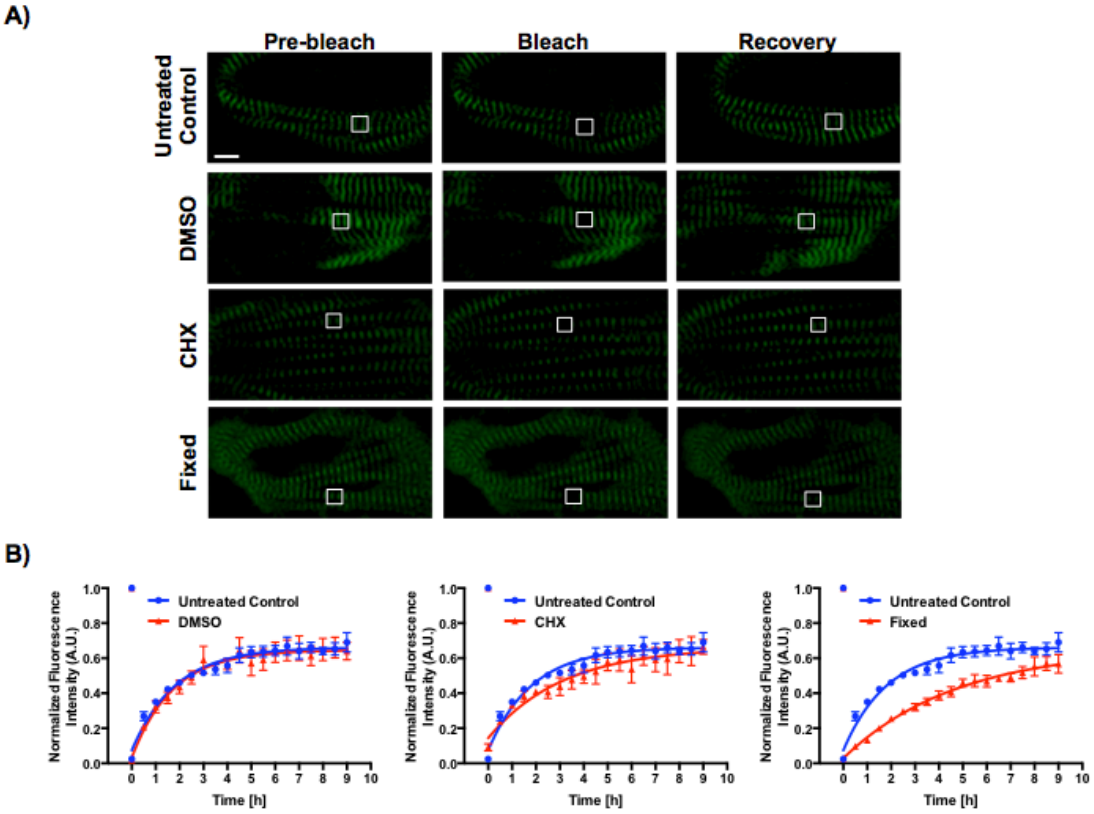

Figure 25. Titin protein dynamics in live and fixed hiPSC-CMs. A) Representative FRAP images (pre-bleach, bleach, recovery) of live and fixed day 30 hiPSC-CMs. Live hiPSC-CMs were treated with 10 µg/mL cycloheximide (CHX), 0.1% DMSO or untreated throughout image acquisition. Fixed hiPSC-CMs were treated with 4% PFA for 15 min and permeablized with 0.5% Triton X-100 in PBS for 15 min before FRAP. An ROI (white outlined box) of 2 sarcomere m-lines were bleached. Scale bar is 5 µm. B) Quantification of FRAP images. FRAP images were acquired every 30 min for 9 hours. Pixel intensities of the ROI, background and whole cell were acquired. Background was subtracted from ROI and whole cell measurements. The ROI was normalized to whole cell pixel intensities. Data was fitted into a one-phase association equation to calculate titin-mEos3.2 exchange half-life. n=4 Control, DMSO, n=3 CHX and Fixed. All data displayed as Mean ± SEM.

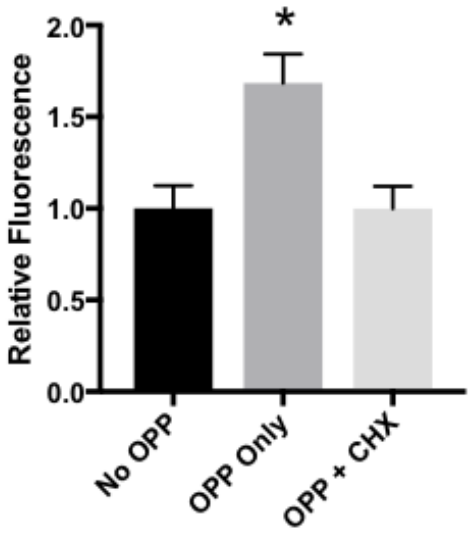

Figure 26. CHX reduces global protein synthesis. Day 30 hiPSC-CMs were pretreated with vehicle or CHX (10 µg/mL) for 30 min in culture. Cells were then treated with a metabolic probe O-propargyl-puromyocin (OPP), OPP+ CHX or no OPP for 1 hour in culture. Cells were then fixed and treated with 5-FAM-Azide for OPP probe detection. Fluorescence was detected (excitation/emission, 485nm/535nm) via Promega Glomax reader. Fluorescence intensity was normalized to no OPP to account for background. Data presented as MEAN ± SEM, *, $p < 0.05$ vs. control, groups compared by ANOVA (n=3-4).

performed whole cell FRAP in CHX and fixed titin-mEos3.2 cells and saw no differences in mobile fractions compared to control (Fig. 27A-C). CHX treatment was included to ensure that any recovery observed must occur via reversible photobleaching and not *de novo* synthesis.

4.3d Cytosolic mEos3.2 display reversible photobleaching properties in non-hiSPC-CMs

To ensure that the fusion of mEos3.2 to titin did not augment mEos3.2 function, we performed FRAP in fixed HEK 293T cells expressing free soluble mEos3.2 protein. FRAP analysis confirmed that reversible photobleaching occurs in fixed unfused mEos3.2 HEK293T cells thus demonstrating that the mEos3.2 tag itself was undergoing this phenomena and was not limited to cell type (Fig 28A-C).

4.5 Discussion

Titin plays a critical role in sarcomere structure and function in striated muscle; however, how titin is incorporated into and dissembled from the sarcomere is poorly understood. With multiple isoforms ranging in molecular weights of 2.97-3.7 mDa, modeling titin dynamics has been problematic. It wasn't until the development of the titin-eGFP knockin mouse model in which titin's dynamic nature was observed[89]. Although, the titin-eGFP mouse model was fundamental in providing initial insight and exploration of titin's rapid exchange at the sarcomere, we sought to test this hypothesis at the human level using CRISPR/Cas9 engineered hiPSC-CMs. Nevertheless, our results differ from those observed in the titin-eGFP cardiomyocyte model.

We report the generation of a novel hiPSC line, titin-mEos3.2 hiPSC, in which one can directly visualize sarcomeres. We focused on tagging the C-terminal end of titin since N-terminal

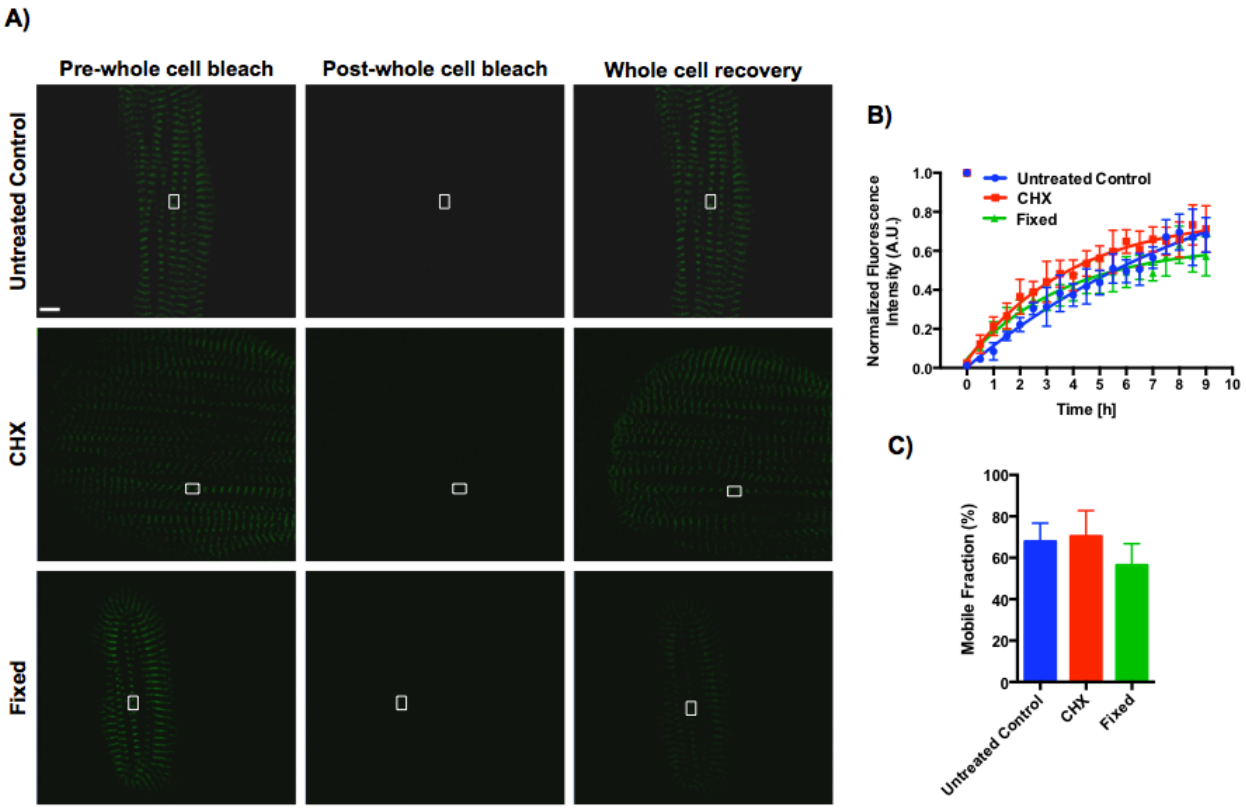

Figure 27. Whole cell titin protein dynamics in live and fixed hiPSC-CMs. A) Representative FRAP images (pre-whole cell post-whole cell bleach, and whole cell recovery) of day 30 hiPSC-CMs. Scale bar is 5 μm. B) Quantification of FRAP images. FRAP images were acquired every 30 min for 9 hours. Pixel intensities of the ROI and background were acquired. Background was subtracted from ROI. Images were normalized to pre-bleach intensities. Data was fitted into a one-phase association equation to extrapolate a recovery rate (n=3). C) Titin-mEos3.2 mobile fractions of untreated control, CHX treated and fixed hiPSC-CMs

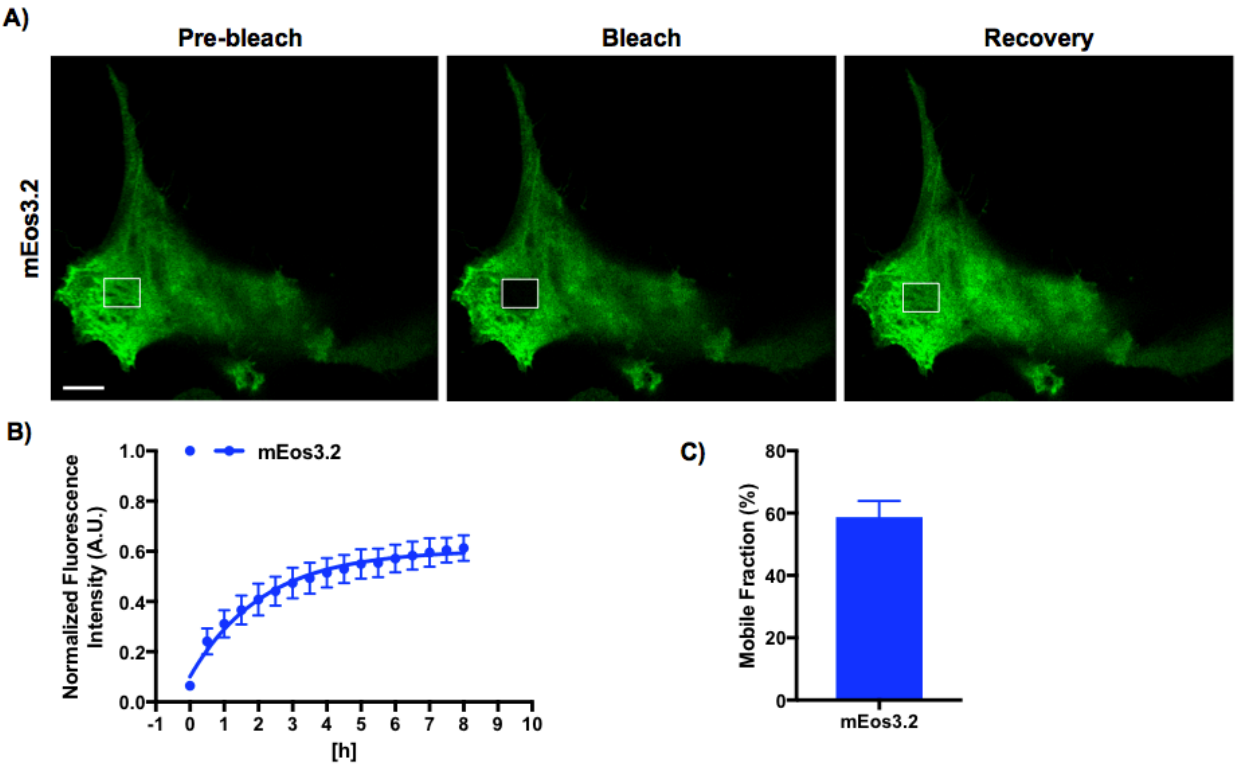

Figure 28. Cytosolic mEo3.2 displays reversible photobleaching in HEK293T cells. A) Representative FRAP images (pre-bleach, bleach, and recovery) of HEK293T cells expressing mEos3.2. Scale bar is 10 µm. B) Quantification of FRAP images. FRAP images were acquired every 30 min for 9 hours. Pixel intensities of the ROI, cell and background were acquired. Background was subtracted from ROI and whole cell. Images were normalized to pre-bleach intensities. Data was fitted into a one-phase association equation to extrapolate a reversible photoswitching rate (n=3). C) Mobile fractions of fixed mEos3.2 expressing HEK293T cells.

tagging of titin with GFP was shown to result in sarcomere dissasembly[153]. At the very C-terminus, titin has been shown to interact with obscurin and obsl1[29]. Our immunolocalization studies demonstrated that the titin-mEos3.2 protein is properly incorporated into the sarcomere suggesting that the mEos3.2 tag does not disrupt sarcomere architecture. We also assessed cell shortening and found no changes in contractility compared to the unedited control line. Our cellular shortening percent is comparable to previously reported ~9% cell shortening in control hiPSC-CMs[100]. Our data demonstrates that the insertion of mEos3.2 into hiPSCs via CRISPR/Cas9 gene editing did not disrupt hiPSC pluripotency, cardiomyocyte differentiation, and cardiomyocyte function.

At the sarcomere, titin binds to over 25 different proteins, each with different affinities. For proper incorporation and removal, titin not only has to overcome these interactions but also the interactions that the binding proteins have with other sarcomere proteins. For example, within the M-band, the titin, obscurin, obscurin-like-1 and myomesin are all crosslinked to form a stable ternary network. Both the titin-obscuin and obscurin-like-1 interactions require at least 30pN for disruption; whereas obsurcin-1-myomesin complex can withstand forces up to ~ 135pN thus making the M-band stable[52,53]. Regarding the A-band, titin is tightly associated with myosin heavy chain and regarded as a molecular ruler for thick filament assembly due to the coincidental ~43 nm spacing of myosin molecules to the spacing of it's 11-domain FnIII/Ig super repeat along the A-band[156,157]. With respect to the Z-disk, the multiple titin/alpha actinin interactions contribute to long-term stability[31]. Therefore, all of these described interactions contribute to the notion that titin movement needs to overcome multiple strong interactions within the sarcomere in order to move fluidly. We performed FRAP as an assay to test the hypothesis that titin was a dynamic and mobile protein.

At baseline, we report a titin exchange half-life 1.2 hours with a 68% mobile fraction. Our results are strikingly similar to the baseline results of da Silva Lopes et al's reporting a 2.5-hour titin-eGFP exchange half-life with 49% mobile fraction. To further confirm the titin recycling model, we performed FRAP on CHX treated cells to assay the role of protein synthesis. Inhibition of protein synthesis did not alter the titin mobile fraction, which supports the idea of recycling as it may serve as a useful strategy instead of only relying on *de novo* synthesis for titin's perceived dynamic incorporation.

Nevertheless, we wanted to perform an additional control to validate our and da Silva Lopes et al's findings. Therefore, we additionally tested the titin exchange model by fixing and permeablizing the titin-mEos3.2 hiPSC-CMs prior to FRAP in order to verify that titin recovery was due to true titin-mEos3.2 movement. However, we found substantial recovery in fixed cells suggesting that the rate and mobile recovery of fixed titin-mEos3.2 was not due to physical movement of titin molecules *per se* but to an intrinsic GFP phenomena known as reversible photobleaching[154].

One presumption in FRAP is the irreversible quenching of GFP from a bright state to a dark state upon photoablation[80]; however, accumulating evidence has demonstrated that reversible photobleaching can impact FRAP studies leading to an artifactual overestimation of protein mobility by as much as 9%, 15%, and 60% under different experimental conditions[154,155,158]. Our 9 hour time-lapse FRAP acquisition demonstrated that fixed cells recovered to the degree of untreated titin-mEos3.2 hiPSC-CMs. Although the fixed titin-mEos3.2 rate was significantly slower, we postulate that the rate represents mEos3.2 achieving reversible fluorescence equilibrium[82]. We further postulate that the observable differences in mobile fractions of titin-mEos3.2 and titin-eGFP are due to their own fluorescent protein's intrinsic

photoswitching properties. It would be interesting to compare the reversible photobleaching phenomena in titin-eGFP or cells expressing eGFP alone.

We further validated our findings by performing whole cell FRAP experiments as a secondary method of confirmation. Whole cell FRAP on CHX, fixed, and control cells recovered to a similar degree with no statistical differences thus confirming the reversible photobleaching phenomena. We postulate that the failure to account for reversible photobleaching led to an overestimation of titin mobility in mouse titin-eGFP cardiomyocytes; therefore, our model and da Silva Lopes et al's titin-eGFP model[89] cannot be confidently used to assay titin dynamics in living cells as the amount of true titin recovery is less and far slower than the rate of reversible photobleaching displayed by fluorescent proteins. Our results may have significant impact on other investigator's work where long term FRAP imaging was conducted such as Ojima et. al[159].

Long-term imaging of single cell dynamics requires effort in the maintenance of culture conditions, minimization of phototoxicity, and maximization of data acquisition[160]. Our results strongly indicate that researchers should exercise caution in the extrapolation of reliable FRAP data in long-term cell imaging.

Chapter 5

Summary and Future directions

5.1 Summary

This dissertation presents novel and unique insight into the homeostatic control of the giant protein, titin, in the cardiac sarcomere. The understanding of the molecular events governing titin turnover still remains poorly understood; nevertheless the projects described in this dissertation served to elucidate key components in our understanding of the titin life cycle. Prior to the dissertation, the field's consensus was that titin was presumably transcribed, exported, translated, and dynamically incorporated/exchanged in the sarcomere before degradation. The experiments described in the previous chapters have addressed 3 major findings.

1) Titin is post-transcriptionally regulated at its 5'-UTR via *cis*-regulatory uORFs.
2) Titin is post-transcriptionally regulated by miR-26a/b at its 3'-UTR.
3) Titin is not a dynamic and mobile protein that is undergoing continuous exchange between myofibrils.

These findings can be summarized in the following revised titin life cycle model (Fig. 29)

5.2 Chapter II: Summary and future directions

In Chapter 2, we demonstrated that titin mRNA is localized in the cytosol and sarcomere with a relatively stable ~66 hour mRNA half-life. We also provide evidence that titin translation is in part regulated via its 5'-UTR through 2 *cis*-regulatory uORFs which serve to negatively regulate translational efficiency. We also demonstrated that this property is resistant to

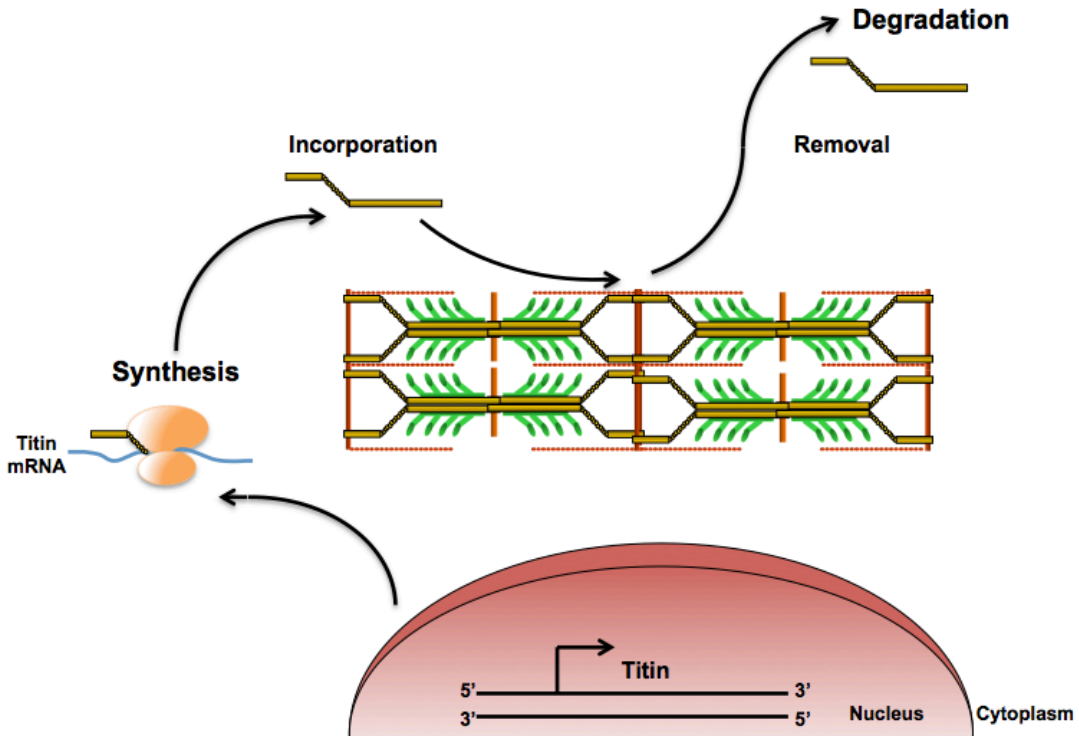

Figure 29. Revised titin life cycle. Titin mRNA is localized in the cytoplasm and sarcomere where it is presumably translated under tight regulation of the 5'-UTR and 3'-UTRs. Newly translated titin protein is incorporated into sarcomere. Over time, titin is removed from the sarcomere and sent for degradation.

hypertrophic stimuli such as growth factors, mechanical stress, and electrical pacing, but altered under specific cardiotoxic stresses. We concluded that the uORFs within the titin 5'-UTR serves a negative regulator in the translation of titin in order to prevent overproduction of titin which is metabolically costly.

5.2a Titin mRNA visualization

Although Chapter 2 provided insight into the translational regulation of titin, many questions regarding titin translation still remain. Spatiotemporal regulation of translation is pertinent for the proper production and transportation of newly synthesized polypeptides. Given titin's stable mRNA half-life, this is particularly relevant for titin as it's molecular weight ranges from ~3.0- 3.8 mDa thus requiring an enormous amount of energy and cellular resources to synthesize and transport this macromolecule. The reporting of striated titin mRNA and titin protein co-localiztion would suggest onsite translation as this notion is supported by the observation of striated 60S ribosomal subunits[121,122,134]. Our titin-mEos3.2 hiPSC-CMs visibly express only striated titin in live cells however, we cannot rule out the existence of a small soluble pool, as confocal microscopy was our only means of detection. Additional support for the sarcomere onsite translation hypothesis stems from our findings where titin is not a mobile and dynamic protein meaning that it would be energetically unfavorable for a molecule of titin to be shuttle around and among myofibrils. Together these observations beget the question, where is titin mRNA transported to and where is it translated? This question would be important to resolve, as insight would provide better understanding of sarcomere homeostasis.

Real-time detection of titin mRNA translation would provide a means to answering this question. Advances in mRNA labeling approaches have been demonstrated to accurately

visualize, with high resolution, active translation at the single mRNA level[161]. For example, the Sun-Tag system is a two-protein approach used to visualize nascent proteins. By the introduction of tandem short peptide GCN4 epitopes via CRISPR/Cas9 editing into the titin loci along with the stable expression of a endogenous single-chain variable fragment (scFv) antibodies fused to GFP, one can visualize active areas titin translation as the scFV binds to the GCNR epitopes[162]. Since multiple ribosomes have been demonstrated to occupy titin, the GFP signal would be a bright fluorescent dot with a higher signal to noise ratio than background scFv-GFP fusion protein alone[69]. Furthermore, to ensure that translation is actively occurring at the site of the mRNA, one can also generate a live cell mRNA reporter via the introduction of PP7 hairpins which have been demonstrated to bind to a tdTomato-labeled PP7-coat protein (tdPCP)[161]. This dual reporter approach would not only identify titin mRNA localization in real-time but illuminate the location of active titin translation thus fulfilling a longstanding question of spatiotemporal regulation of titin synthesis.

5.2b Functional significance of the uORF in hiPSC-CMs

With regards to the uORF, it would be pertinent to determine if they have any physiological relevance to titin. Our initial studies examined how the *cis*-regulatory elements affected titin translation via a surrogate reporter gene. It would be important to determine if these uORFs do in fact affect titin translation by using CRISPR/Cas9 gene editing to disrupt the uORFs in titin-mEos3.2 hiPSC-CMs creating a new titin-mEos3.2-uORFdel model. This *in vitro* approach would allow one to quantify titin protein levels via biochemical approaches, which was something that our initial studies lacked and would provide insight into the functional consequences of disrupting the uORFs in a living cell. If the uORFs regulate titin protein

expression, it would be interesting to observe the functional consequence of titin overproduction since it has not been possible to generate such a model before. Would there be titin aggregation? Having the uORFdel in the titin-mEos3.2 line would allow for a quick visualization of aggregation. Polysome profiling would be an effective assay to use to determine if the uORF regulate titin translation as disrupting the uORF would in theory lead to more ribosomes occupying titin mRNA. Another interesting approach would be to determine if the titin uORFs result in the expression of a small regulatory peptide, (small ORF, smORF) that affects biological activity as recent studies suggest that approximately 10-15% genome encodes these bioactive smORFs[163].

5.3 Chapter III: Summary and future directions

In Chapter 2, we tested the hypothesis that titin is regulated by *cis*-regulatory sequences at the 5'-UTR and found that titin is regulated via uORFs. This finding led us to consider the role the titin 3'-UTR in regulating its translational efficiency. We tested the hypothesis that titin is post-transcriptionally regulated by its 3'-UTR. We identified two titin 3'-UTRS in both mouse and human heart tissue. Using the canonical titin 3-UTR sequence, we generated a mouse titin 3'-UTR reporter and found that it significantly repressed translation efficiency. *In silco* analysis of titin 3'-UTR identified a conserved miRNA binding site, miR-26a/b therefore we tested hypothesis that miR-26a/b regulate titin gene expression. We demonstrated titin miR-26a/b dependent regulation. Our results imply that titin is post-transcriptionally regulated by miR-26a/b.

5.3a Alternative cleavage and polyadenylation (APA)

Our 3' RACE assay identified two titin 3'-UTRs. One hypothesis could be that titin mRNA undergoes APA. APA is an important widespread 3' processing event as approximately 70% of mammalian genes undergo APA. APA has been shown to affect mRNA metabolism, localization and stability[144]. Given the identification of multiple titin 3'-UTRs in both human and mouse heart tissue, we speculate that titin mRNA may undergo APA; however, a second method such as 3' end deep sequencing should be used to verify the existence of a short titin 3'-UTR.

In the context of the heart, cardiac hypertrophy is generally associated with increased gene transcription; however, post-transcriptional regulation by global 3'-UTR shortening has emerged as an important mode of modulating protein expression independent of transcriptional input[164,165]. Shorter 3'-UTRs are generally associated with cell growth and proliferation as the truncated 3'-UTRs may remove *cis*-regulatory sequences associated with repression[144]. It would be interesting to determine which titin 3'-UTR is preferentially expressed under growth stimulation.

Fluorescent *in situ* hybridization of titin mRNA localized titin to both the cytosol and sarcomere[134]. Subcellular targeting via alternate 3'-UTRs could explain the heterogeneity in titin mRNA localization as there are zipcode sequences within the 3'-UTRs of genes that localize mRNAs[166]. Evidence for this stem from short brain-derived neurotrophic factor (BDNF) studies where the short BDNF 3'-UTR is restricted to the somata of hippocampal neurons and the long BDNF 3'-UTR is localized in at the dendrites[167].

5.3b Role of miR-26a/b

We sought to determine if titin expression was regulated in part by miRNAs therefore we performed an *in silico* analysis and identified miR-26a/b as a putative target. In Chapter 3 we provided preliminary evidence suggesting that miR-26a treatment downregulates titin protein expression in NRVM. This experiment was an N=1 hence the need for further replication and validation. Although we provided evidence demonstrating that miR-26a/b target the mouse titin 3'-UTR, it would be important to recapitulate this interaction and determine if this interaction is conserved in humans. Furthermore, it would also be beneficial to confirm a miR-26a/b titin interaction *in vivo* to demonstrate that there is a physiological interaction. One method would be to use an unbiased approach such as crosslinking immunoprecipitation coupled with high-throughput sequencing (HITS-CLIP) in mouse and human tissue[147]. Such an experiment would also allow for the validation of miR-26a/b binding to titin as well as the identification of other novel binding miRNAs as mRNAs have been shown to be the target of multiple miRNAs[148].

5.4 Chapter 4: Summary and future directions

The titin-mEos3.2 model is the first of its kind and allows for real-time visualization of titin in contracting human cardiomyocytes. In Chapter 4, we described the generation of the titin-mEos3.2 cell line to test the hypothesis that titin was a dynamic and mobile protein. Our work was built upon the assumption of da Silva Lopes et al initial study where they observed a titin ~45% mobile fraction and 2.4 hour exchange half-life in their mouse titin-eGFP line[89]. Originally, our work was to build and expand on the mechanisms that control titin incorporation and degradation by identifying potential cell biological pathways such as proteasomal degradation and microtubules trafficking in hopes to better understand titin movement. Our early

FRAP studies initially confirmed da Silva Lopes et al's findings; however, when examined closely, we discovered a discrepancy in titin mobility. Upon performing a control FRAP experiment in 4% PFA fixed and permeablized titin-mEos3.2 hiPSC-CMs, we observed titin-mEos3.2 recovery. We found that titin-mEos3.2 recovered to the same extent as it did in live hiPSC-CMs which prompted us to raise concern regarding the original titin recycling model put forth by da Silva Lopes et al. In our results, at least ~81% of the mobility could be explained by reversible photobleaching. Furthermore, we confirmed our findings by performing whole cell FRAP on untreated, CHX treated and fixed titin-mEos3.2 hiPSC-CMs where we demonstrated that each group recovered to a similar extent. We concluded that the reason why titin-mEos3.2 recovered in a fixed cell was to due to reversible photobleaching. Our findings also raise significant concerns for any investigator preforming long-term FRAP studies regarding myofilaments proteins or other proteins in general where reversible photobleaching was not accounted for.

Despite our initial studies, the titin-mEos3.2 model still has potential uses that extend beyond that of sarcomere biology; the hiPSC titin-mEos3.2 cell line can be used as a robust high throughput *in vitro* platform for preclinical discovery and/or screening of drugs that affect the contractile properties of the heart.

5.4a Reevaluating titin turnover in hiPSC-CMs

Our model was initially developed to assay titin turnover *in situ*. It appears that the use of mEos3.2, let alone any other photoconvertabile GFP may not be accurate in quantifying the true exchange and turnover of titin. It would then be appropriate to use pulse chase assays to quantify titin turnover in hiPSC-CMs; however, these studies would only assay global titin turnover.

These experiments would be technically challenging as solubilization and loading of titin lysates require unconventional methods. These types of experiments would be important in our understanding the regulation of the giant protein; however, they lack the spatiotemporal component of turnover at the sarcomere.

Therefore, it is still crucial to develop a novel live cell reporter with an appropriate fluorophore that displays no reversible photoswitching in order to assess true titin dynamics. The organic fluorophore, tetramethylrhodamine (TMR), bound to a modified haloalkane dehalogenase (HaloTag) has been successfully used for FRAP and does not display any reversible photobleaching unlike conventional fluorescent proteins[82]. The HaloTag is a 2-part detection system where the HaloTag covalently binds to a chloroalkane linker that is chemically attached to a fluorescent dye[168]. Initially this technology was developed in order to circumvent the use of one specific tagging system for proteins, meaning that the HaloTag can bind to multiple types of synthetic HaloTag ligands that are applicable for various types of functions from visualization to purification[168].

Ideally, we should use this type of tagging system with titin by adopting a similar strategy of the mEos3.2 knock-in approach. By using CRISPR/Cas9 gene editing to insert a HaloTag to the C-terminal end of titin in control un-CRISPR/Cas9 edited line, one can generate an endogenously tagged titin molecule. The HaloTag ligand is cell permeable and can easily covalently attach to the HaloTag protein under physiological conditions. At this time, there aren't any commercially available photoconvertabile dyes; until one is developed, the model is limited to only quantifying exchange and mobility. With this novel model, titin-HaloTag hiPSC-CM, one can then begin to address true titin exchange and mobility within the sarcomere complex, which has yet to be described.

After establishing the true baseline titin kinetics, we can begin to address the importance of titin movement as titin molecules may require some form of cellular transport machinery. Microtubules have been implicated in sarcomere myosin movement and organization during myofibrillogenesis sarcomere assembly[169-171]. Regardless, with a valid model, one can reliably test how certain perturbations from microtubules to chaperones affect titin dynamics.

5.4b Sarcomere homeostasis in dilated cardiomyopathy

Dilated cardiomyopathy (DCM) is the leading cause heart failure in the United States. Although the etiology is heterogeneous, many mutations key sarcomeric, cytoskeletal and splicing genes lead to the development of DCM[63]. HiPSC-CMs can serve as a useful surrogate to model cardiovascular disease *in vitro*[67]. Coupling CRISPR/Cas9 gene editing to hiPSC technology, one can then begin to edit in patient specific mutations, gene corrections or knock out genes at the human genome level in order to gain insight into cardiomyocyte biology and disease pathophysiology. In a landmark study, titin-truncating variants (TTNtvs) were found to be the cause of ~25% of idiopathic dilated cardiomyopathy; therefore, homeostatic control is crucial in titin turnover, as damaged proteins would presumably be degraded[65]. The question then becomes, what happens to titin in the context of disease? It is currently unknown how these truncating variants cause disease. One arching question in the field stems from whether these mutant proteins are even expressed and incorporated into the sarcomere.

The next step would be to use CRISPR/Cas9 gene editing to knock-in a TMR-Halo-tag to the c-terminal end of a truncating titin variant in order to elucidate it's role in sarcomere function. This model would have to be a heterozygous truncating mutation as homozygous mutations fail to form sarcomeres[67,86,172]. This dual labeling strategy would allow for the

visualization of both full-length titin-mEos3.2 and truncated titin-TMR-Halo-Tag proteins in live hiPSC-CMs. The TMR-Halo-Tag can be used for FRAP without fear of reversible photobleaching[82]. The absence of truncated protein would be crucial as this particular titin mutation may result in an unstable protein that is degraded quickly. The absence or presence of a truncated titin would resolve this dilemma in the field. This is a possible second step in elucidating titin's role in disease as preliminary evidence highlights the feasibility of this approach (Fig. 29). Figure 29 demonstrates the generation of a TTNtv in hiPSC-CMs. Work in this field would expand our current knowledge of titin turnover.

There is a caveat with this model since the structure of a C-terminal end of a titin-truncating variant or any TTNtvs are unknown. Therefore a possible confounder would be that the tag disrupts titin binding to myosin heavy chain or myosin binding protein c as the A-band domain of titin is divided into Ig and FNII super-repeats that are important in thick filament orientation[22]. An important control to generate would be a TTNtv line without a CRISPR/Cas9 edited TMR-Halo-Tag would be important to determine if the tag itself disrupts sarcomere architecture more so than the truncated titin itself. Given that the central importance of titin in cardiac structure and function, the potential identification, expression, and incorporation of TTNtvs in the sarcomere would answer a current longstanding debate.

5.3c Microcontact printing for high throughput screening

HiPSC-CMs display myofibrils with varying size, shape and organization on 1:200 Matrigel substrate. Although the substrate allows for the promotion of sarcomerogenesis/sarcomere maintenance, these cells do not shorten. When seeded on undiluted.

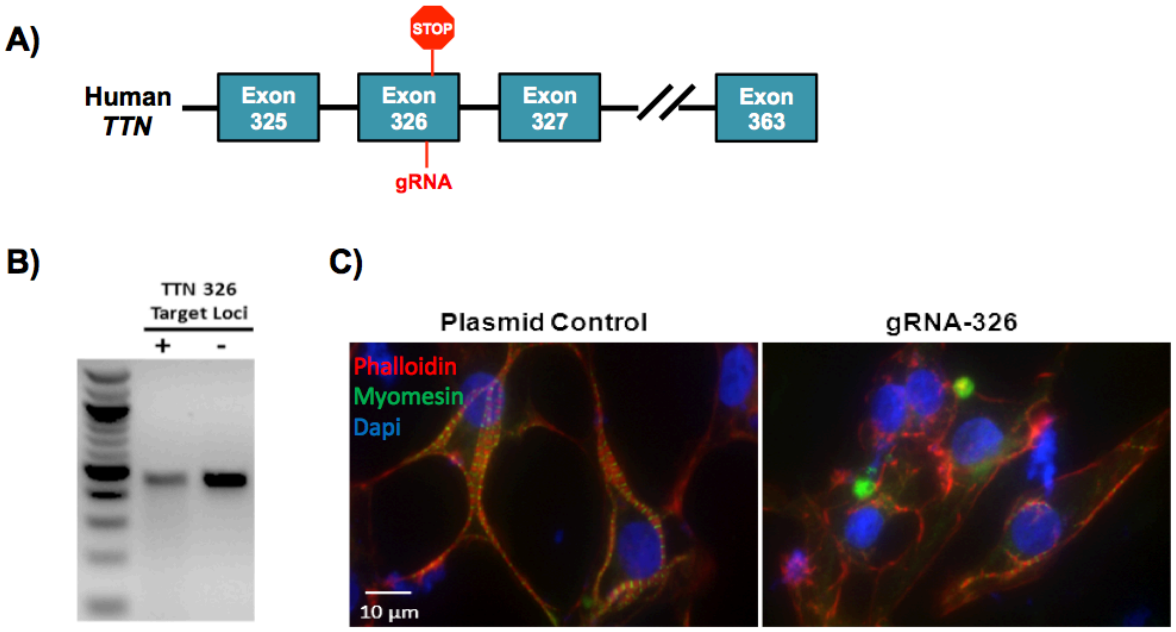

Figure 29. TTNtv gRNA 326 targets titin resulting in sarcomere disarray. A) TTNtv gRNA 326 knock out strategy. B) TTNtv 326 gRNA targets titin in T7 endonculease assay. + denotes T7 endonuclease, - denotes no nuclease. C) Day 14 hiPSC-CMs were transiently transfected with plasmid control or TTNtv326 gRNA.

Matrigel (Matrigel Mattress), we found that the cells took an elongated rod shape with anisotropic myofibrils that allowed for the ability to shorten[100]. This technological breakthrough. allowed for the first single cell assessment of contractility in hiPSC-CMs. This was a novel platform in evaluating hiPSC-CM function; however, 48hr time-lapse microscopy revealed that these cells were quite mobile and dynamic (Data not shown) on the Mattress. HiPSC-CMs plated on the mattress therefore could not be reliably used for FRAP experiments in Chapter 4 as they would move throughout the 9 hr recording. Furthermore, undiluted Matrigel displays autofluorescence in the 488 nm channel which is the same wavelength used to detect titin-mEos3.2 as this property decreases the signal to noise ratio in titin-mEos3.2 detection.

Geometric cues have been demonstrated to influence cardiomyocyte morphology and sarcomere alignment[173]. A method to circumvent this issue and allow for the standardization of myofibril alignment would be microcontact printing. Microcontact printing coupled to a soft hydrogel polymer at an ideal 7:1 aspect ratio would allow for a more physiological assessment of sarcomere architecture[101]. This approach is feasible as Figure 30 shows the titin-mEos3.2 hiPSC-CMs on a microcontact print. Future research could develop this platform with the goal to screen for cardiotoxic/cardioprotective compounds, as one would only have to score myofibril alignment. This offers a unique advantage than conventional staining as this approach could be assayed in real-time in living cells. An example would be to pre-treat titin-mEos3.2 hiPSC-CMs with a cardiotoxic compound and score sarcomere disarray. After scoring, the titin-mEos3.2 hiPSC-CMs would be washed and treated with compounds form library. Restoration in sarcomere architecture would be used to identify a potential hit. This is only one example that the titin-mEos3.2 hiPSC-CMs could be used for in drug discovery. The approach just described only takes into consideration hiPSC-CMs cultured on two-dimensions. Three-dimensional

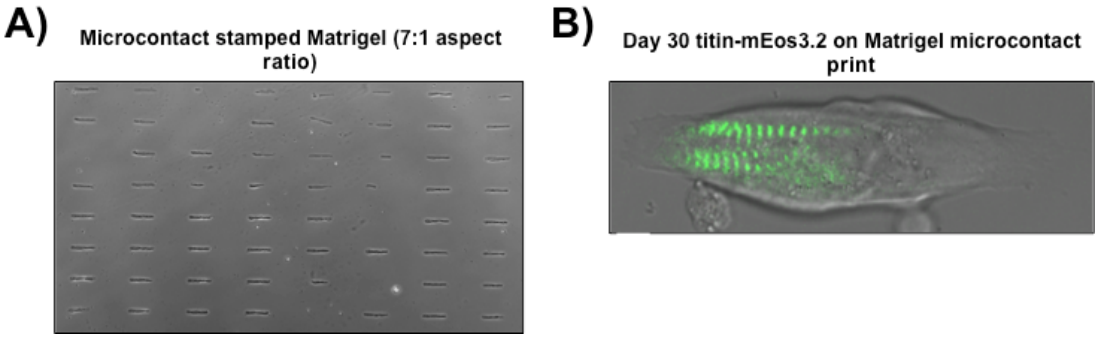

Figure 30. Matrigel micropatterned printing technologies standardize mophological analysis of hiPSC-CMs. A) A polydimethylsiloxane stamp was designed using a 7:1 aspect ratio pattern and was utilized to establish a Matrigel micropatterned array. Live cell image of day 30 titin-mEos3.2 hiPSC-CM conferring to the micropattern. Scale bar is 5 μm.

approaches using engineered heart tissue (EHT) seeded with hiPSC-CMs have been adopted to generate a more physiological model as they display organized sarcomeres and relatively mature protein expression profile[174]. Ideally it would be interesting to use the titin-mEos3.2 with EHT to assess sarcomere architecture and function, as they are closer to tissue for drug screening purposes.

APPENDIX

Photoconversion

Our titin-mEos3.2 hiPSC line has an endogenous photoconvertable GFP, mEos3.2, genetically encoded into the C-terminal of exon 363 in the titin gene. Our main finding in Chapter 4 concluded that titin is not a dynamic and mobile protein in hiPSC-CMs since we discovered that that majority of fluorescence recovery was due to reversible photobleaching. Understanding this caveat, we wanted to test the hypothesis that titin is recycled at the level of the sarcomere.

Irradiation of mEos3.2 with UV light results in irreversible transition from green into a very photostable, bright-red fluorescence, that can be tracked for days without significant photobleaching[152]. This fluorescent "pulse chase" of titin-mEos3.2 allows for accurate and continuous tracking of a subpopulation of photoconverted "red" titin proteins that are easily distinguishable from *de novo* synthesized "green" titin proteins. This method is superior as it does not require cycloheximide to block potential secondary effects of global protein translation and obviates the limitations of standard FRAP in that photobleached protein populations cannot be tracked beyond the point of photobleaching.

We photoconverted whole hiPSC-CMs from green fluorescing titin-mEos3.2 signal to red. After photoconversion, an ROI encompassing two sarcomeres was photoablated. Within 2 hour, red-titin-mEos3.2 proteins reincorporated into the photoablated area, potentially demonstrating that *de novo* titin synthesis may not required for sarcomeric titin exchange (Fig 31A). We found the recycled exchange half-life to be ~6 min with ~20% mobile fraction (Fig. 31B). However, we cannot confidently state that the signal recovery is indeed recycled titin. 3

potential explanations may account for the measured signal. 1) The photoconverted titins may be recycled from pre-existing sarcomeres. 2) The signal recovery may be due to freshly translated and transported titins from cytosolic precursor pool. 3) The signal recovery was due to reversible photoswitching from the red mEos3.2 dark state to a bright state. Given our observations that reversible photobleaching accounts for titin recovery in PFA fixed hiPSC-CMs, we cannot rule out the possibility that the red photoconverted titin-mEos3.2 proteins are from reversible photobleaching and not recycling or cytosolic transport. This experiment should be conducted in PFA fixed and permeablized hiPSC-CMs before any conclusion be confidently drawn.

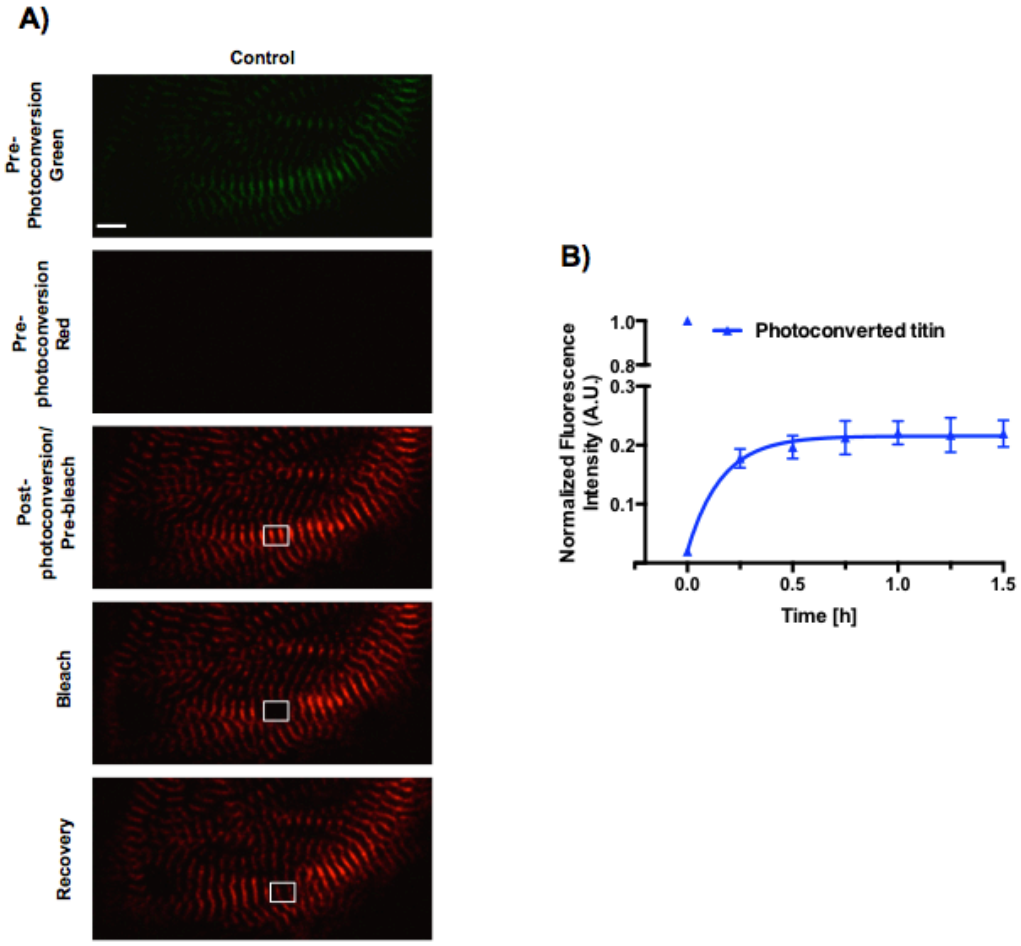

Figure 31 In situ titin recycling rate. A) Representative images of dual photoconversion/ FRAP experiments. Cells were then photoconverted prior to FRAP. After photoconversion, a ROI was photoablated in titin-mEos3.2 hiPSC-CMs using 100% laser power at 561nm. Images were collected every 15 min post-photoablation. Scale bar is 5 μm. B) Quantification of titin recycling. Pixel intensities of the ROI, background and whole cells were acquired every 15 min for 2 hours. Background was subtracted from ROI and whole cell measurements. The ROI was normalized to whole cell pixel intensities. Data was fitted into a one-phase association equation to calculate titin-mEos3.2 exchange half-life and mobility. Percent titin recycling was quantified by (photoconverted titin mobile fraction/ titin baseline mobile fraction)*100 at the 1.2 h exchange half-life.

REFERENCES

1 Tirziu, D., Giordano, F. J. & Simons, M. Cell communications in the heart. *Circulation* **122**, 928-937, doi:10.1161/CIRCULATIONAHA.108.847731 (2010).

2 Hooke, R. & Royal, S. Philosophical collections. 7 v. in 1 (1679).

3 Krause, W. *Die motorischen Endplatten der quergestreiften Muskelfasern. Mit einem Vorwort, die Lebensbeschreibung von C. Krause enthaltend*. (Hahn, 1869).

4 Schafer, E. A. On the Minute Structure of the Muscle-Columns or Sarcostyles Which form the Wing-Muscles of Insects. Preliminary Note. *Proceedings of the Royal Society of London* **49**, 280-286 (1890).

5 Tskhovrebova, L. & Trinick, J. Titin: properties and family relationships. *Nature reviews. Molecular cell biology* **4**, 679-689, doi:10.1038/nrm1198 (2003).

6 LeWinter, M. M. & Granzier, H. Cardiac titin: a multifunctional giant. *Circulation* **121**, 2137-2145, doi:10.1161/CIRCULATIONAHA.109.860171 (2010).

7 Huxley, A. F. & Niedergerke, R. Structural Changes in Muscle During Contraction: Interference Microscopy of Living Muscle Fibres. *Nature* **173**, 971-973 (1954).

8 Huxley, H. & Hanson, J. Changes in the Cross-Striations of Muscle during Contraction and Stretch and their Structural Interpretation. *Nature* **173**, 973-976 (1954).

9 Hanson, J. & Huxley, H. E. Structural basis of the cross-striations in muscle. *Nature* **172**, 530-532 (1953).

10 Squire, J. M. Muscle contraction: Sliding filament history, sarcomere dynamics and the two Huxleys. *Global Cardiology Science and Practice* **2016**, doi:10.21542/gcsp.2016.11 (2016).

11 Huxley, H. E. & Hanson, J. Quantitative studies on the structure of cross-striated myofibrils. I. Investigations by interference microscopy. *Biochimica et biophysica acta* **23**, 229-249 (1957).

12 Hanson, J. & Huxley, H. E. Quantitative studies on the structure of cross-striated myofibrils. II. Investigations by biochemical techniques. *Biochimica et biophysica acta* **23**, 250-260 (1957).

13 Wang, K. Sarcomere-associated cytoskeletal lattices in striated muscle. Review and hypothesis. *Cell Muscle Motil* **6**, 315-369 (1985).

14 Huxley, A. F. & Peachey, L. D. The maximum length for contraction in vertebrate straiated muscle. *The Journal of physiology* **156**, 150-165 (1961).

15 Locker, R. H. & Leet, N. G. Histology of highly-stretched beef muscle. IV. Evidence for movement of gap filaments through the Z-line, using the N2-line and M-line as markers. *J Ultrastruct Res* **56**, 31-38 (1976).

16 Maruyama, K., Natori, R. & Nonomura, Y. New elastic protein from muscle. *Nature* **262**, 58-60 (1976).

17 Maruyama, K. Connectin, an elastic protein from myofibrils. *J Biochem* **80**, 405-407 (1976).

18 Etlinger, J. D., Zak, R. & Fischman, D. A. Compositional studies of myofibrils from rabbit striated muscle. *The Journal of cell biology* **68**, 123-141 (1976).

19 Wang, K., McClure, J. & Tu, A. Titin: major myofibrillar components of striated muscle. *Proceedings of the National Academy of Sciences of the United States of America* **76**, 3698-3702 (1979).

20 Maruyama, K., Kimura, S., Ohashi, K. & Kuwano, Y. Connectin, an elastic protein of muscle. Identification of "titin" with connectin. *J Biochem* **89**, 701-709 (1981).

21 Bang, M. L. *et al.* The complete gene sequence of titin, expression of an unusual approximately 700-kDa titin isoform, and its interaction with obscurin identify a novel Z-line to I-band linking system. *Circulation research* **89**, 1065-1072 (2001).

22 Linke, W. A. & Hamdani, N. Gigantic business: titin properties and function through thick and thin. *Circulation research* **114**, 1052-1068, doi:10.1161/CIRCRESAHA.114.301286 (2014).

23 Kontrogianni-Konstantopoulos, A., Ackermann, M. A., Bowman, A. L., Yap, S. V. & Bloch, R. J. Muscle giants: molecular scaffolds in sarcomerogenesis. *Physiol Rev* **89**, 1217-1267, doi:10.1152/physrev.00017.2009 (2009).

24 Cazorla, O. *et al.* Differential expression of cardiac titin isoforms and modulation of cellular stiffness. *Circulation research* **86**, 59-67 (2000).

25 Granzier, H. L. & Labeit, S. The giant protein titin: a major player in myocardial mechanics, signaling, and disease. *Circulation research* **94**, 284-295, doi:10.1161/01.RES.0000117769.88862.F8 (2004).

26 Helmes, M., Trombitas, K. & Granzier, H. Titin develops restoring force in rat cardiac myocytes. *Circulation research* **79**, 619-626 (1996).

27 Neagoe, C. *et al.* Titin Isoform Switch in Ischemic Human Heart Disease. *Circulation* **106**, 1333-1341, doi:10.1161/01.cir.0000029803.93022.93 (2002).

28 Neagoe, C., Opitz, C. A., Makarenko, I. & Linke, W. A. Gigantic variety: expression patterns of titin isoforms in striated muscles and consequences for myofibrillar passive

stiffness. *Journal of Muscle Research & Cell Motility* **24**, 175-189, doi:10.1023/a:1026053530766 (2003).

29 Gautel, M. & Djinovic-Carugo, K. The sarcomeric cytoskeleton: from molecules to motion. *The Journal of experimental biology* **219**, 135-145, doi:10.1242/jeb.124941 (2016).

30 Bertz, M., Wilmanns, M. & Rief, M. The titin-telethonin complex is a directed, superstable molecular bond in the muscle Z-disk. *Proceedings of the National Academy of Sciences of the United States of America* **106**, 13307-133310, doi:10.1073/pnas.0902312106 (2009).

31 Grison, M., Merkel, U., Kostan, J., Djinovic-Carugo, K. & Rief, M. alpha-Actinin/titin interaction: A dynamic and mechanically stable cluster of bonds in the muscle Z-disk. *Proceedings of the National Academy of Sciences of the United States of America* **114**, 1015-1020, doi:10.1073/pnas.1612681114 (2017).

32 Linke, W. A. *et al.* Actin-titin interaction in cardiac myofibrils: probing a physiological role. *Biophysical journal* **73**, 905-919, doi:http://dx.doi.org/10.1016/S0006-3495(97)78123-2 (1997).

33 Granzier, H. L. & Irving, T. C. Passive tension in cardiac muscle: contribution of collagen, titin, microtubules, and intermediate filaments. *Biophysical journal* **68**, 1027-1044, doi:10.1016/S0006-3495(95)80278-X (1995).

34 Freiburg, A. *et al.* Series of exon-skipping events in the elastic spring region of titin as the structural basis for myofibrillar elastic diversity. *Circulation research* **86**, 1114-1121 (2000).

35 Guo, W., Bharmal, S. J., Esbona, K. & Greaser, M. L. Titin Diversity—Alternative Splicing Gone Wild. *Journal of Biomedicine and Biotechnology* **2010**, 8, doi:10.1155/2010/753675 (2010).

36 Guo, W. *et al.* RBM20, a gene for hereditary cardiomyopathy, regulates titin splicing. *Nature medicine* **18**, 766-773, doi:10.1038/nm.2693 (2012).

37 Wells, Q. S. *et al.* Whole exome sequencing identifies a causal RBM20 mutation in a large pedigree with familial dilated cardiomyopathy. *Circulation. Cardiovascular genetics* **6**, 317-326, doi:10.1161/CIRCGENETICS.113.000011 (2013).

38 Granzier, H. & Labeit, S. Cardiac titin: an adjustable multi-functional spring. *The Journal of physiology* **541**, 335-342, doi:10.1113/jphysiol.2001.014381 (2002).

39 Radke, M. H. *et al.* Targeted deletion of titin N2B region leads to diastolic dysfunction and cardiac atrophy. *Proceedings of the National Academy of Sciences* **104**, 3444-3449, doi:10.1073/pnas.0608543104 (2007).

40 Chung, C. S. *et al.* Shortening of Titin's Elastic Tandem Ig Segment Leads to Diastolic Dysfunction. *Circulation*, doi:10.1161/circulationaha.112.001268 (2013).

41 Granzier, H. L. *et al.* Truncation of Titin's Elastic PEVK Region Leads to Cardiomyopathy With Diastolic Dysfunction. *Circulation research* **105**, 557-564, doi:10.1161/circresaha.109.200964 (2009).

42 Labeit, D. *et al.* Calcium-dependent molecular spring elements in the giant protein titin. *Proceedings of the National Academy of Sciences* **100**, 13716-13721, doi:10.1073/pnas.2235652100 (2003).

43 Linke, W. A. *et al.* PEVK Domain of Titin: An Entropic Spring with Actin-Binding Properties. *Journal of structural biology* **137**, 194-205, doi:http://dx.doi.org/10.1006/jsbi.2002.4468 (2002).

44 Sheikh, F. *et al.* An FHL1-containing complex within the cardiomyocyte sarcomere mediates hypertrophic biomechanical stress responses in mice. *The Journal of clinical investigation* **122**, 1584-1584, doi:10.1172/JCI63742 (2012).

45 Lange, S. *et al.* Subcellular targeting of metabolic enzymes to titin in heart muscle may be mediated by DRAL/FHL-2. *Journal of cell science* **115**, 4925-4936, doi:10.1242/jcs.00181 (2002).

46 Zhong, L. *et al.* Targeted inhibition of ANKRD1 disrupts sarcomeric ERK-GATA4 signal transduction and abrogates phenylephrine-induced cardiomyocyte hypertrophy. *Cardiovascular research* **106**, 261-271, doi:10.1093/cvr/cvv108 (2015).

47 Houmeida, A. *et al.* Evidence for the Oligomeric State of 'Elastic' Titin in Muscle Sarcomeres. *Journal of molecular biology* **384**, 299-312, doi:http://doi.org/10.1016/j.jmb.2008.09.030 (2008).

48 Freiburg, A. & Gautel, M. A molecular map of the interactions between titin and myosin-binding protein C. Implications for sarcomeric assembly in familial hypertrophic cardiomyopathy. *European journal of biochemistry / FEBS* **235**, 317-323 (1996).

49 Agarkova, I. & Perriard, J.-C. The M-band: an elastic web that crosslinks thick filaments in the center of the sarcomere. *Trends in cell biology* **15**, 477-485, doi:http://doi.org/10.1016/j.tcb.2005.07.001 (2005).

50 Lange, S. *et al.* The kinase domain of titin controls muscle gene expression and protein turnover. *Science* **308**, 1599-1603, doi:10.1126/science.1110463 (2005).

51 Musa, H. *et al.* Targeted homozygous deletion of M-band titin in cardiomyocytes prevents sarcomere formation. *Journal of cell science* **119**, 4322-4331, doi:10.1242/jcs.03198 (2006).

52 Pernigo, S. *et al.* Binding of Myomesin to Obscurin-Like-1 at the Muscle M-Band Provides a Strategy for Isoform-Specific Mechanical Protection. *Structure* **25**, 107-120, doi:10.1016/j.str.2016.11.015 (2017).

53 Pernigo, S. *et al.* Structural insight into M-band assembly and mechanics from the titin-obscurin-like-1 complex. *Proceedings of the National Academy of Sciences of the United States of America* **107**, 2908-2913, doi:10.1073/pnas.0913736107 (2010).

54 Obermann, W. M. J., Gautel, M., Weber, K. & Fürst, D. O. Molecular structure of the sarcomeric M band: mapping of titin and myosin binding domains in myomesin and the identification of a potential regulatory phosphorylation site in myomesin. *The EMBO journal* **16**, 211-220, doi:10.1093/emboj/16.2.211 (1997).

55 Puchner, E. M. *et al.* Mechanoenzymatics of titin kinase. *Proceedings of the National Academy of Sciences* **105**, 13385-13390, doi:10.1073/pnas.0805034105 (2008).

56 Mayans, O. *et al.* Structural basis for activation of the titin kinase domain during myofibrillogenesis. *Nature* **395**, 863-869 (1998).

57 Peng, J. *et al.* Cardiac hypertrophy and reduced contractility in hearts deficient in the titin kinase region. *Circulation* **115**, 743-751, doi:10.1161/CIRCULATIONAHA.106.645499 (2007).

58 Lyon, R. C., Lange, S. & Sheikh, F. Breaking down protein degradation mechanisms in cardiac muscle. *Trends in molecular medicine* **19**, 239-249, doi:10.1016/j.molmed.2013.01.005 (2013).

59 Centner, T. *et al.* Identification of muscle specific ring finger proteins as potential regulators of the titin kinase domain. *Journal of molecular biology* **306**, 717-726, doi:10.1006/jmbi.2001.4448 (2001).

60 Mrosek, M. *et al.* Molecular determinants for the recruitment of the ubiquitin-ligase MuRF-1 onto M-line titin. *FASEB journal : official publication of the Federation of American Societies for Experimental Biology* **21**, 1383-1392, doi:10.1096/fj.06-7644com (2007).

61 Beckmann, J. S. & Spencer, M. Calpain 3, the "gatekeeper" of proper sarcomere assembly, turnover and maintenance. *Neuromuscular disorders : NMD* **18**, 913-921, doi:10.1016/j.nmd.2008.08.005 (2008).

62 Heidenreich, P. A. *et al.* Forecasting the impact of heart failure in the United States: a policy statement from the American Heart Association. *Circulation. Heart failure* **6**, 606-619, doi:10.1161/HHF.0b013e318291329a (2013).

63 McNally, E. M., Golbus, J. R. & Puckelwartz, M. J. Genetic mutations and mechanisms in dilated cardiomyopathy. *The Journal of clinical investigation* **123**, 19-26, doi:10.1172/JCI62862 (2013).

64 Roberts, A. M. *et al.* Integrated allelic, transcriptional, and phenomic dissection of the cardiac effects of titin truncations in health and disease. *Science translational medicine* **7**, 270ra276, doi:10.1126/scitranslmed.3010134 (2015).

65 Herman, D. S. *et al.* Truncations of titin causing dilated cardiomyopathy. *The New England journal of medicine* **366**, 619-628, doi:10.1056/NEJMoa1110186 (2012).

66 Gramlich, M. *et al.* Stress-induced dilated cardiomyopathy in a knock-in mouse model mimicking human titin-based disease. *Journal of molecular and cellular cardiology* **47**, 352-358, doi:10.1016/j.yjmcc.2009.04.014 (2009).

67 Hinson, J. T. *et al.* HEART DISEASE. Titin mutations in iPS cells define sarcomere insufficiency as a cause of dilated cardiomyopathy. *Science* **349**, 982-986, doi:10.1126/science.aaa5458 (2015).

68 Gerull, B. *et al.* Mutations of TTN, encoding the giant muscle filament titin, cause familial dilated cardiomyopathy. *Nature genetics* **30**, 201-204, doi:10.1038/ng815 (2002).

69 Schafer, S. *et al.* Titin-truncating variants affect heart function in disease cohorts and the general population. *Nature genetics* **49**, 46-53, doi:10.1038/ng.3719 (2017).

70 Levine, H. J. Rest heart rate and life expectancy. *Journal of the American College of Cardiology* **30**, 1104-1106 (1997).

71 HALL, C. E., JAKUS, M. A. & SCHMITT, F. O. AN INVESTIGATION OF CROSS STRIATIONS AND MYOSIN FILAMENTS IN MUSCLE. *The Biological Bulletin* **90**, 32-50, doi:doi:10.2307/1538060 (1946).

72 Thompson, B. R. & Metzger, J. M. Cell biology of sarcomeric protein engineering: disease modeling and therapeutic potential. *Anat Rec (Hoboken)* **297**, 1663-1669, doi:10.1002/ar.22966 (2014).

73 Martin, A. F. Turnover of cardiac troponin subunits. Kinetic evidence for a precursor pool of troponin-I. *The Journal of biological chemistry* **256**, 964-968 (1981).

74 Everett, A. W., Prior, G. & Zak, R. Equilibration of leucine between the plasma compartment and leucyl-tRNA in the heart, and turnover of cardiac myosin heavy chain. *The Biochemical journal* **194**, 365-368 (1981).

75 Sanger, J. W., Mittal, B. & Sanger, J. M. Formation of myofibrils in spreading chick cardiac myocytes. *Cell Motil* **4**, 405-416 (1984).

76 Sanger, J. M., Mittal, B., Pochapin, M. B. & Sanger, J. W. Myofibrillogenesis in living cells microinjected with fluorescently labeled alpha-actinin. *The Journal of cell biology* **102**, 2053-2066 (1986).

77 Peter, A. K., Bjerke, M. A. & Leinwand, L. A. Biology of the cardiac myocyte in heart disease. *Molecular biology of the cell* **27**, 2149-2160, doi:10.1091/mbc.E16-01-0038 (2016).

78 Imanaka-Yoshida, K., Sanger, J. M. & Sanger, J. W. Contractile protein dynamics of myofibrils in paired adult rat cardiomyocytes. *Cell motility and the cytoskeleton* **26**, 301-312, doi:10.1002/cm.970260405 (1993).

79 Shimomura, O., Johnson, F. H. & Saiga, Y. Extraction, purification and properties of aequorin, a bioluminescent protein from the luminous hydromedusan, Aequorea. *J Cell Comp Physiol* **59**, 223-239 (1962).

80 Reits, E. A. & Neefjes, J. J. From fixed to FRAP: measuring protein mobility and activity in living cells. *Nature cell biology* **3**, E145-147, doi:10.1038/35078615 (2001).

81 Loren, N. *et al.* Fluorescence recovery after photobleaching in material and life sciences: putting theory into practice. *Q Rev Biophys* **48**, 323-387, doi:10.1017/S0033583515000013 (2015).

82 Morisaki, T. & McNally, J. G. Photoswitching-free FRAP analysis with a genetically encoded fluorescent tag. *PloS one* **9**, e107730, doi:10.1371/journal.pone.0107730 (2014).

83 Skwarek-Maruszewska, A., Hotulainen, P., Mattila, P. K. & Lappalainen, P. Contractility-dependent actin dynamics in cardiomyocyte sarcomeres. *Journal of cell science* **122**, 2119-2126, doi:10.1242/jcs.046805 (2009).

84 Wolny, M. *et al.* Cardiomyopathy mutations in the tail of beta-cardiac myosin modify the coiled-coil structure and affect integration into thick filaments in muscle sarcomeres in adult cardiomyocytes. *The Journal of biological chemistry* **288**, 31952-31962, doi:10.1074/jbc.M113.513291 (2013).

85 Wang, J., Fan, Y., Dube, D. K., Sanger, J. M. & Sanger, J. W. Jasplakinolide reduces actin and tropomyosin dynamics during myofibrillogenesis. *Cytoskeleton* **71**, 513-529, doi:10.1002/cm.21189 (2014).

86 van der Ven, P. F., Bartsch, J. W., Gautel, M., Jockusch, H. & Furst, D. O. A functional knock-out of titin results in defective myofibril assembly. *Journal of cell science* **113 (Pt 8)**, 1405-1414 (2000).

87 Person, V., Kostin, S., Suzuki, K., Labeit, S. & Schaper, J. Antisense oligonucleotide experiments elucidate the essential role of titin in sarcomerogenesis in adult rat cardiomyocytes in long-term culture. *Journal of cell science* **113 Pt 21**, 3851-3859 (2000).

88 Ehler, E. & Gautel, M. The sarcomere and sarcomerogenesis. *Advances in experimental medicine and biology* **642**, 1-14 (2008).

89 da Silva Lopes, K., Pietas, A., Radke, M. H. & Gotthardt, M. Titin visualization in real time reveals an unexpected level of mobility within and between sarcomeres. *The Journal of cell biology* **193**, 785-798, doi:10.1083/jcb.201010099 (2011).

90 Isaacs, W. B., Kim, I. S., Struve, A. & Fulton, A. B. Biosynthesis of titin in cultured skeletal muscle cells. *The Journal of cell biology* **109**, 2189-2195 (1989).

91 Global, regional, and national life expectancy, all-cause mortality, and cause-specific mortality for 249 causes of death, 1980–2015: a systematic analysis for the Global Burden of Disease Study 2015. *The Lancet* **388**, 1459-1544, doi:10.1016/s0140-6736(16)31012-1 (2016).

92 Martin, G. R. Isolation of a pluripotent cell line from early mouse embryos cultured in medium conditioned by teratocarcinoma stem cells. *Proceedings of the National Academy of Sciences of the United States of America* **78**, 7634-7638 (1981).

93 Evans, M. J. & Kaufman, M. H. Establishment in culture of pluripotential cells from mouse embryos. *Nature* **292**, 154-156 (1981).

94 Thomson, J. A. *et al.* Embryonic stem cell lines derived from human blastocysts. *Science* **282**, 1145-1147 (1998).

95 Hynes, R. O. US policies on human embryonic stem cells. *Nature reviews. Molecular cell biology* **9**, 993-997, doi:10.1038/nrm2528 (2008).

96 Takahashi, K. & Yamanaka, S. Induction of pluripotent stem cells from mouse embryonic and adult fibroblast cultures by defined factors. *Cell* **126**, 663-676, doi:10.1016/j.cell.2006.07.024 (2006).

97 Takahashi, K. *et al.* Induction of pluripotent stem cells from adult human fibroblasts by defined factors. *Cell* **131**, 861-872, doi:10.1016/j.cell.2007.11.019 (2007).

98 Burridge, P. W. *et al.* Chemically defined generation of human cardiomyocytes. *Nature methods* **11**, 855-860, doi:10.1038/nmeth.2999 (2014).

99 Mummery, C. L. *et al.* Differentiation of human embryonic stem cells and induced pluripotent stem cells to cardiomyocytes: a methods overview. *Circulation research* **111**, 344-358, doi:10.1161/CIRCRESAHA.110.227512 (2012).

100 Feaster, T. K. *et al.* Matrigel Mattress: A Method for the Generation of Single Contracting Human-Induced Pluripotent Stem Cell-Derived Cardiomyocytes. *Circulation research* **117**, 995-1000, doi:10.1161/CIRCRESAHA.115.307580 (2015).

101 Ribeiro, A. J. *et al.* Contractility of single cardiomyocytes differentiated from pluripotent stem cells depends on physiological shape and substrate stiffness. *Proceedings of the National Academy of Sciences of the United States of America* **112**, 12705-12710, doi:10.1073/pnas.1508073112 (2015).

102 Rodriguez, M. L. *et al.* Measuring the contractile forces of human induced pluripotent stem cell-derived cardiomyocytes with arrays of microposts. *Journal of biomechanical engineering* **136**, 051005, doi:10.1115/1.4027145 (2014).

103 Ahola, A. *et al.* Video image-based analysis of single human induced pluripotent stem cell derived cardiomyocyte beating dynamics using digital image correlation. *Biomedical engineering online* **13**, 39, doi:10.1186/1475-925X-13-39 (2014).

104 Liu, J., Sun, N., Bruce, M. A., Wu, J. C. & Butte, M. J. Atomic force mechanobiology of pluripotent stem cell-derived cardiomyocytes. *PloS one* **7**, e37559, doi:10.1371/journal.pone.0037559 (2012).

105 Sander, J. D. & Joung, J. K. CRISPR-Cas systems for editing, regulating and targeting genomes. *Nature biotechnology* **32**, 347-355, doi:10.1038/nbt.2842 (2014).

106 Hsu, P. D., Lander, E. S. & Zhang, F. Development and applications of CRISPR-Cas9 for genome engineering. *Cell* **157**, 1262-1278, doi:10.1016/j.cell.2014.05.010 (2014).

107 Barrett, L. W., Fletcher, S. & Wilton, S. D. Regulation of eukaryotic gene expression by the untranslated gene regions and other non-coding elements. *Cellular and molecular life sciences : CMLS* **69**, 3613-3634, doi:10.1007/s00018-012-0990-9 (2012).

108 Houseley, J. & Tollervey, D. The many pathways of RNA degradation. *Cell* **136**, 763-776, doi:10.1016/j.cell.2009.01.019 (2009).

109 Tian, Q. *et al.* Integrated genomic and proteomic analyses of gene expression in Mammalian cells. *Molecular & cellular proteomics : MCP* **3**, 960-969, doi:10.1074/mcp.M400055-MCP200 (2004).

110 Cox, B., Kislinger, T. & Emili, A. Integrating gene and protein expression data: pattern analysis and profile mining. *Methods* **35**, 303-314, doi:10.1016/j.ymeth.2004.08.021 (2005).

111 Schwanhausser, B. *et al.* Global quantification of mammalian gene expression control. *Nature* **473**, 337-342, doi:10.1038/nature10098 (2011).

112 Sonenberg, N. & Hinnebusch, A. G. Regulation of translation initiation in eukaryotes: mechanisms and biological targets. *Cell* **136**, 731-745, doi:10.1016/j.cell.2009.01.042 (2009).

113 Barbosa, C., Peixeiro, I. & Romao, L. Gene expression regulation by upstream open reading frames and human disease. *PLoS genetics* **9**, e1003529, doi:10.1371/journal.pgen.1003529 (2013).

114 Calvo, S. E., Pagliarini, D. J. & Mootha, V. K. Upstream open reading frames cause widespread reduction of protein expression and are polymorphic among humans. *Proceedings of the National Academy of Sciences of the United States of America* **106**, 7507-7512, doi:10.1073/pnas.0810916106 (2009).

115 Lim, C. C. *et al.* Anthracyclines induce calpain-dependent titin proteolysis and necrosis in cardiomyocytes. *The Journal of biological chemistry* **279**, 8290-8299, doi:10.1074/jbc.M308033200 (2004).

116 Cripe, L., Morris, E. & Fulton, A. B. Vimentin mRNA location changes during muscle development. *Proceedings of the National Academy of Sciences of the United States of America* **90**, 2724-2728 (1993).

117 Zuker, M. Mfold web server for nucleic acid folding and hybridization prediction. *Nucleic acids research* **31**, 3406-3415, doi:10.1093/nar/gkg595 (2003).

118 Martin, K. C. & Ephrussi, A. mRNA localization: gene expression in the spatial dimension. *Cell* **136**, 719-730, doi:10.1016/j.cell.2009.01.044 (2009).

119 Kozak, M. Point mutations define a sequence flanking the AUG initiator codon that modulates translation by eukaryotic ribosomes. *Cell* **44**, 283-292 (1986).

120 Pisarev, A. V. *et al.* Specific functional interactions of nucleotides at key -3 and +4 positions flanking the initiation codon with components of the mammalian 48S translation initiation complex. *Genes & development* **20**, 624-636, doi:10.1101/gad.1397906 (2006).

121 Larsen, T. H. & Saetersdal, T. Translocation of 60S Ribosomal Subunit in Spreading Cardiac Myocytes. *Journal of Histochemistry & Cytochemistry* **46**, 963-969, doi:10.1177/002215549804600810 (1998).

122 Fulton, A. B. & Alftine, C. Organization of protein and mRNA for titin and other myofibril components during myofibrillogenesis in cultured chicken skeletal muscle. *Cell structure and function* **22**, 51-58 (1997).

123 Capell, A., Fellerer, K. & Haass, C. Progranulin transcripts with short and long 5'-untranslated regions (UTR) are differentially expressed via post transcriptional and translational repression. *The Journal of biological chemistry*, doi:10.1074/jbc.M114.560128 (2014).

124 Wegrzyn, J. L., Drudge, T. M., Valafar, F. & Hook, V. Bioinformatic analyses of mammalian 5'-UTR sequence properties of mRNAs predicts alternative translation initiation sites. *BMC bioinformatics* **9**, 232, doi:10.1186/1471-2105-9-232 (2008).

125 van Zalen, S., Nijenhuis, M., Jonkman, M. F. & Pas, H. H. Two major 5'-untranslated regions for type XVII collagen mRNA. *Journal of dermatological science* **43**, 11-19, doi:10.1016/j.jdermsci.2006.02.008 (2006).

126 Spruill, L. S. & McDermott, P. J. Role of the 5'-untranslated region in regulating translational efficiency of specific mRNAs in adult cardiocytes. *FASEB journal : official publication of the Federation of American Societies for Experimental Biology* **23**, 2879-2887, doi:10.1096/fj.08-128447 (2009).

127 Nikcevic, G., Heidkamp, M. C., Perhonen, M. & Russell, B. Mechanical activity in heart regulates translation of alpha-myosin heavy chain mRNA but not its localization. *The American journal of physiology* **276**, H2013-2019 (1999).

128 Yang, J. *et al.* Translational up-regulation of polycystic kidney disease protein PKD2 by endoplasmic reticulum stress. *FASEB journal : official publication of the Federation of American Societies for Experimental Biology* **27**, 4998-5009, doi:10.1096/fj.13-236075 (2013).

129 Mohan, R. A. *et al.* A mutation in the Kozak sequence of GATA4 hampers translation in a family with atrial septal defects. *American journal of medical genetics. Part A*, doi:10.1002/ajmg.a.36703 (2014).

130 van Rooij, E. & Olson, E. N. MicroRNAs: powerful new regulators of heart disease and provocative therapeutic targets. *The Journal of clinical investigation* **117**, 2369-2376, doi:10.1172/JCI33099 (2007).

131 Allis, C. D. & Jenuwein, T. The molecular hallmarks of epigenetic control. *Nature reviews. Genetics* **17**, 487-500, doi:10.1038/nrg.2016.59 (2016).

132 Spitz, F. & Furlong, E. E. Transcription factors: from enhancer binding to developmental control. *Nature reviews. Genetics* **13**, 613-626, doi:10.1038/nrg3207 (2012).

133 Bentley, D. L. Coupling mRNA processing with transcription in time and space. *Nature reviews. Genetics* **15**, 163-175, doi:10.1038/nrg3662 (2014).

134 Cadar, A. G., Zhong, L., Lin, A., Valenzuela, M. & Lim, C. C. Upstream Open Reading Frame in 5'-Untranslated Region Reduces Titin mRNA Translational Efficiency. *Biochemical and biophysical research communications*, doi:10.1016/j.bbrc.2014.09.085 (2014).

135 Gebauer, F. & Hentze, M. W. Molecular mechanisms of translational control. *Nature reviews. Molecular cell biology* **5**, 827-835, doi:10.1038/nrm1488 (2004).

136 Kahvejian, A., Svitkin, Y. V., Sukarieh, R., M'Boutchou, M. N. & Sonenberg, N. Mammalian poly(A)-binding protein is a eukaryotic translation initiation factor, which acts via multiple mechanisms. *Genes & development* **19**, 104-113, doi:10.1101/gad.1262905 (2005).

137 Mayr, C. Evolution and Biological Roles of Alternative 3'UTRs. *Trends in cell biology* **26**, 227-237, doi:10.1016/j.tcb.2015.10.012 (2016).

138 van Rooij, E. & Olson, E. N. MicroRNA therapeutics for cardiovascular disease: opportunities and obstacles. *Nat Rev Drug Discov* **11**, 860-872, doi:10.1038/nrd3864 (2012).

139 Yeo, M., Lin, P. S., Dahmus, M. E. & Gill, G. N. A novel RNA polymerase II C-terminal domain phosphatase that preferentially dephosphorylates serine 5. *The Journal of biological chemistry* **278**, 26078-26085, doi:10.1074/jbc.M301791200 (2003).

140 Zhu, Y. *et al.* MicroRNA-26a/b and their host genes cooperate to inhibit the G1/S transition by activating the pRb protein. *Nucleic acids research* **40**, 4615-4625, doi:10.1093/nar/gkr1278 (2012).

141 Han, M. *et al.* GATA4 expression is primarily regulated via a miR-26b-dependent post-transcriptional mechanism during cardiac hypertrophy. *Cardiovascular research* **93**, 645-654, doi:10.1093/cvr/cvs001 (2012).

142 Molkentin, J. D., Lin, Q., Duncan, S. A. & Olson, E. N. Requirement of the transcription factor GATA4 for heart tube formation and ventral morphogenesis. *Genes & development* **11**, 1061-1072 (1997).

143 Warren, C. M., Krzesinski, P. R. & Greaser, M. L. Vertical agarose gel electrophoresis and electroblotting of high-molecular-weight proteins. *Electrophoresis* **24**, 1695-1702, doi:10.1002/elps.200305392 (2003).

144 Tian, B. & Manley, J. L. Alternative cleavage and polyadenylation: the long and short of it. *Trends in biochemical sciences* **38**, 312-320, doi:10.1016/j.tibs.2013.03.005 (2013).

145 He, L. & Hannon, G. J. MicroRNAs: small RNAs with a big role in gene regulation. *Nature reviews. Genetics* **5**, 522-531, doi:10.1038/nrg1379 (2004).

146 Zhao, Y., Samal, E. & Srivastava, D. Serum response factor regulates a muscle-specific microRNA that targets Hand2 during cardiogenesis. *Nature* **436**, 214-220, doi:10.1038/nature03817 (2005).

147 Chi, S. W., Zang, J. B., Mele, A. & Darnell, R. B. Argonaute HITS-CLIP decodes microRNA-mRNA interaction maps. *Nature* **460**, 479-486, doi:10.1038/nature08170 (2009).

148 Peter, M. E. Targeting of mRNAs by multiple miRNAs: the next step. *Oncogene* **29**, 2161-2164, doi:10.1038/onc.2010.59 (2010).

149 Crippa, S. *et al.* Comparative transcriptome profiling of the injured zebrafish and mouse hearts identifies miRNA-dependent repair pathways. *Cardiovascular research* **110**, 73-84, doi:10.1093/cvr/cvw031 (2016).

150 Zhang, Z. H. *et al.* MicroRNA-26 was decreased in rat cardiac hypertrophy model and may be a promising therapeutic target. *Journal of cardiovascular pharmacology* **62**, 312-319, doi:10.1097/FJC.0b013e31829b82e6 (2013).

151 Ran, F. A. *et al.* Genome engineering using the CRISPR-Cas9 system. *Nature protocols* **8**, 2281-2308, doi:10.1038/nprot.2013.143 (2013).

152 Zhang, M. *et al.* Rational design of true monomeric and bright photoactivatable fluorescent proteins. *Nature methods* **9**, 727-729, doi:10.1038/nmeth.2021 (2012).

153 Turnacioglu, K. K., Mittal, B., Dabiri, G. A., Sanger, J. M. & Sanger, J. W. An N-terminal fragment of titin coupled to green fluorescent protein localizes to the Z-bands in

living muscle cells: overexpression leads to myofibril disassembly. *Molecular biology of the cell* **8**, 705-717 (1997).

154 Mueller, F., Morisaki, T., Mazza, D. & McNally, J. G. Minimizing the impact of photoswitching of fluorescent proteins on FRAP analysis. *Biophysical journal* **102**, 1656-1665, doi:10.1016/j.bpj.2012.02.029 (2012).

155 Sinnecker, D., Voigt, P., Hellwig, N. & Schaefer, M. Reversible photobleaching of enhanced green fluorescent proteins. *Biochemistry* **44**, 7085-7094, doi:10.1021/bi047881x (2005).

156 Furst, D. O., Nave, R., Osborn, M. & Weber, K. Repetitive titin epitopes with a 42 nm spacing coincide in relative position with known A band striations also identified by major myosin-associated proteins. An immunoelectron-microscopical study on myofibrils. *Journal of cell science* **94 (Pt 1)**, 119-125 (1989).

157 Isaacs, W. B., Kim, I. S., Struve, A. & Fulton, A. B. Association of titin and myosin heavy chain in developing skeletal muscle. *Proceedings of the National Academy of Sciences of the United States of America* **89**, 7496-7500 (1992).

158 Dayel, M. J., Hom, E. F. & Verkman, A. S. Diffusion of green fluorescent protein in the aqueous-phase lumen of endoplasmic reticulum. *Biophysical journal* **76**, 2843-2851, doi:10.1016/S0006-3495(99)77438-2 (1999).

159 Ojima, K., Ichimura, E., Yasukawa, Y., Wakamatsu, J. & Nishimura, T. Dynamics of myosin replacement in skeletal muscle cells. *American journal of physiology. Cell physiology* **309**, C669-679, doi:10.1152/ajpcell.00170.2015 (2015).

160 Jones, R. B. *et al.* A Subset of Latency-Reversing Agents Expose HIV-Infected Resting CD4+ T-Cells to Recognition by Cytotoxic T-Lymphocytes. *PLoS pathogens* **12**, e1005545, doi:10.1371/journal.ppat.1005545 (2016).

161 Wang, C., Han, B., Zhou, R. & Zhuang, X. Real-Time Imaging of Translation on Single mRNA Transcripts in Live Cells. *Cell* **165**, 990-1001, doi:10.1016/j.cell.2016.04.040 (2016).

162 Tanenbaum, M. E., Gilbert, L. A., Qi, L. S., Weissman, J. S. & Vale, R. D. A protein-tagging system for signal amplification in gene expression and fluorescence imaging. *Cell* **159**, 635-646, doi:10.1016/j.cell.2014.09.039 (2014).

163 Saghatelian, A. & Couso, J. P. Discovery and characterization of smORF-encoded bioactive polypeptides. *Nat Chem Biol* **11**, 909-916, doi:10.1038/nchembio.1964 (2015).

164 Sayed, D., He, M., Yang, Z., Lin, L. & Abdellatif, M. Transcriptional Regulation Patterns Revealed by High Resolution Chromatin Immunoprecipitation during Cardiac Hypertrophy. *The Journal of biological chemistry* **288**, 2546-2558, doi:10.1074/jbc.M112.429449 (2013).

165 Park, J. Y. *et al.* Comparative analysis of mRNA isoform expression in cardiac hypertrophy and development reveals multiple post-transcriptional regulatory modules. *PloS one* **6**, e22391, doi:10.1371/journal.pone.0022391 (2011).

166 Jansen, R. P. mRNA localization: message on the move. *Nature reviews. Molecular cell biology* **2**, 247-256, doi:10.1038/35067016 (2001).

167 An, J. J. *et al.* Distinct role of long 3' UTR BDNF mRNA in spine morphology and synaptic plasticity in hippocampal neurons. *Cell* **134**, 175-187, doi:10.1016/j.cell.2008.05.045 (2008).

168 Los, G. V. *et al.* HaloTag: a novel protein labeling technology for cell imaging and protein analysis. *ACS Chem Biol* **3**, 373-382, doi:10.1021/cb800025k (2008).

169 Pizon, V., Gerbal, F., Diaz, C. C. & Karsenti, E. Microtubule-dependent transport and organization of sarcomeric myosin during skeletal muscle differentiation. *The EMBO journal* **24**, 3781-3792, doi:10.1038/sj.emboj.7600842 (2005).

170 Rothen-Rutishauser, B. M., Ehler, E., Perriard, E., Messerli, J. M. & Perriard, J. C. Different behaviour of the non-sarcomeric cytoskeleton in neonatal and adult rat cardiomyocytes. *Journal of molecular and cellular cardiology* **30**, 19-31 (1998).

171 Pizon, V. *et al.* Transient association of titin and myosin with microtubules in nascent myofibrils directed by the MURF2 RING-finger protein. *Journal of cell science* **115**, 4469-4482 (2002).

172 Weinert, S., Bergmann, N., Luo, X., Erdmann, B. & Gotthardt, M. M line-deficient titin causes cardiac lethality through impaired maturation of the sarcomere. *The Journal of cell biology* **173**, 559-570, doi:10.1083/jcb.200601014 (2006).

173 Parker, K. K., Tan, J., Chen, C. S. & Tung, L. Myofibrillar architecture in engineered cardiac myocytes. *Circulation research* **103**, 340-342, doi:10.1161/CIRCRESAHA.108.182469 (2008).

174 Chen, I. Y., Matsa, E. & Wu, J. C. Induced pluripotent stem cells: at the heart of cardiovascular precision medicine. *Nature reviews. Cardiology* **13**, 333-349, doi:10.1038/nrcardio.2016.36 (2016).